12-2014

Calibration of Resistance Factors for Driven Piles using Static and Dynamic Tests

Deshinka A. Bostwick
University of Arkansas, Fayetteville

Calibration of Resistance Factors for Driven Piles using Static and Dynamic Tests

Calibration of Resistance Factors for Driven Piles using Static and Dynamic Tests

A thesis submitted in partial fulfillment
of the requirements for the degree of
Master of Science in Civil Engineering

By

Deshinka Arimena Bostwick
University of Arkansas
Bachelor of Science in Civil Engineering, 2011

December 2014
University of Arkansas

This thesis is approved for recommendation to the Graduate Council.

Dr. Norman D. Dennis
Thesis Director

Dr. Richard A. Coffman
Committee Member

Dr. Rodney D. Williams
Committee Member

Abstract

The field of geotechnical engineering has evolved from Allowable Stress Design (ASD) to Load Factor and Resistance Design (LRFD) which has led to a need to quantify the measures of uncertainty and the level of reliability associated with a project. The measures of uncertainty are quantified by load and resistance factors, while the level of reliability is driven by the amount of risk an owner is willing to take and is quantified by the reliability index. The load factors are defined through structural design codes, but the resistance factors have uncertainties that can be mitigated through reliability based design. The American Association of State Highway and Transportation Officials (AASHTO) have recommended resistance factors that are dependent on the type of load tests conducted and are available as a reference to state agencies. The objective of this study was to improve the AASHTO recommended resistance factors used by the Arkansas State Highway and Transportation Department (AHTD), thereby, increasing allowable pile capacity and reducing deep foundation costs. Revised resistance factors for field acceptance based on dynamic testing were established through the analysis of pile load test data where both static and dynamic load testing was conducted. Pile load tests were separated by pile type and soil type. It was important that the load test data analyzed represented soil and geologic conditions similar to those found in Arkansas. The resistance factors determined from this analysis improved AHTD current practice, but indicated that the factors recommended by AASHTO may be unconservative for this region.

Acknowledgments

A note of appreciation is extended to my family for their support throughout this journey, also to the professors and lecturers throughout my academic career.

Table of Contents

List of Tables

List of Figures

1 Introduction

Pile foundations become a critical aspect in construction when the structural loads from buildings and bridges must be transferred from relatively weak surface soils to stronger soil or rock stratigraphy. Pile foundations offer additional load carrying capability that is essential for foundations that must sustain large structural loads with relatively small settlements. The design of pile foundations is subject to a large number of uncertainties which can lead to over conservative or unconservative designs if care is not taken to address these uncertainties in a logical and realistic manner. These uncertainties can be mitigated through the proper application of factors of safety to design loads and full scale pile testing. Clearly, managing uncertainty is necessary to ensure economic and efficient use of resources, time, and money.

When piles are installed, seldom are full scale load tests performed that provide definitive values for capacity. When capacity is known precisely for test piles, production piles can be redesigned or pile groups redistributed thereby reducing costs. Pile capacity is truly measured by performing static load testing (SLT). Unfortunately, SLT is very expensive, the cost ranges from $50,000 to $2 million depending on the intended size and capacity of the pile, the need for sophisticated reaction pile systems, and mobilization costs (Loadtest USA 2012). As a distinct result, industry practice is to use other less costly procedures to predict pile capacity.

Dynamic load testing (DLT) through signal matching and the use of program interface software such as the pile driving analyzer (PDA) and CAse Pile Wave Analyses Program (CAPWAP) have become an accepted means to predict pile capacity in conjunction with wave equation analysis. However, dynamic load testing is normally performed on only a small selection of test piles to determine the driving criteria for the project and the possible pile

capacity development within the site. It would be ideal to test every pile driven on a site and have capacity quantified, but due to time and money constraints, very few production piles are actually tested. Testing a larger population of piles specific to a region can positively impact current pile driving practices, prompting more efficient designs and better classification of uncertainties.

Arkansas reportedly monitors fewer than 5% of production piles with signal matching to establish a final production pile driving criteria (Brown et al. 2011). Due to having very little applicable load test data, Arkansas pile design and field acceptance is guided by the guidelines of the American Association of State Highway and Transportation Official (AASHTO) Load Factor and Resistance Design (LRFD) Bridge Design Specifications. This guide provides recommendations based on worldwide data than may misrepresent pile driving conditions in Arkansas.

1.1 Problem Statement

Pile capacity is definitively measured through static load testing (SLT). While its use is limited, this is the methodology that most accurately measures the ultimate capacity of pile foundations. Unfortunately, this test method is often cost prohibitive, and as such, has seldom been carried out in the state of Arkansas.

The Arkansas Highway and Transportation Department (AHTD) has estimated that 99 percent of the projects conducted by the agency involve pile foundations (Brown et al. 418 2011). Piles are driven to a specified driving resistance, characterized by blow count, which is based on bearing capacity. Evidently, AHTD determines bearing capacity utilizing three distinct methodologies: Empirical Pile Driving Formula (Method A), Wave Equation Analysis of Piles

(WEAP) (Method B), and Dynamic Load Testing (Method C) (Arkansas Specifications 2014). The empirical formulas used in Method A calculate bearing capacity based solely on the weight and stroke of the hammer used in driving (driving energy), and the penetration of the pile into the soil per hammer blow. The safe bearing value for Method A is obtained when the target value is maintained through the last five feet of driving or when practical refusal is observed. Practical refusal occurs when the calculated safe bearing value is three times the required safe bearing value. The current practice within AHTD is to implement a resistance factor of 0.1, which corresponds to a dated Engineering News Record dynamic formula which does not consider the pile-soil-hammer system.

Bearing capacity obtained through Method B, Wave Equation Analysis of Piles (WEAP), matches the pile hammer to the pile and soil conditions. This method requires soil, pile, and driving equipment properties, determined by the Engineer, to be entered into the Wave Equation Analysis Program (WEAP). The analysis provides the Engineer with a bearing graph that shows a hammer-blow count relationship for the required ultimate bearing capacity. The design bearing capacity would be 40 % of the ultimate bearing capacity determined through WEAP, with a ϕ factor of 0.40 (AASHTO 2010).

The bearing capacity obtained from Method C, Dynamic Load Testing, uses signal matching to establish soil resistance to determine pile capacity. Bearing graphs are produced that shows a hammer blow count relationship for 90% to 100% of the required ultimate bearing capacity. The design bearing capacity of a pile shall be 40% of the ultimate bearing capacity as determined by dynamic testing (AHTD 2007). In normal practice, however, piles are usually driven to practical refusal or to rock. Currently, test piles on AHTD construction projects

constitute far less than 5% of production piles that are monitored by high strain dynamic testing with signal matching (Brown et al. 2011).

Performing load testing on test piles provides the engineer with confirmation of design capacity that is usually inferred through the analysis of boring log data and the use of empirical design methods that may have unclear or unstated assumptions. The information obtained through load testing, such as the pile ultimate bearing capacity and the load-settlement relationship of the pile-soil system, can lead to a more informed decision on the allowable load per pile, which may reduce the number and length of piles required for a given project, thereby providing cost savings. The potential in cost savings may be sufficiently beneficial to encourage the State of Arkansas to perform load testing on an increased number of test piles and to extend testing to production piles. The expansion of pile testing should positively impact the development of a pile load test database. A robust pile load database will allow for the improvement of resistance factors used for the design and acceptance of pile foundations in the State of Arkansas.

1.2 Research Objectives

The focus of this research effort will be to explore the correlation between SLT and DLT methods. The endeavor is not to dissuade the use of SLT to measure pile capacity, but rather to build a platform from which the AHTD can infer capacity predictions while implementing appropriate resistance factors that are specific to the soil and pile type in question.

Accordingly, static and dynamic load test data from neighboring states with similar land forms as Arkansas (Alabama, Missouri, Iowa, and Louisiana), will be collected, compiled and analyzed. The information gathered is expected to allow AHTD to categorize projects by soil and

pile type, then choose the appropriate resistance factor for the project. The load test data would encompass as many landforms as possible to allow observations on how different pile types perform in a given stratigraphy.

The data reduction will be conducted by the University of Arkansas research team. The main objectives of this research are: (1) Compare SLT capacities to DLT capacities; (2) Perform statistical analysis of the load test data; (3) Develop resistance factors applicable to Arkansas; (4) Determine the level of reliability of these design factors; (5) Refine a driven pile database for Arkansas; (6) Provide guidance on field acceptance during pile driving.

To evaluate these objectives, several statistical methods will be performed at various levels of reliability. Methods used to analyze the data will include a regression analysis, resistance factor calibration through First Order Second Moment (FOSM), First Order Reliability Methods (FORM), and the Monte Carlo Simulation (MCS) to determine a suitable resistance factors (ϕ) appropriate for use in AHTD designs.

2 Literature Review

2.1 Introduction

Pile foundations have been the center of construction and the advancement of civilization for thousands of years. The first records of pile use extend to the late Neolithic Period, about 9500 BC, with dwellings built in flood-prone areas. These early piles were formed by using small trees which were denuded of branches. These timbers were then installed into the soil with the small diameter at the bottom by a stone driving mechanism. These ancient pilings were also used as the sub-structure of wooden bridges erected during the reign of Julius Caesar, 55 BC (Ulitskii 1995).

Scientific studies involving the driving of piles were conducted as early as the 18th century (Ulitskii 1995). These studies resulted in the use of dynamic capacity prediction equations, the earliest of which were introduced by Woltmann and Eytelwein during the 19th century (Ulitskii 1995; Chrimes 2008). These early dynamic equations considered the energy of the pile driving hammer and the resulting pile set to determine bearing capacity (GRL Engineers, Inc. 2014). Predicting pile capacity through dynamic formulae is variable and relies on the expertise of the Engineer. Dynamic formulas can provide a wide range of capacity predictions, depending on the input variables (soil properties, hammer efficiency, stroke of the ram, ram weight, etc.) and thus may lead to over or under predicted capacities and expensive or unreliable pile foundations.

To accurately measure pile capacity, an axial load is applied at the pile top and direct measurements of displacement of the pile head are recorded. This type of capacity measurement is termed Static Load Testing (SLT). The SLT is the most fundamental form of pile load testing and is considered to be the bench-mark for pile load testing due to its repeatability and consistent

performance. Static Load Testing has been used to measure pile capacities ranging from 22 kips to 2700 kips. Static Load Testing for piles with high capacities requires expensive pile reaction systems. Pile capacity has also been determined through a less costly and more commonly employed method called dynamic load testing (DLT). Dynamic load testing is a predictive method, and is only as good as the inputs provided by the designer. Other methods to measure pile capacity are the Statnamic Load Test and A Preferred Pile Load Evaluator (Newton's APPLE). Information necessary to accurately predict the pile capacity through dynamic methods are the soil's resistance, quake (displacement required to develop full soil capacity) and damping coefficients. Both SLT and DLT are standardized by the American Society for Testing and Materials (ASTM) and the American Association of State Highway and Traffic Officials. (AASHTO) and provide the user with several testing methods which provide a varying array of capacity measurement options.

2.1 Overview of Design and Testing of Pile Foundations

Determining the geometric and material properties of a pile for a deep foundation project begins with the static design process. The following is a typical course the design process may take: (1) The engineer is provided with the design loads and functions of the structure (critical or non-critical), (2) sub surface soils investigations in which the engineer determines the number, location and depth of borings needed to model the subsurface stratigraphy where the pile foundation is to be constructed. The engineer must also specify sampling and testing protocols, (3) Soil properties are evaluated through the interpretation of boring logs or cone penetration data and laboratory testing (4) Empirical static analysis methods are conducted to determine the pile size and length, and the number of piles necessary to safely resist the design load, (5) Dynamic formulas are sometimes used to determine ultimate capacity of a pile based upon blow

counts of a particular hammer delivering a certain energy level. (6) Alternatively a stress wave analysis could be conducted which integrates hammer, pile and soil properties to predict a pile capacity as a function of blow count. (7) After all the initial calculations are made; field testing should be conducted to measure pile capacity. The test pile may be instrumented and driven while DLT is preformed or the pile may be subjected to SLT at some time after the pile driving. Many agencies use a form of DLT called signal matching which has been shown to provide a reliable correlation to SLT capacities. However, this DLT method is subject to some uncertainties that may affect the predicted pile capacity. It is recommended that DLT and/or SLT be performed after a 7 to 14 day waiting period to allow the soil time to either setup or relax after the significant disturbance created by the driving operation. This would be the point in time when the pile is most likely to exhibit its long-term capacity. When time and economics permit SLT should be performed as this procedure is still the most reliable and truest measure of capacity.

2.2 Static Design

Static analysis is an initial step in the pile foundation design and construction process that establishes the geometry of the pile or pile group to develop a required resistance in a specified soil profile. The essential soil parameters needed for design normally include: particle size, plasticity, specific weight, strength, and location of the ground water table. These properties are obtained through sub-surface exploration with the standard penetration test (SPT), cone penetration tests (CPT), or undisturbed sampling of the soil. Interpretation of the information obtained from sub-surface exploration will determine the method of analysis. Many transportation agencies use the design methods contained in the computer program, DRIVEN 1.0 (FHWA 1998). This analysis program uses the Norlund β-method for sands or the Tomlinson α-

method for clays. Ultimate pile capacity (Q_{ult}) is determined through the summation of side capacity (Q_s) and tip capacity (Q_p) for either method expressed in Eqn. 2.1, Eqn. 2.2, and Eqn. 2.3:

$$Q_{ult} = Q_s + Q_p \quad \text{Eqn. 2.1}$$

$$Q_s = f_s A_s \quad \text{Eqn. 2.2}$$

Where: f_s is the unit side resistance, A_s is the area of the pile side in contact with the soil.

$$Q_p = q_p A_p \quad \text{Eqn. 2.3}$$

Where: q_p is the unit tip resistance, A_p is the area of the pile tip. For Norlund's method the unit side capacity, and the unit tip resistance are given by Eqn. 2.4:

$$f_s = \beta \sigma'_{avg}, \quad \beta = K tan\delta \quad \text{and} \quad q_p = \sigma'_v N_q \quad \text{Eqn. 2.4}$$

Where σ'_{avg} is the average effective stress along the pile side, K is the earth pressure coefficient, δ is the coefficient of wall friction, σ'_v is the effective stress at the pile tip, and N_q is the overburden bearing capacity factor. For the Tomlinson method the unit side and tip resistance are given by Eqn. 2.5:

$$f_s = \alpha C_u \text{ and } q_p = 9C_u \quad \text{Eqn. 2.5}$$

Where: α is the adhesion factor, C_u is the undrained shear stress.

The Norlund β-method (Eqn. 2.4) for cohesionless soils and piles of uniform dimensions was presented in 1963 by R. L. Norlund. It uses standard penetration blow count data to arrive at a value of beta to be used in the equations described above (Norlund 1963). The Tomlinson α-method (Eqn. 2.5) for cohesive soils was presented by M. J. Tomlinson (1957) and addresses the change in the in-situ conditions of the soil as it is remolded while the pile is driven. Tomlinson

suggested a range of alpha values less than or equal to one that effectively reduce the soil's undrained shear strength. Other static design methods in common use include Meyerhof's method (Meyerhof 1976) for sands (Meyerhof 1976), American Petroleum Institute (API) (API 1984) for both sands and clays, and the Lambda I (Vijayvergiya et al. 1972) and Lambda II (Kraft et al. 1981) methods for clays.

2.3 Dynamic Formulae

Once the pile geometry is established through static design methods, dynamic driving formulas may be used to predict capacity as a function of pile penetration per hammer blow. Dynamic formulae have been a common tool to predict pile capacity since the early 1900s (Likins et al. 2012). The dynamic formula presented in Eqn. 2.6 is a potential energy balance equation that relates the work energy transferred from the pile hammer to the pile as it penetrates through a specific distance in the soil (Long et al. 2009). Dynamic formulae are generally expressed as:

$$eWH = Rs \qquad \text{Eqn. 2.6}$$

Where: e is the efficiency of the hammer, W is the weight of ram, H is the vertical drop of hammer or stroke of ram, R is the pile resistance, and s is the pile permanent set. There have been varied approaches to the development of dynamic formula throughout the years. The more common methods include: the Engineering News (EN) formula; the Modified Engineering News (EN) formula; the Gates formula; the Federal Highway Administration (FHWA) Gates formula; and the Washington State Department of Transportation (WSDOT) formula.

2.3.1 Engineering News (EN) Formula

The Engineering News (EN) formula, illustrated in Eqn. 2.7, was developed in 1888 by Arthur Mellen Wellington a railway civil engineer (Likins et al. 2012). This formula was empirically developed for timber piles driven in sand with a drop hammer (Hannigan et al. 1998). Owing to the units used in the equation, it has a built-in factor of safety of six to produce a safe load that a pile can support.

$$L = F\,\frac{WH}{(s+c)} \qquad \text{Eqn. 2.7}$$

Where: L is the safe load, F is a constant determined from experience, W is the ram weight, H is the drop height of ram in feet (assumes single acting hammer), s is the penetration of pile in inches per blow, and c is a constant to account for the elastic compression of the hammer-pile-soil system. Historically, the EN formula has been considered the least accurate dynamic predictive method. However, it is widely used among transportation departments due to its simple formulation and ease of use. The EN formula has been proven to have factor of safeties ranging from as low 0.5 to as high as 20 (FHWA 1998), yet 45% of respondents to the state of practice survey reported in NCHRP Report 507 claim that they use the EN formula (Paikowsky 2004).

2.3.2 The Gates Formula

The Gates formula was proposed in 1957 by Marvin Gates, and is given in Eqn. 2.8. It is an empirical equation that was developed by simplifying the form of existing equations and adding an adjustment factor to achieve the allowable bearing capacity with a recommended factor of safety of three.

$$Q_u = \left(\frac{6}{7}\right)\sqrt{eE_r}\ \log(10N_b) \qquad \text{Eqn. 2.8}$$

Where: Q_u is the ultimate pile capacity (kips), e is the efficiency of the hammer (taken as 75% for drop hammers and 85% for all others), E_r is the theoretical delivered energy of the pile hammer (ft-lb), and N_b is the number of blows to cause one inch of pile penetration. The Gates formula tends to over-predict resistance at low driving resistances and under-predict resistance at high driving resistances (Allen 2005).

2.3.1 Modified Gates Formula

The analysis of 100 pile load tests (Olson et al. 1967) allowed for an adjustment in the Gates formula to provide a better statistical fit through the measured and predicted data. The formula was modified for timber with Eqn. 2.9, concrete with Eqn. 2.10, steel with Eqn. 2.11, and all piles with Eqn. 2.12.

$$R_u = 1.11\sqrt{eE_r}\log(10N_b) - 34 \qquad \text{Eqn. 2.9}$$

$$R_u = 1.39\sqrt{eE_r}\log(10N_b) - 54 \qquad \text{Eqn. 2.10}$$

$$R_u = 2.01\sqrt{eE_r}\log(10N_b) - 166 \qquad \text{Eqn. 2.11}$$

$$R_u = 1.55\sqrt{eE_r}\log(10N_b) - 96 \qquad \text{Eqn. 2.12}$$

Where: R_u is the ultimate pile capacity (kips), e is the efficiency of the hammer (75% for drop hammers or 85% for all others), E_r is the theoretical delivered energy of the pile hammer (ft-lb), and N_b is the number of blows to cause one inch of pile penetration.

2.3.2 Modified Engineering News (EN) Formula

The Modified Engineering News (EN) formula modifies the original EN formula by accounting for the weight of the pile and the energy that may be lost in the transfer from hammer

to pile. Several modified EN formulas have been developed, but in 1965, the Michigan State Highway Commission proposed an equation, expressed as Eqn. 2.13, that included a factor of safety of 6.0 (Fragaszy et al. 1985).

$$R_u = \frac{e_h E_h}{(s+c)} \frac{W + n^2 w}{W + w} \qquad \text{Eqn. 2.13}$$

Where: R_u is the ultimate bearing capacity of pile in soil, e_h is the efficiency of the striking hammer (<1.0), E_h is the manufacturer's hammer energy rating, s is the pile penetration for the last blow count (set) in inches, c is a constant (0.1 for steam hammers or 1.0 for drop hammers), W is the weight of the hammer ram, w is the weight of the pile, and n is the coefficient of restitution of the pile material.

2.3.3 The FHWA Gates Formula

The FHWA Gates formula, presented in Eqn. 2.14, is the preferred dynamic formula to predict bearing capacity (AASHTO 2010). Equation 2.8 is the original Gates formula modified by Olson and Flaate in 1967 with the objective to have a better statistical fit through the predicted and measured data (Long et al. 2009). The FHWA subsequently introduced more modifications to the already modified Gates formula, producing the FHWA Gates formula which takes the average of the equations for steel and concrete piles used in of the Modified Gates equation. The FHWA Gates formula reduced the tendency to under predict capacity and has demonstrated improved accuracy relative to the EN formula (Paikowsky et al. 2004; Allen 2005).

$$R_n = 1.75\sqrt{E_d}\,\log(10N_b) - 100 \qquad \text{Eqn. 2.14}$$

Where: R_n is the ultimate bearing resistance (kips), E_d is the developed hammer energy, and N_b is the number of blows for one inch of pile penetration.

2.3.4 Washington State Department of Transportation (WSDOT) Formula

The WSDOT also attempted to improve upon the Gates (1957) formula which resulted in significant changes as illustrated in Eqn. 2.15. The WSDOT formula was developed to maintain the low prediction variability of the Gates Formula while simultaneously minimizing the tendency to under- or over-predict resistance.

$$R_n = 6.6F_{eff}E\,\mathrm{Ln}(10N) \qquad \text{Eqn. 2.15}$$

Where: R_n is the ultimate bearing resistance (kips), F_{eff} is the hammer efficiency factor, E is the developed energy (ft-kips), Ln is the natural logarithm, in base "e", and N is the average penetration resistance in blows per inch for the last 4 inches of driving (WSDOT 2010).

Dynamic formulas are only one means of supplying an estimate of the pile capacity, it addresses the kinetic energy of driving but not the entire driving system. It does not account for pile cap, pile cushion, and other energy damping factors in the hammer-pile-soil system. It also assumes constant soil resistance along the pile side (Long et al. 2009). In fact no soil parameters are input into the equations, and they ignore the viscoelastic effects of the soil. Dynamic formulae neglect pile axial stiffness effects while driving and assume the pile to be rigid (Hannigan et al. 1998).

2.4 Wave Equation Analysis

The wave equation is a dynamic predictive method that represents a better relationship between capacity and driving resistance. It relates pile penetration to stresses within the pile and soil that presents a more complete picture of the hammer-pile-soil system and prevents the pile from being loaded beyond the pile material capacity. The wave equation was first introduced by Pochhaammer in 1876 as the analysis of a stress wave propagating through an infinitely long

cylindrical bar with a circular cross-section (Valsamos et al. 2013). As originally proposed, it provides an equation of motion in an elastic medium and predicts no energy transfer (Kolsky 1963). After Pochhaammer, there were contributions made by Chree (1889) with an independent theory on wave equations, Lord Rayleigh (1894) discussed it in sound theory, and Field (1931) considered longitudinal waves (Kolsky 1963). In 1931 D.V. Isaacs had the idea of applying the wave equation to pile driving.

However, it was not until 1960 that E.A.L. Smith proposed an approach that utilized a numerical closed form solution to investigate the effects of the ram weight, ram velocity, cushion, pile properties, and the soil's dynamic behavior during driving. During Smith's investigation, the pile-soil model was fashioned into discretized lumped masses connected with springs as illustrated in Figure 2.1. The governing equation for one-dimensional wave propagation in a rod is a linear second order differential equation illustrated in Eqn. 2.16:

$$\sigma = \rho \frac{\partial^2 u}{\partial t^2} - E \frac{\partial^2 u}{\partial t^2} \qquad \text{Eqn. 2.16}$$

Where: σ is the stress in the pile, ρ is the mass density of the pile, u is the axial displacement of a point at location x on the pile at time t, $\partial^2 u/\partial t^2$ is acceleration of point x, and $\partial^2 u/\partial x^2$ is the strain gradient at x at time t. Performing a wave equation analysis allows for the establishment of a driving criterion and selection of the correct driving equipment for pile installation. The drivability analysis of the system is predicated on the predicted static pile capacity with depth.

The wave equation provides a relationship between two sets of variables. The first set of variables comprise: force, stress, and strain (Goble 2008). While the second set of variables encompasses: displacement, velocity, and acceleration (Goble 2008). These variables help to determine the stresses within the pile during driving. This method is semi-theoretical because it

depends on the accuracy of the soil, pile and hammer parameters entered into the equations. The results of the wave equation provide rational and reliable pile capacities when compared to values obtained from field tests (Reese et al. 2006). Wave equation analyses are performed on a number of assumed pile capacities to construct a bearing graph that relates ultimate capacity to driving resistance (Hannigan et al. 1998). The wave equation is used normally in conjunction with SLT and DLT on pile foundations and appears to be a reliable predictor of the friction and end bearing capacities of the pile.

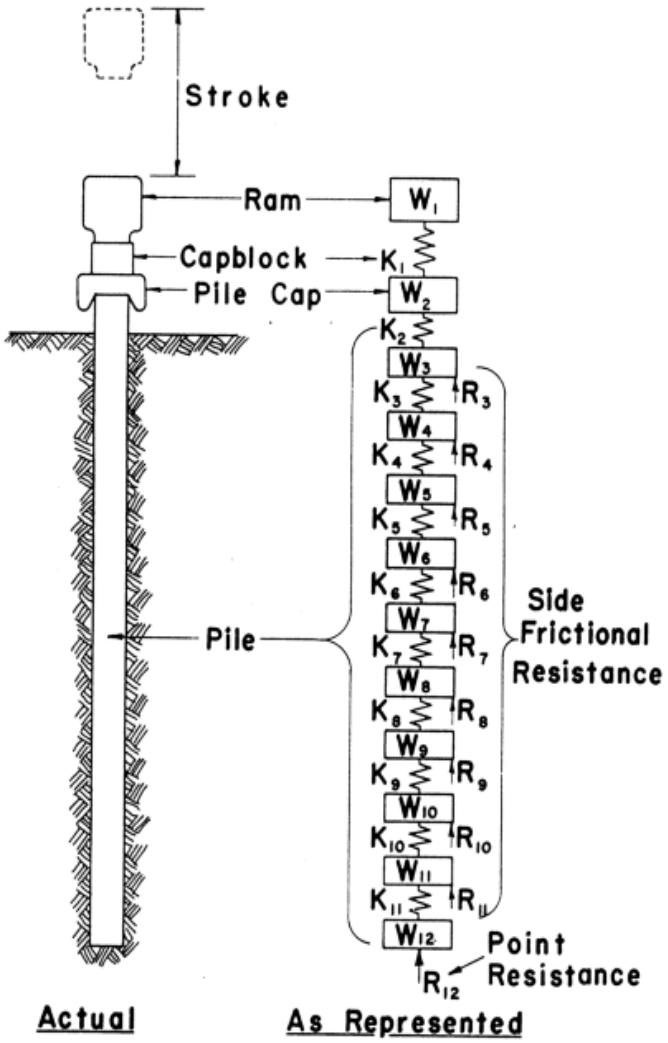

Figure 2.1. Pile-soil model for wave equation calculations (Smith 1962)

2.5 Static Load Testing

The Static Load Test (SLT) is considered the most reliable testing method in the verification of pile capacity in axial loading (Hannigan et al. 1997). Specifications for the standard test method are stated in ASTM D1143/D1143M, 'Standard Test Method for Piles Under Static Axial Compressive Load'. This test specification defines seven SLT test procedures, which are defined as follows: Quick Test (Procedure A), Maintained Load Test (Procedure B), Loading in Excess of Maintained Test (Procedure C), Constant Time Interval Test (Procedure D), Constant Rate of Penetration Test (Procedure E), Constant Movement Increment Test (Procedure F), and the Cyclic Loading Test (Procedure G).

In all of the listed procedures the pile is loaded axially to failure or to a specified safe structural capacity with the use of hydraulic jacks acting against the pile head and a reaction frame as illustrated in Figure 2.2. Displacement gages or transducers and load cells are used to acquire sufficient data to produce a load-settlement curve, which can be used to interpret ultimate pile capacity. During research efforts, instrumented test piles make use of gages and transducers attached to or embedded within the pile to record deformation measurements that can be used to interpret the magnitude and the distribution of the static soil resistance along the pile side and at the pile tip (Walton et al. 1998). Static load tests should be performed on driven piles that have had equilibrium reestablished to the surrounding soil. Normally, a rest period from 3 to 30 days between driving and testing is needed to allow for any setup or relaxation in the surrounding soil.

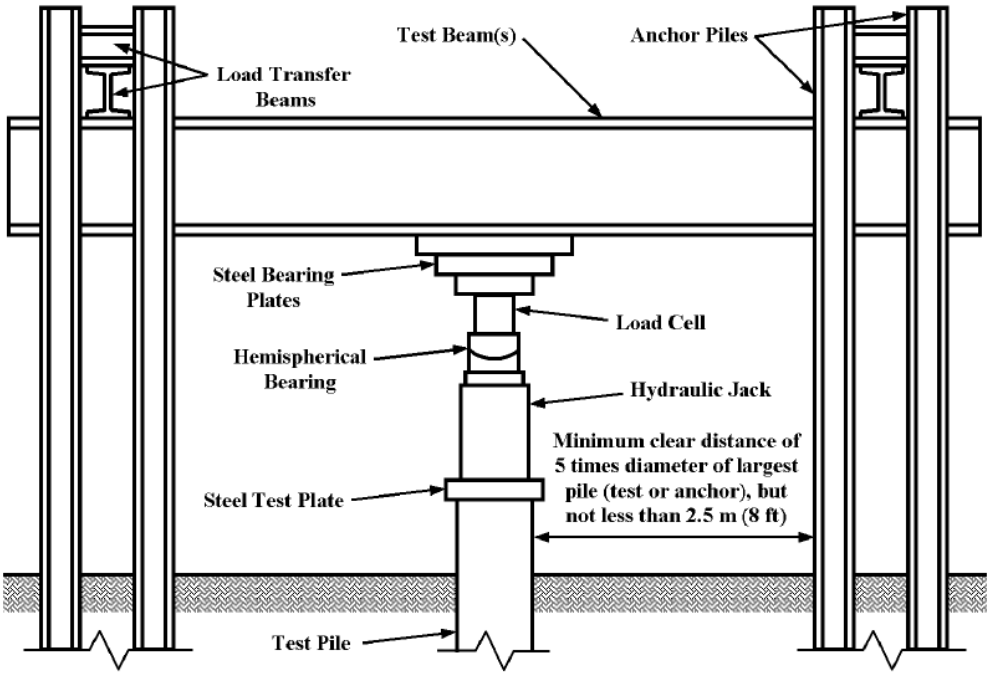

Figure 2.2. Schematic of static load testing (ASTM D1143/D1143M 2007)

Pile setup refers to the increase in effective stress with time as excess pore pressure, generated during pile driving, is dissipated, which leads to increased pile capacity. When a pile is driven into to clay, silt, or fine sand, excess positive pore pressure is developed as the water is not able to translocate freely, given the nature of cohesive type soils. The soil and water is displaced, causing the buildup of positive pore pressure, which results in lower effective stresses around the pile (Hannigan 2009). As time passes, excess pore pressure dissipates and the soil resistance around the pile increases, thereby increasing pile capacity. Relaxation on the other hand is the reduction in effective stress with time; which reduces pile capacity. Driving a pile into saturated dense silts or shales gives rise to negative pore pressures. As the soil and water are displaced by the pile, the dense material dilates. This expansion under undrained conditions

essentially creates a vacuum in the void spaces, causing negative pore pressure (Hannigan 2009). The phenomenon of set up and relaxation is summarized in Table 2.1.

Table 2.1. Effective stress and capacity development in driven piles (Long et al 1999)

Phenomena	**Effective Stress Equation**	**End of Driving (EOD)**	**After Pore Pressures Dissipate**
Setup	$\bar{\sigma} = \sigma - (+u) = \sigma - u$	Low Effective Stress, Low Capacity	Higher Effective Stress, Higher Capacity
Relaxation	$\bar{\sigma} = \sigma - (-u) = \sigma + u$	High Effective Stress, High Capacity	Lower Effective Stress, Lower Capacity

Note: $\bar{\sigma}$ is effective stress, σ is total stress, and u is pore water pressure.

The Quick Test (Procedure A), is the most common method utilized by transportation agencies due to its ease of use and satisfactory results (AASHTO 2010). The test pile is loaded in increments of five percent (5%) of the anticipated failure load capacity. The load is maintained for a fixed period of time that varies from four to fifteen (4-15) minutes. After achieving pile failure, load is removed in approximately ten (10) equal decrements, the duration of the unloading stages mirrors the duration for the loading stages (ASTM D1143/D1143M 2007). The report provided from this test is an interpreted load-settlement curve which is illustrated in Figure 2.3. Static load testing can range from $50,000 to $2 million depending on the reaction pile setup (PDI 2013). A pile testing project for Milwaukee Stadium documents that SLT cost $100,000 per test (PDI 2002).

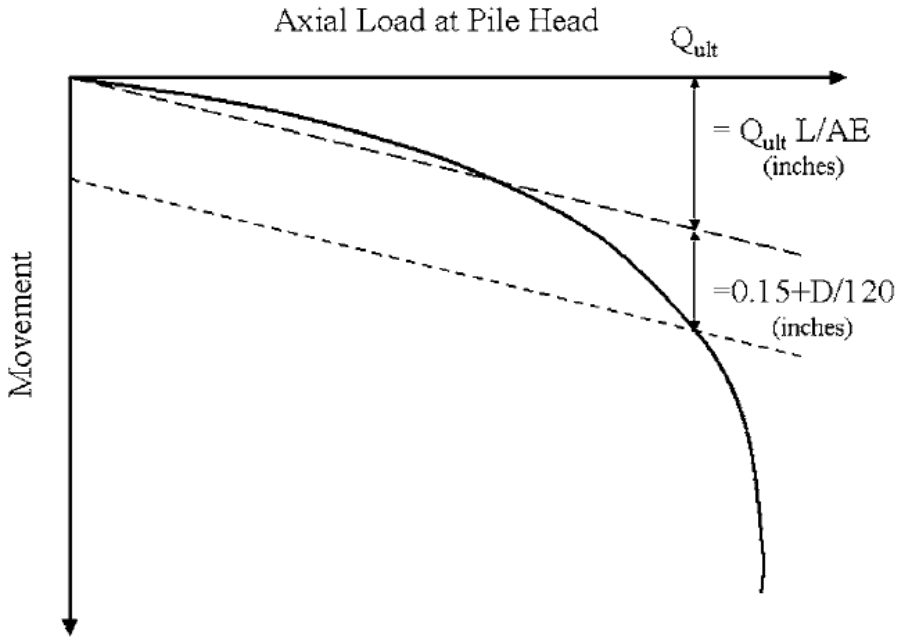

Figure 2.3. SLT load-settlement curve illustrating loading to plunging failure and illustrating the application of the Davisson-offset failure criterion (Reese et al. 2006)

2.5.1 Failure Criteria

The data generated from the static load test allows the ultimate capacity of a pile to be identified according to a predefined failure criterion. According to a Manual presented in 1940 titled 'Pile-Driving Formulas', failure was defined as "the load that produced an increase in pile movement disproportional to the increase in load" (Likins et al. 2012). In 1942 after review of the Manual Report B, and through ASCE Journal Discussions, Karl Terzaghi sought the need to add provisions to define the term "load at failure" (Terzaghi et al. 1942). Load at failure was then defined as the load required to have the pile head move at least 10% of the pile tip diameter. This standard was applicable to pile diameters of 12 inches, which was the typical pile diameter installed during the period.

Since 1942, several researchers have developed improved techniques for determining ultimate pile capacity through defining various failure criterion. It was necessary to develop these techniques due to some load-test curves not having a well-defined failure load, and some piles may never achieve ultimate capacity because of large toe capacities (Goble et al. 2000). Ultimate pile capacity has been defined by: the Davisson Offset Limit, the DeBeer Yield Limit, the Hansen 80% criterion, the Chin-Kondner Extrapolation, and the Decourt Extrapolation.

The most widely accepted method for defining ultimate pile capacity in North America is the Davisson Offset Limit method proposed in 1972 (Davisson 1972). This technique, presented in Eqn.2.17, produces a straight line parallel to and offset from a plot of the elastic compression of the pile under load. This parallel line is superimposed on the load settlement curve illustrated in Figure 2.3, at an offset of 0.15 inches plus the pile diameter (in inches) divided by 120. The ultimate pile capacity is defined as the intersection of the Davisson offset and the load-settlement curve, as illustrated in Figure 2.3. Pile head movement for piles with diameter less than 24 inches is determined from Eqn.2.17 and Eqn.2.18 for piles with diameter larger than 24 inches. The later equation, Eqn.2.18, is referred to as the modified Davisson Offset criterion recommended by Kyfor et al. (1992):

$$\delta_u = \frac{QL}{AE} + \frac{B}{120} + 0.15(in.) \qquad \text{Eqn.2.17}$$

$$\delta_u = \frac{QL}{AE} + \frac{B}{30} \qquad \text{Eqn.2.18}$$

Where: δ_u is pile head movement, Q is the applied load, L is the pile length, A is the pile cross-section area, E is the pile Modulus of Elasticity, and B is the pile diameter.

Another criterion used to identify the pile failure load is the DeBeer Yield Load, introduced in 1968 (DeBeer 1968). It is an extrapolation method that is used when the data from a load-settlement curve does not indicate a clear failure load. The load and settlement are plotted using logarithmic scales, illustrated in Figure 2.5. At the development of the ultimate load, the early linear portion of the load settlement curve begins to change slope, the point of the slope change is classified as the yield load.

Another available extrapolation method is the Hansen 80% criterion introduced in 1963 (Hansen 1963). It uses the load-settlement curve to identify the point at which the applied load produces four times the settlement that was observed for 80% of the same applied load. The settlement is plotted against the square root of settlement divided by the load, illustrated in Figure 2.6. The 80% criterion usually agrees with the plunging failure of the pile, and is usually identified visually or can be computed by Eqn.2.19:

$$Q_u = \frac{1}{2\sqrt{C_1 C_2}} \qquad \text{Eqn.2.19}$$

Where: Q_u is the capacity or ultimate load, C_1 is the slope of the straight line, and C_2 is the y-intercept of the straight line.

The Chin-Kondner Extrapolation (1970) method is similar to the Hansen method. The settlement is divided by its corresponding load then plotted against the settlement value as illustrated in Figure 2.7. The ultimate load as defined by the Chin-Kondner Extrapolation is the inverse of the slope of the line from the load-settlement curve given in Eqn.2.20. It is useful to use this method during load testing as a kink in the plotted line would suggest a weakness developing in the pile. The Chin-Kondner Extrapolation can be applied to both quick and slow loading cases, provided constant time increments are used.

$$Q_u = \frac{1}{C_1} \qquad \text{Eqn.2.20}$$

Where: Q_u is the capacity or ultimate load and C_1 is the slope of the straight line.

The Decourt Extrapolation (1999) is constructed similar to the Chin-Kondner Extrapolation and Hansen methods; each load is divided by its corresponding settlement and plotted against the applied load presented in Eqn.2.21 and illustrated in Figure 2.8. The results of the Decourt Extrapolation are similar to the Chin-Kondner Extrapolation and allow projected capacity to be determined as the SLT is in progress. The Hanson 80% Criterion, Chin-Kondner Extrapolation, and the Decourt Extrapolation all have an equation that represents an ideal load curve (Q) that compares with the ultimate load curves.

$$Q_u = \frac{C_2}{C_1} \qquad \text{Eqn.2.21}$$

Where: Q_u is the capacity or ultimate load, C_1 is the slope of the straight line, and C_2 is the y-intercept of the straight line.

To illustrate the differences among the aforementioned methodologies, Bengt H. Fellenius presented the graphs in Figures 2.4 through 2.8 in his presentation to the Deep Foundation Institute in 2001. A SLT was performed on a 12 inch precast concrete pile and various failure criteria were used to evaluate ultimate capacity.

Figure 2.4 which indicates an ultimate capacity of 375 kips. The DeBeer Yield Limit produced an ultimate capacity of 360 kips in Figure 2.5. The Hansen 80% criterion produced an ultimate capacity of 418 kips in Figure 2.6. Whereas the Chin-Kondner Extrapolation in Figure 2.7 gave an ultimate capacity of 475 kips and the Decourt Extrapolation in Figure 2.8 produced an ultimate capacity of 474 kips. The example presented gave capacities which varied by 114

kips and serves to illustrate the uncertainty associated with reporting ultimate pile capacity if the pile cannot be loaded to plunging failure. The Davisson Offset Limit criterion is one of the more conservative methods to determine ultimate capacity and its ease of use through analysis has increased its popularity among professionals.

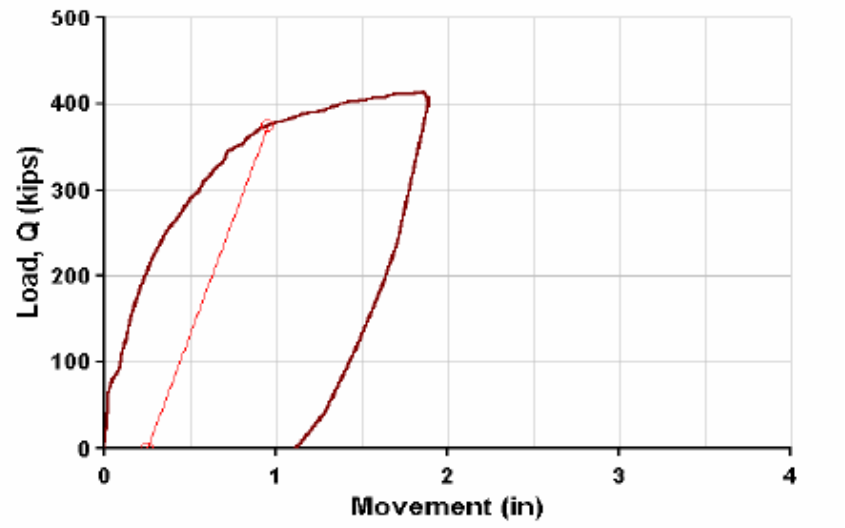

Figure 2.4. Davisson Offset Limit example (Fellenius 2001)

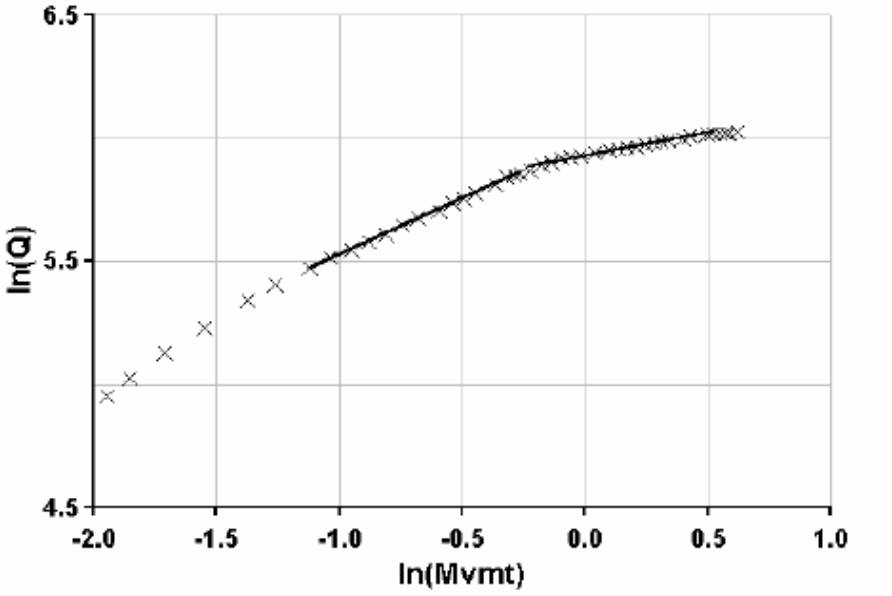

Figure 2.5. DeBeer Yield Limit example (Fellenius 2001)

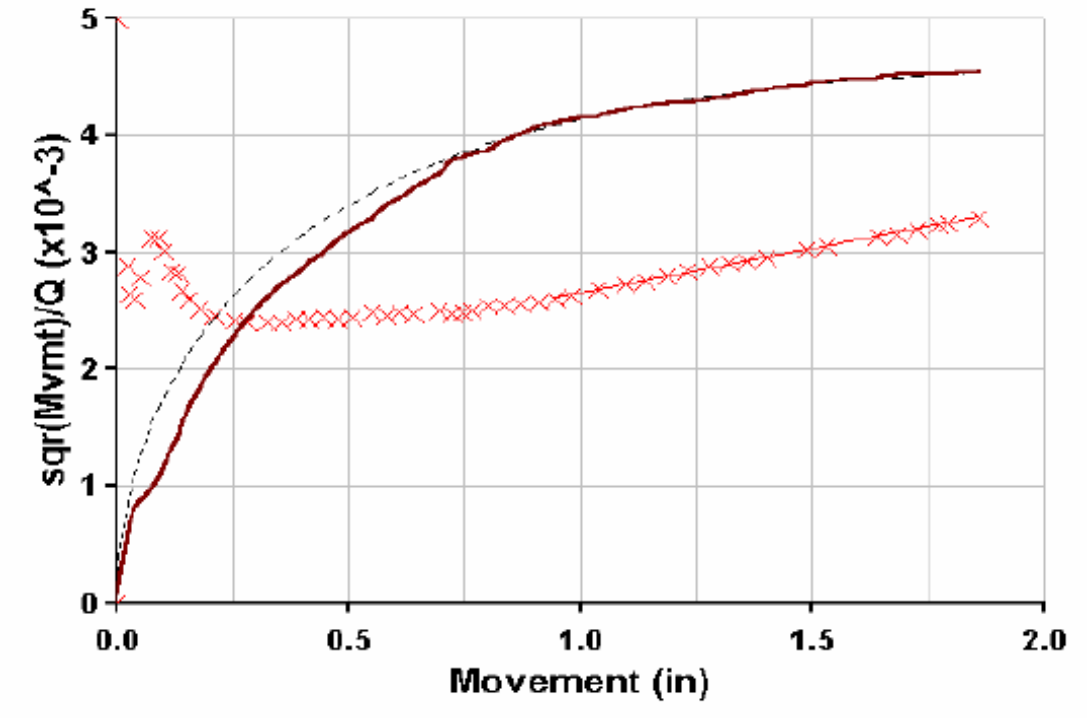

Figure 2.6. Hansen 80% criterion example (Fellenius 2001)

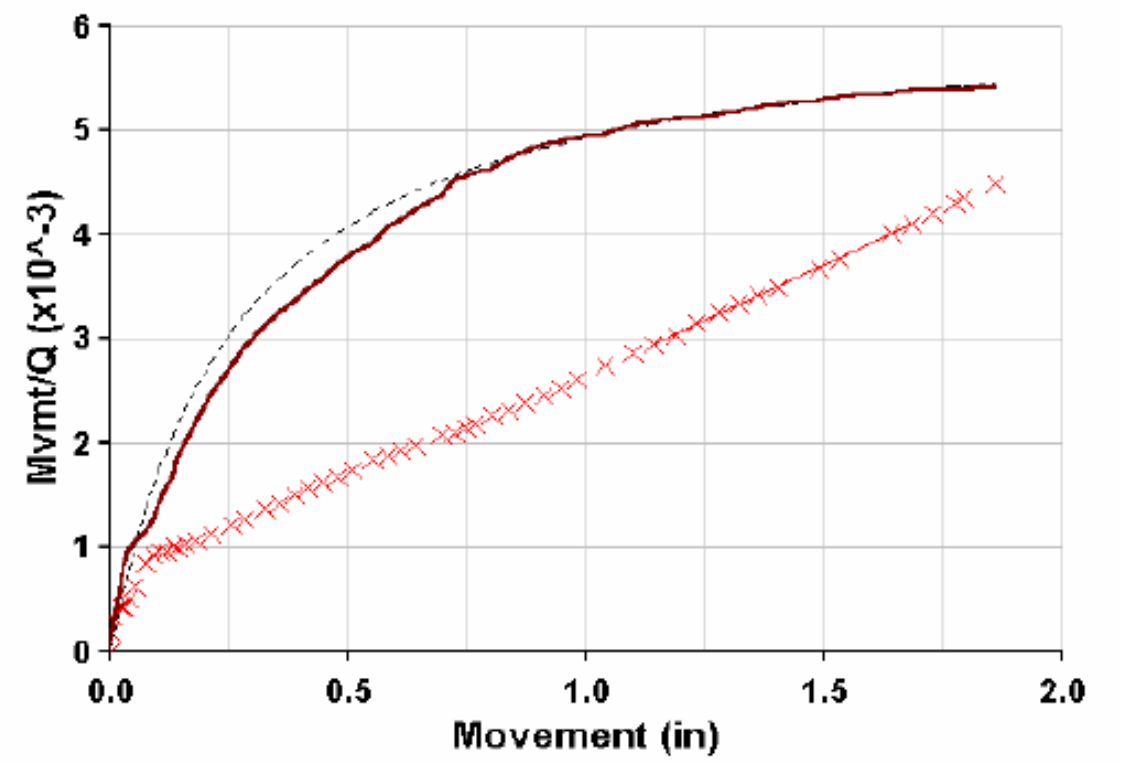

Figure 2.7. Chin-Kondner Extrapolation example (Fellenius 2001)

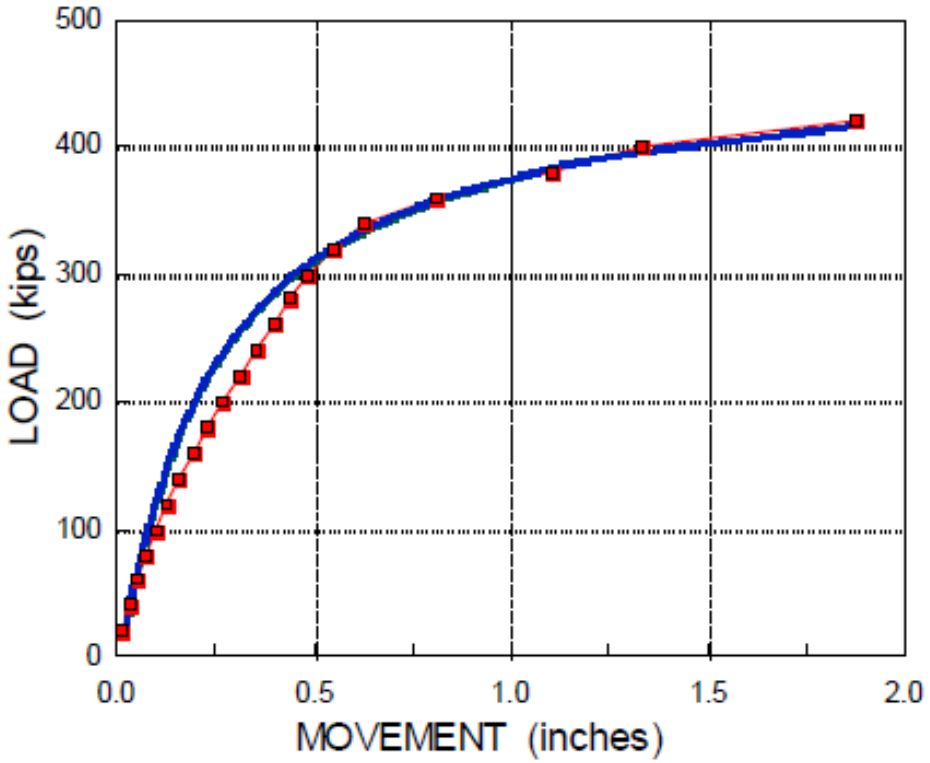

Figure 2.8. Decourt Extrapolation example (Fellenius 2001)

2.6 Dynamic Load Tests

The dynamic load test (DLT) is a testing method that measures strain and acceleration near the pile top as it is driven with an axial compressive force. The force exerted is often from a pile driving hammer, but can take the form of a Newton's APPLE (Section 2.7) or impulse load (Section 2.8). The use of a pile driving hammer is more common and the hammer can be powered via diesel, air or hydraulic power. Strain and acceleration measurements are evaluated to verify the capacity of the pile and to detect pile damage, and monitor hammer performance. The procedures for dynamic load testing are prescribed in ASTM D4945, 'Standard Test Method of High-Strain Dynamic Testing of Deep Foundations'. Dynamic load testing utilizes one dimensional wave mechanics; it measures strain and acceleration at the pile top via stress waves conveyed along the pile, to determine the response of the soil to the induced stress waves.

Dynamic load testing can provide real time results, and is relatively inexpensive (Steele et al. 1990). Instrumentation for DLT requires accelerometers and strain gauges that are bolted, welded, or glued onto the side of the pile near its top illustrated in Figure 2.9. The signals from these transducers produce time traces of force and velocity for every hammer blow. A software program is used to manipulate soil resistance and dynamic damping and quake values to produce a calculated force curve that matches the measured force curve. This process is called signal matching. Dynamic load testing is less reliable than static load testing due to the analysis not providing a unique solution and the dependence on the user's ability to model the system accurately.

Figure 2.9. Strain gauge and accelerometer attached to a pile for dynamic testing (GRL Engineers, Inc. 2014)

2.6.1 Dynamic Load Testing with Signal Matching

In 1964, the Ohio Department of Transportation initiated a research project at Case Institute of Technology that explored the idea of using a dynamic approach to determine pile capacity (Goble et al. 1975). The research effort used strain gages and recorded the data on high

speed oscillographs. This method was slow, recording only a few blows per pile, and was prone to errors while converting analog signals to digital data during calibrations. In 1970 the portable tape recorder replaced the oscillograph and eliminated the need for digital conversions. This allowed for faster data collection, recording results for every blow of the hammer with more accuracy.

Today, most dynamic testing is conducted with the use of the signal matching. Signal matching is a type of high strain dynamic testing that measures strain and acceleration at the pile top through strain gages and accelerometers attached to the pile. Electrical signals are transmitted with wires or through wireless radios to a device which conditions the signals and performs the signal matching analysis. Strain transducers measure the force while the accelerometers measure the motion of the pile. The pile-soil system is modeled using the CAse Pile Wave Analyses Program (CAPWAP) which attempts to find a tip and side resistance that produces a force versus time signal which matches the measured data. Signal matching is useful in measuring the activated soil resistance and distribution, along with the maximum compressive and tensile stresses within the pile shaft, pile integrity, and hammer performance (Likins 1998).

CAPWAP is a signal matching software program offered by Pile Dynamics, Inc. CAPWAP is based on the wave equation model which analyses the hammer-pile-soil system as a series of elasto-plastic elements with damping characteristics (Alvarez et al. 2006). CAPWAP predicts the side and toe resistance, as well as the total capacity of the pile (Pile Dynamics 2012). The program uses the measured force based on the strain data collected and Hooke's Law, to give an expression of force (F) to be the product of strain (ε), the modulus of elasticity (E) of the material, and the cross-sectional area (A) of the pile ($F = \varepsilon EA$). The velocity is determined by integrating the measured acceleration over time. CAPWAP performs an iterative process that

maintains dynamic equilibrium of the system with a calculated resistive force that is generated by varying tip and side resistance and by manipulating the damping factors for the soil and pile. An illustration of the force-time graph is presented in Figure 2.10 where the measured force in the pile is compared to the calculated force as a function of time. This graph shows a good signal match up to 40 ms, but would require more iterations to create a better fit the remainder of the curve.

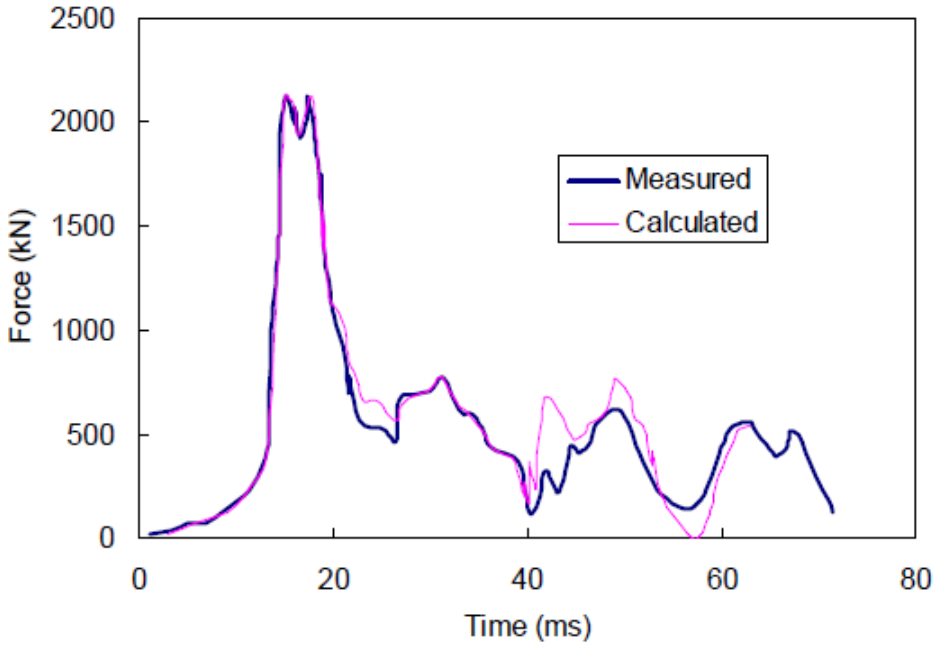

Figure 2.10. Example of CAPWAP signal matching (Bradshaw et al. 2006)

Dynamic load testing using signal matching can cost up to $25,000 to $45,000 per test site with mobilization costs included (PDI 2013). A pile testing project for Milwaukee Stadium documents the cost of signal matching at $3,000 per test (PDI 2002).

2.7 A Preferred Pile Load Evaluator (Newton's APPLE)

The Newton's APPLE loading system, illustrated in Figure 2.11, is large strain dynamic testing system, named after Sir Isaac Newton's second law of motion (Force = Mass x Acceleration). The loading system is a rigid frame that allows a ram to freely drop from various heights and has the ability to generate proof loads up to 400 tons (4000 kN) (GRL-PDI 2000). This method measures force at the pile top and provides more accurate force values than from strain transducers attached to concrete piles with questionable values for modulus of elasticity.

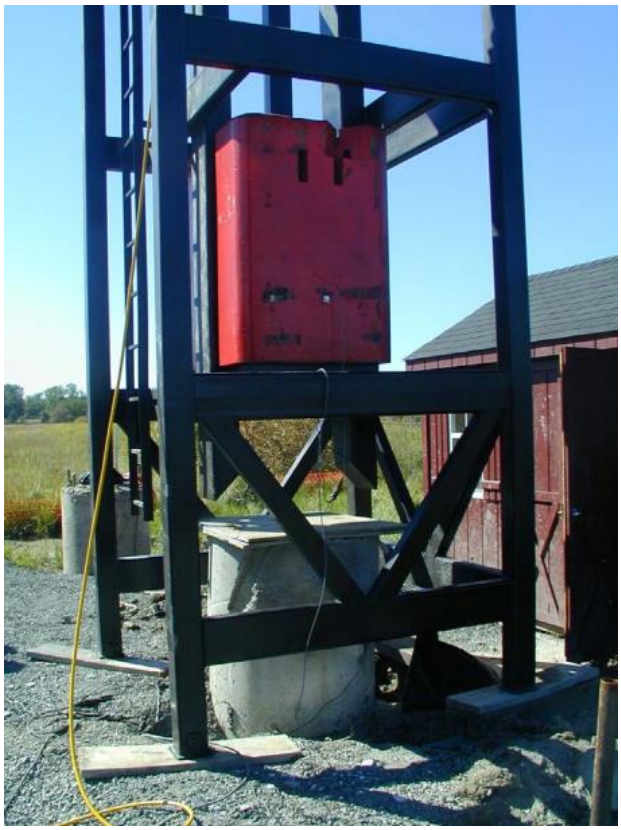

Figure 2.11. Newton's APPLE loading system (PDI 2002)

2.8 Statnamic Load Testing

The statnamic load test was developed by Patrick Birmingham in 1989. It is based on Newton's second and third law of motion which state that force (F) is equal to mass (M) times acceleration (A) (Force = MA) and that for every action there is an equal and opposite reaction. Statnamic load testing is standardized by ASTM D7383, Standard Test Methods for Axial Compressive Force Pulse (Rapid) Testing of Deep Foundations. It can be used as an alternative to ASTM D1143 (static load testing in compression) or as a higher quality alternative to ASTM D4945 (high strain dynamic testing). Statnamic load testing is a rapid load test which combines the simple analysis of static testing with the efficiency and cost effectiveness of dynamic testing (Hannigan et al. 2006). The impulse load is provided through the buildup of pressure in a heavy cylindrical vessel which acts as a reaction mass that rests on top of the pile. A nitrocellulose based explosive material used in shotgun shells is burned inside the cylinder at a rapid rate to generate gas pressure (an explosion), as the pressure builds, it propels the reaction mass upward, initiating a downward force applied to the pile top. The load generated can range from 10 kips (44.5 kN) to 10,000 kips (44,482 kN). The set up time is a fraction of the cost and time of static tests; the exception in this case is that reaction piles, reaction beam, and the hydraulic jack are not required (Statnamic Load Testing 2012).

2.9 Case Study - A Comparison of SLT to DLT Capacity Values

The Caminada Bay Bridge project in Louisiana compares SLT and DLT performed on production piles (Yoon et al. 2011). Static analyses were performed with the Tomlinson α-Method for cohesive soils and the Norlund β-Method for cohesionless soils and resulted in a target capacity of 1,129 kips, comparatively drawing on experience, it was projected that a capacity of 1,219 kips was achievable. Wave equation analysis confirmed that the selected pile

with the chosen pile hammer could achieve pile resistance between 190 kips to 2,000 kips. Static load testing (quick loading method) was conducted 27-days after the initial pile driving. Dynamic load testing was conducted with signal matching at a 7-day restrike after the static load test. Signal matching was performed at the end of drive (EOD), and at two beginning-of-restrike (BOR) conditions. The result of the SLT, which was combined with internal strain gauge monitoring indicated a plunging load of 558 kips. Using the load-settlement curve provided from the SLT and the Davisson Offset Limit criteria, the ultimate capacity was determined to be 540 kips. The DLT (after static load test restrike) capacity using signal matching was 600 kips. All load test data are summarized in Table 2.2. While the dynamic analysis over predicted the pile capacity, the measured SLT and DLT results were within an acceptable range of ten percent (10%). This evidence confirms SLT and DLT are comparable, and promotes the idea that performing DLT on all installed piles can quantify the capacity and quality of the piles used in foundation design.

Table 2.2 Pile capacity with time for static analysis, SLT, and DLT performed on the Caminada Bay Bridge Project.

Pile Testing	**Capacity (kips)**
Static Analysis (Tomlinson and Norlund)	1,219
DLT - End of initial drive (EOD)	450
DLT - 7-day restrike	570
SLT - 27-days after initial pile driving (Plunging)	558
SLT - 27-days after initial pile driving (Davisson)	540
DLT - Restrike after static load test	600

2.10 Geotechnical Design Process and Reliability

Geotechnical engineering is a field where great uncertainty exists. These uncertainties are prevalent in various empirical design methodologies, site characterization, soil behavior, and

construction quality (Paikowsky et al. 2004). Since the early 1800s, the Allowable Stress Design (ASD), also known as working stress design, method was used to design foundations. In ASD, the design load is compared to the nominal resistance with a factor of safety applied to the resistance using Eqn. 2.22. An appropriate factor of safety was determined through engineering experience to account for the uncertainties listed above, this apparent trial and error approach lacked suitable support to quantify the reliability and performance of the resulting designs. Due to the lack of a rational approach to assign factors of safety, this method often produces conservative results that reflect highly over-designed and expensive foundations.

$$Q \leq Q_{all} = \frac{R_n}{FS} = \frac{Q_{ult}}{FS} \qquad \text{Eqn. 2.22}$$

Where: Q is the design load, Q_{all} is the allowable design load, R_n is the nominal resistance of the element or the structure, FS is the factor of safety, and Q_{ult} is the ultimate geotechnical foundation resistance.

Due to the desire for a more economical approach to design, Limit State Design (LSD) was employed to address safety factor concerns, serviceability, and economic requirements (Paikowsky et al. 2010, NCHRP 651). Additionally, LSD identifies the limit where the structure fails to fulfill the purpose for which it was designed. There are two types of limit states when referring to LSD, the ultimate limit state (ULS) considers the strength of the structure, and the serviceability limit state (SLS) which considers the functionality and service requirements of a structure for adequate performance under expected loading conditions (Paikowsky et al. 2010). The ULS approach depends on the predicted loads and the ability of the structure to resist such loads. The uncertainties that arise in design are quantified through probability based methods and use a format called load and resistance factor design (LRFD). This method separates the

uncertainties due to load and the uncertainties due to resistance and ensures an acceptable margin of safety through the application of probability theory. In the LRFD method, load factors (γ) are applied to nominal loads to obtain a factored load. Likewise, resistance factors (ϕ), known as strength reduction factors, are applied to the ultimate capacity (Coduto 2001).

The American Association of State and Highway and Transportation Officials (AASHTO) LRFD Bridge Design Specifications recommends Eqn. 2.23 for strength limit state in foundation design as:

$$R_r = \phi R_n \geq \sum \eta_i \gamma_i Q_i \qquad \text{Eqn. 2.23}$$

Where: the factored resistance (R_r),the product of the nominal (ultimate) resistance (R_n) and its resistance factor (ϕ) must be greater than or equal to the summation of loads (Q_i) multiplied by their corresponding load factors (γ_i) and a modifier (η_i) (AASHTO 2010). The modifier (η_i) is taken as:

$$\eta_i = \eta_D \eta_R \eta_I > 0.95 \qquad \text{Eqn. 2.24}$$

Where: η_D accounts for the ductility of the structure, η_R accounts for the redundancy in the structure, and η_I is operational importance of the structure (AASHTO 2010).

The theory of LRFD can be illustrated through the use of probability density functions (PDF) representing load (Q) and resistance (R) and their relation to the limit state function (g). The limit state function (g) is defined by Eqn. 2.25 for a normal distribution of data and Eqn. 2.26 for a lognormal distribution of data. The probability of failure (P_f) is defined by Eqn. 2.27:

$$\bar{g} = R - Q \qquad \text{Eqn. 2.25}$$

$$\bar{g} = \ln(R) - \ln(Q) = \ln(R/Q) \quad \text{Eqn. 2.26}$$

$$P_f = P(R < \bar{Q}) \quad \text{Eqn. 2.27}$$

The limit state function is related to the margin of safety by the difference in value of the resistance and the load effect. When looking at Figure 2.12, one can see that the PDF curve for the load effect, which is the nominal load acting on a structure, is much narrow than the PDF for nominal resistance., This is due to smaller variations in the factors affecting load than the uncertainty affecting resistance (Paikowsky et al. 2010). A probability of failure occurs when the two PDFs overlap (shaded region), indicating the load exceeds the resistance illustrated in Figure 2.12.

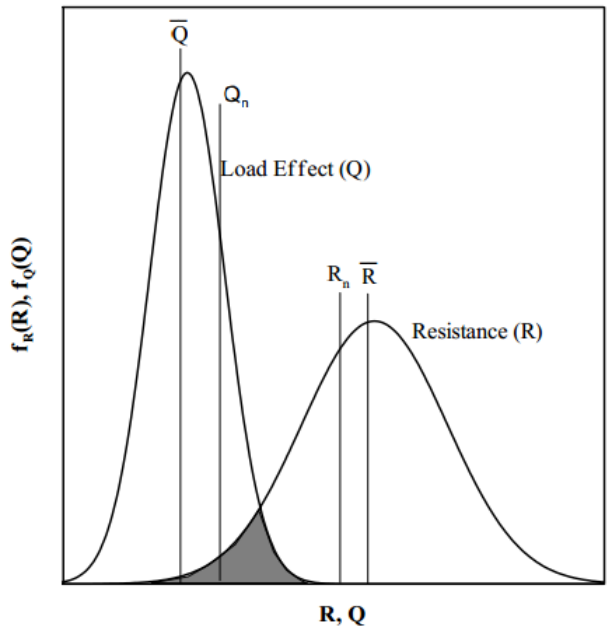

Figure 2.12 An illustration of the probability density function for load factor and resistance factors (Paikowsky 2002)

In the AASHTO Specification, suggested resistance factors for Eqn. 2.23 are presented and are based on the specific design and acceptance methods utilized. An excerpt of the

Specification Table 10.5.5.2.3-1 (AASHTO 2010) is presented in Table 2.3 which gives resistance factors ranging from 0.65 to 0.8 depending on the use of either SLTs or DLTs and the number of load tests that are performed. Statistical analysis tools available range from the simple averaging of values to more elaborate methods such as First Order Second Moment (FOSM), First Order Reliability Methods (FORM), and the Monte Carlo Simulation (MCS).

Table 2.3 Excerpt for resistance factors for driven piles (AASHTO 2010)

Condition/Resistance Determination Method		Resistance Factor
Nominal Bearing Resistance of Single Pile—Dynamic Analysis and Static Load Test Methods, φ_{dyn}	Driving criteria established by successful static load test of at least one pile per site condition and dynamic testing* of at least two piles per site condition, but no less than 2% of the production piles	0.80
	Driving criteria established by successful static load test of at least one pile per site condition without dynamic testing	0.75
	Driving criteria established by dynamic testing* conducted on 100% of production piles	0.75
	Driving criteria established by dynamic test with signal matching at beginning of redrive (BOR) conditions only of at least one production pile per pier, but no less than the number of tests per site provided in Table 10.5.5.2.3-3.	0.65
	Wave equation analysis, without pile dynamic measurements or load test, at end of drive conditions only	0.40
	FHWA-modified Gates dynamic pile formula (End of Drive condition only)	0.40
	Engineering News Record (as defined in Article 10.7.3.8.5) dynamic pile formula (End of Drive condition only)	0.10

2.11 Reliability and LRFD Design

In geotechnical engineering design, the probability that a structure will not fail can be defined as the probability of failure (p_f) or the level of reliability ($1-p_f$) ,and is usually 99% or higher. The reliability level in LRFD is often represented by the reliability index (β) presented in Eqn. 2.28, which is the number of standard deviations (σ) separating the mean value ($\bar{g}$) load from the origin on the PDF in Figure 2.13. Load and resistance factors are calculated and adjusted to meet a target reliability index (β_T) (Paikowsky et al. 2010).

$$\beta = \frac{m_g}{\sigma_g} = \frac{(m_{RN} - m_{QN})}{\sqrt{\sigma_{QN}^2 + \sigma_{RN}^2}} = \frac{\ln\left[\left(\bar{R}/\bar{Q}\right)\sqrt{(1 + COV_Q^2)/(1 + COV_R^2)}\right]}{\sqrt{\ln(1 + COV_R^2)(1 + COV_Q^2)}} \quad \text{Eqn. 2.28}$$

Where: m_g is the mean of the nominal safety margin, σ_g is the standard deviation of the safety margin defined by the limit state function g, m_{RN} and m_{QN} are mean of the natural logarithm of the load and the resistance, σ_{QN}^2 and σ_{QN}^2 are standard deviations of the natural logarithm of the load and the resistance, $\bar{R}$ and $\bar{Q}$ are the mean of the load and the resistance, and COV_Q and COV_R are the coefficient of variation of the load and resistance assuming a normal distribution (Paikowsky et al. 2010).

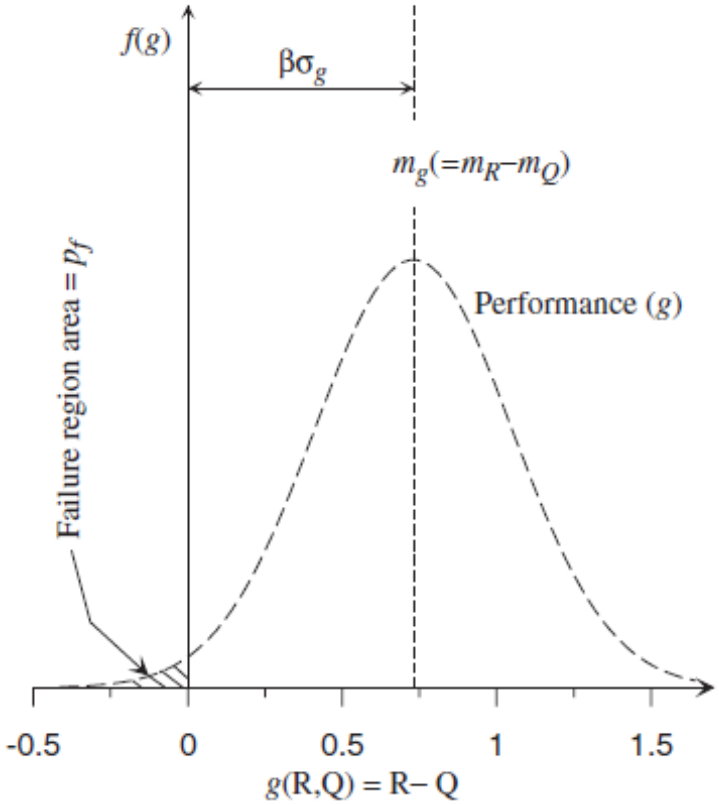

Figure 2.13 The performance function for a normal distribution (g(R,Q)) demonstrating the margin of safety (p_f) and its relation to the reliability index, β (σ_g = standard deviation of g) (Paikowsky et al. 2010)

2.11.1 Statistical Terms

The methods used to quantify the state function include: First Order Second Moment, First Order Reliability Method, and the Monte Carlo Simulation. These methods are an integral part of determining the resistance factor. However, prior to explaining these methods, it is essential to define the common statistical parameters used in each method. The common parameters are mean, standard deviation, sample variance, and coefficient of variation. The mean (μ) is the average value of the sample and calculated with Eqn. 2.29:

$$\mu = \frac{1}{n}\sum_{i} x_i \qquad \text{Eqn. 2.29}$$

The standard deviation (σ) indicates how much variation there is from the mean and calculated with Eqn. 2.30:

$$\sigma = \sqrt{\frac{1}{N-1}\sum_{i}(x_i - \bar{x})^2} \qquad \text{Eqn. 2.30}$$

The sample variance (σ^2) is a measure of how spread out the values are and calculated using Eqn. 2.31:

$$\sigma^2 = \frac{1}{N-1}\sum_{i}(x_i - \bar{x})^2 \qquad \text{Eqn. 2.31}$$

The coefficient of variation (COV) measures the normalized dispersion of a sample population and is determined using Eqn. 2.32, which enables a comparison of several data sets (Miller et al. 1985):

$$COV = \frac{\sigma}{\mu} \qquad \text{Eqn. 2.32}$$

2.11.2 First Order Second Moment (FOSM)

First Order Second Moment (FOSM) is a closed form solution and a probabilistic reliability method that produces a resistance (ϕ) factor for a given reliability index (β). It is based on the lower order terms from a Taylor series expansion of the performance function to approximate the variance of the performance function (Baecher et al. 2003). The FOSM is a first-order expansion about the mean value and a linear approximation of the second moment (the variance) (Patev 2010). First Order Second Moment requires the limiting state function, the mean, and standard deviations of the design parameters. FOSM has had a presence in geotechnical engineering since 1969 when it was originally proposed by C. A. Cornell. It was subsequently used by Barker et al. (1991) for NCHRP Report 343 titled "The calibration of geotechnical resistance factors using closed form solutions".

The limit state occurs when the state equation equals zero, $g(x) = 0$, a value greater than zero is considered a safe state, $g(x) > 0$, and a value less than zero is at considered a failure state, $g(x) < 0$. The geotechnical resistance (ϕ) factors can be derived from Eqn. 2.23 by setting η to one and following the procedure described in Becker et al. (1991) and FHWA (2001):

$$\phi R_n \geq \sum \gamma_i Q_i \qquad \text{Eqn. 2.33}$$

From which:

$$\phi \geq \sum \gamma_i \frac{Q_i}{R_n} \qquad \text{Eqn. 2.34}$$

The nominal resistance (R_n) is replaced by the mean value divided by the bias factor, $\bar{R}/\lambda_R$, which gives:

$$\phi \geq \lambda_R \sum \gamma_i \frac{Q_i}{\bar{R}} \qquad \text{Eqn. 2.35}$$

Using the lognormal form of Eqn. 2.28, the mean value of the resistance ($\bar{R}$):

$$\bar{R} = \frac{\bar{Q} exp\left\{\beta\sqrt{\ln(1+COV_R^2)(1+COV_Q^2)}\right\}}{\sqrt{(1+COV_Q^2)/(1+COV_R^2)}} \qquad \text{Eqn. 2.36}$$

Then substituting $\bar{R}$ into Eqn. 2.35 and replacing β with the target reliability (β_T) the expression for ϕ becomes:

$$\phi = \frac{\lambda_R(\sum \gamma_i Q_i)\sqrt{\frac{1+COV_Q^2}{1+COV_R^2}}}{\bar{Q}exp\left\{\beta_T\sqrt{\ln\left[(1+COV_R^2)(1+COV_Q^2)\right]}\right\}} \qquad \text{Eqn. 2.37}$$

Where: λ_R is the resistance bias factor which in the context of pile capacity is the mean of the ratio of measured pile capacity over predicted pile capacity, γ_i is the load factor for the specific type of load, Q_i is the specific type of load applied (dead load, live load, environmental load, etc.), $\bar{Q}$ is the mean of the load and subsequently referred to as λ_Q, COV_Q is the coefficient of variation of the load, COV_R is the coefficient of variation of the resistance, and β_T is the target reliability index (Paikowsky 2004). Eqn. 2.37 can be restated in a simpler form when only the dead and live loads are considered as was presented in the NCHRP Report 507 and illustrated in Eqn. 2.38 (Paikowsky 2004):

$$\phi = \frac{\lambda_R\left(\frac{\gamma_D Q_D}{Q_L}+\gamma_L\right)\sqrt{\frac{\left(1+COV_{Q_D}^2+COV_{Q_L}^2\right)}{1+COV_R^2}}}{\left(\frac{\lambda_{Q_D}Q_D}{Q_L}+\lambda_{Q_L}\right)exp\left\{\beta_T\sqrt{\ln\left[(1+COV_R^2)\left(1+COV_{Q_D}^2+COV_{Q_L}^2\right)\right]}\right\}} \qquad \text{Eqn. 2.38}$$

Where: γ_D, γ_L are the dead and live load factors respectively, Q_D/Q_L is the dead to live load ratio, and λ_{QD}, λ_{QL} are the dead and live load bias factors respectively. Eqn. 2.38 presents an oversimplified version of the FOSM equation when it considers the COV_Q from Eqn. 2.37 as simply the sum of coefficient of variation of the dead load (COV_{QD}) and coefficient of variation of the live load (COV_{QL}). The proper way to account for the variation in loads is illustrated in Eqn. 2.39. An improvement to the FOSM equation is achieved by considering the expansion of COV_Q and is illustrated in Eqn. 2.39:

$$COV_Q^2 = \frac{\sigma_Q}{\mu_Q} = \frac{\sqrt{\sigma_D^2 + \sigma_L^2}}{\mu_D + \mu_L} \qquad \text{Eqn. 2.39}$$

Where: σ_Q, σ_D, and σ_L are the standard deviations of the load, dead load, and live load respectively, and, μ_Q, μ_D, and μ_L are the mean values of the load, dead load, and live load respectively. The corrected expression for the ϕ factor becomes Eqn. 2.40:

$$\phi = \frac{\lambda_R \left(\frac{\gamma_D Q_D}{Q_L} + \gamma_L\right) \sqrt{\frac{\left(1 + \frac{\sqrt{\sigma_D^2 + \sigma_L^2}}{\mu_D + \mu_L}\right)}{1 + COV_R^2}}}{\left(\frac{\lambda_{Q_D} Q_D}{Q_L} + \lambda_{Q_L}\right) \exp\left\{\beta_T \sqrt{\ln\left[(1 + COV_R^2)\left(1 + \frac{\sqrt{\sigma_D^2 + \sigma_L^2}}{\mu_D + \mu_L}\right)\right]}\right\}} \qquad \text{Eqn. 2.40}$$

The FOSM method has made two assumptions to derive a closed form solution. The first assumption is that the moments of failure can be estimated when the mean values of the variables are known (Baecher et al. 2003). The second is an assumption about the type of probability distribution which describes the data. When this distribution is known, the probability of failure

and the reliability index can be computed (Baecher et al. 2003). While closed form solutions are easy to apply, they can be too simplistic for foundation design (Phoon et al. 2003).

2.11.3 First Order Reliability Method (FORM)

The First Order Reliability Method (FORM) was first proposed for use in 1974 by Hasofer and Lind (Baecher et al. 2003) to address the limitations of the FOSM by identifying a geometric interpretation of the reliability index (β) and not relying on assumptions or extrapolations. The reliability index (β) is the measured distance in dimensionless space between the mean of the limit state function or performance function as $\bar{g}$ = R-Q and the failure function (g = 0) (Baecher et al. 2003). The First Order Reliability Method is the preferred method to calibrate resistance factors (Baecher et al. 2003) and has been used in structural design for years. It provides an estimate of the probability of failure (p_f) as expressed in Eqn. 2.41:

$$p_f = \Phi(-\beta) \qquad \text{Eqn. 2.41}$$

Where: Φ( ) is the cumulative distribution function of the standard normal distribution (Paikowsky 2004). The First Order Reliability Method is an iterative process that allows for the calculation of partial safety factors for load and resistance factors with respect to a target level of reliability (β_T). It requires the first and second moment (mean and variance) information for the load and resistance factors and an assumed shape for the distribution (Paikowsky et al. 2010).

The FORM assumes an initial design point (x_i^*) on the failure surface. The design point is usually the point on the failure surface closest to the mean point, the highest point on the probability density curve (Phoon et al. 2003). This assumption creates a situation that is constrained, nonlinear, and requires minimization (Maier 2001). The design point is transformed

into standard normal variable (x'^{*}_i) which is dimensionless with zero mean and a standard deviation of one using Eqn. 2.42:

$$x'^{*}_i = \frac{x^{*}_i - \mu_{X_i}}{\sigma_{X_i}} \qquad \text{Eqn. 2.42}$$

Where: $\mu_{X_i}$is the mean value of the random variable X and $\sigma_{X_i}$is the standard deviation of the random variable for the distribution (Paikowsky et al. 2004). The random variable (X) is the vector of the difference between the strength and load variables. An equivalent normal distribution at the design point may be necessary for non-normal distributions, such as lognormal distributions. The equations needed to convert a non-normal mean and standard deviation to an equivalent mean and equivalent standard deviation are illustrated in Eqn. 2.43 and Eqn. 2.44 (Phoon et al. 2003):

$$\mu_X^N = x^* - \Phi^{-1}\left(F_x(x^*)\sigma_X^N\right) \qquad \text{Eqn. 2.43}$$

$$\sigma_X^N = \frac{\phi\left(\Phi^{-1}\left(F_X(x^*)\right)\right)}{f_X(x^*)} \qquad \text{Eqn. 2.44}$$

Where: μ_X^N is the mean of the equivalent normal distribution, σ_X^N is the standard deviation of the equivalent normal distribution, $F_X(x^*)$ is the original cumulative distribution function (CDF) of X_i evaluated at the design point, $f_X(x^*)$ is the original PDF of X_i evaluated at the design point, and $\phi(\ )$ is the PDF of the standard normal distribution (Paikowsky 2004). Once the necessary equivalent moments are established the random variable can be used to minimize the function:

$$x'^{*}_i = \alpha^{*}_i \beta \qquad \text{Eqn. 2.45}$$

Where: α^{*}_i is the directional cosine expressed in Eqn. 2.46 and normalize to a unit vector:

$$\alpha_i^* = \frac{\left(\frac{\partial g}{\partial x_i'}\right)_*}{\sqrt{\sum_{i=1}^{n}\left(\frac{\partial g}{\partial x_i'}\right)_*^2}} \qquad for\ i = 1, 2, \ldots n \qquad \text{Eqn. 2.46}$$

Where:

$$\left(\frac{\partial g}{\partial x_i'}\right)_* = \left(\frac{\partial g}{\partial x_i}\right)_* \sigma_{X_i}^N \qquad \text{Eqn. 2.47}$$

The reliability index (β) can then be determined using Eqn. 2.48 once the variables α_i^*, $\mu_{X_i}^N$, and $\sigma_{X_i}^N$ are known:

$$g\left[\left(\mu_{X_1}^N - \alpha_{X_1}^* \sigma_{X_1}^N \beta\right)\right] \cdots \left(\mu_{X_n}^N - \alpha_{X_n}^* \sigma_{X_n}^N \beta\right) = 0 \qquad \text{Eqn. 2.48}$$

A new design point is obtained using Eqn. 2.49 with the β found in Eqn. 2.45:

$$x_i^* = \mu_{X_i}^N - \alpha_i^* \sigma_{X_i}^N \beta \qquad \text{Eqn. 2.49}$$

These procedures are repeated until calculated values of β converge to a common value. The mean value of the resistance (μ) and the design point (x_i^*) are used to calculate the resistance factor (ϕ) (Paikowsky 2004):

$$\phi = \frac{R^*}{\mu_R} = \frac{x_R^*}{\mu_{X_R}} \qquad \text{Eqn. 2.50}$$

The difference between FOSM and FORM is that FORM allows the failure function to take any shape as long as the failure criterion remains constant, meaning the safety factor equates to one, or the margin of safety equates to zero (Baecher et al. 2003).

2.11.4 Monte Carlo Simulation

Monte Carlo Simulation (MCS) is a form of experimental mathematics that provides probabilistic or deterministic solutions to problems. The MCS was considered a strong research tool in 1944 during the era of the Second World War (Hammersley et al. 1964). Since then the method has been refined and proper applications have been identified that make it a strong tool for solving deterministic problems. Prior to the refinement of the MCS method, researchers attempted to use it as a solution technique for all problems (Hammersley et al. 1964) and discovered the MCS had inefficiencies and some problems modeling certain situations. The use of the MCS regained popularity once specific cases that would benefit from this type of analysis were identified and variance reducing techniques made the computations more efficient (Hammersley et al. 1964).

The MCS applications are ideal tools for problems where an exact result is unattainable through normal sampling techniques. It is useful in modeling events with great uncertainty, or in solving problems with multiple sources of uncertainty. The MCS lends itself to complex multidimensional integrals and to problems where realism is modeled with complex and involved problem descriptions (Rubinstein 1981). The MCS method has become AASHTO's preferred calibration tool and is recommended for all AASHTO related calibrations of LRFD factors (Paikowsky et al. 2010).

As in the previous FORM, the MCS attempts to estimate the probability of failure. The MCS method generates random values of load (Q) and resistance (R) based on the mean, COV, and distribution of the sample. The limit state function, $g = Q-R$ or $g = \ln(Q/R)$, is formed with the random values and evaluated for failure. Failure is defined when $g < 0$. A predetermined

quantity of simulations are executed with the random values and a tally of the total times failure occurred is divided by the number of simulations gives the probability of failure (p_f).

The MCS estimates a probability of failure (p_f) by solving Eqn. 2.55. However, before Eqn. 2.55 can be used, the design variables need to be identified and their distributions determined. The number of simulations (N) are determined using Eqn. 2.51:

$$N = \frac{1 - p_f}{COV_{pf}^2 \times (p_f)} \quad \text{Eqn. 2.51}$$

Where: COV_{pf} is the desired coefficient of variation. An estimate of the lognormal variable (x_i) is determined using Eqn. 2.52:

$$x'_i = exp(\lambda + z_i \xi) \quad \text{Eqn. 2.52}$$

$$\xi^2 = \ln\left[1 + \left(\frac{\sigma}{\mu}\right)^2\right] \quad \text{Eqn. 2.53}$$

$$\lambda = \ln(\mu) - 0.5\xi^2 \quad \text{Eqn. 2.54}$$

Where: σ and μ are the standard deviation and mean of the lognormal distribution, λ and ξ are the equivalent normal standard deviation and mean, and z_i is the random standard normal variable. Based on the distribution of the random variable (x_i), the limit state function (g) is evaluated N times and evaluated by the indicator function (J) in Eqn. 2.55. The indicator function (J) is equal to 1 when $g_i \leq 0$ (the failure region), and equal to 0 when $g_i > 0$ (the safe region). Through the simulation, a total of the failures are recorded and defined as N_f. The p_f is represented in Eqn. 2.56 (Paikowsky et al. 2010).

$$p_f = P(g \leq 0) = \frac{1}{N}\sum_{i-1}^{N} J[g_i \leq 0] \quad \text{Eqn. 2.55}$$

$$p_f = \frac{N_f}{N} \quad \text{Eqn. 2.56}$$

Where: N is the number of simulations carried out (Paikowsky et al. 2010). The reliability index (β) is then calculated with Eqn. 2.41 rearranged to give Eqn. 2.57:

$$\beta = \Phi^{-1}(1 - p_f) \quad \text{Eqn. 2.57}$$

2.12 Summary

The adoption of reliability concepts, namely LRFD, in geotechnical engineering has attempted to bridge the gap between structural design and foundation design. The conservative factors of safety used in ASD are steadily being replaced by load and resistance factors that better classify the uncertainties related to ultimate capacity determination. Static load testing is a full scale load test that measures the actual capacity of a pile and costly to perform, whereas, dynamic load testing predicts the pile capacity and can be more economical. The load test capacities collected within this study will allow for a comparison of the testing methods whose parameters are dependent on the ratio of SLT to DLT and the respective coefficient of variation. The reliability analyses, First Order Second Moment, First Order Reliability Method, and the Monte Carlo Simulation, are useful in determining suitable resistance factors, given the pile driving condition.

3 Methodology

3.1 Introduction

In order to compare and analyze the relationship between pile capacities obtained from Static and Dynamic load testing, it was necessary to understand all the conditions under which the tests were performed. Information regarding the soil profile the piles were driven into, the pile material type and geometry to establish design capacities, were necessary to group load cases into special sub-categories. The particulars of the driving operation which might include information on pre-boring, jetting or delays in driving, as well as information about testing conditions, such as the delay between driving and testing, might be useful in discerning the reasons for anomalous data. The governing standards and practices of the agencies performing the tests may also affect the results of the test. Essentially, all information about a load test is considered important in some manner when establishing a load test database. Once the data is collected, preliminary statistical evaluations were performed to identify any correlative trends and the general scatter of the relationship between dynamic and static capacities. Preliminary information on the distribution of the data may also be developed to inform the reliability analyses that will be used to establish resistance factors for various categories of pile load cases.

The pile load test cases found suitable for analysis in this study consisted of those for which the following information was available: capacity from a static load test (SLT) carried to at least 2.0 times the design load, capacity from a dynamic load test (DLT) at end-of-driving (EOD) and/or at the beginning-of-restrike (BOR), established with signal matching analysis. The piles should have been driven in a landform similar to that found in Arkansas. Sufficient information should be available to classify the soil profile in which the pile was driven. The pile itself was one of four pile types: Precast or Precast-Prestressed Concrete Piles, H-Piles, or Pipe

Piles. Of the more than 1000 pile load cases investigated, only 138 piles were found that met all of these criteria.

3.1 Database Development

The preliminary step in gathering the data for this study was reviewing case studies and reports from Departments of Transportation in neighboring states where both static (SLT) and dynamic load tests (DLT) had been performed, and where soils information was provided. The primary states of interest were Louisiana, Missouri, and Alabama. The state of Arkansas itself had no load cases where static load testing had been conducted.

3.1.1 Determining Soil Profile

The objective of the data search was to find load tests that were performed in soil types similar to those found in Arkansas. Arkansas has two distinct regions, as illustrated in Figure 3.1, where the soil profile can vary: the highlands in the northwest and the lowlands in the south and east. The highland region consists of sandstone, shale, limestone, thin layers of unconsolidated clays, sands, and gravel (residual soils). The lowlands consist of unconsolidated clays, sands, gravel of the Quaternary Period, poorly consolidated deposits of clay, silt, limestone, and lignite of the Tertiary Period (AGS 2012). Once a load tests had been identified, the geology of the area was examined to accept or reject the case based on the soils present in Arkansas.

Figure 3.1. The geology of Arkansas (AGS 2012)

Using the pile driving records, or the information provided in the DOT reports, soil profiles were broken into three major categories; clay, sand and mixed. The designation of a soil profile was determined by using the 70% rule. The 70% rule considers the soil types along the length of the pile. The soil type which represents 70% or greater of the pile length is considered to be the dominating soil type that would be evaluated for friction piles (pipe and PPC piles). When considering the H-Piles, the soil type relevant to end bearing capacities was ideally the soil type located at the pile tip. For piles where detailed driving records or bore log data were available, the soil type was classified accordingly using information from these records. When these records were not present, the soil type was classified as recorded in the initial report. For example, if 72% of the soil along the side of a pile consisted of clay or clayey soil, the recorded soil profile would be clay. Similarly, if more that 70% of the soil along the pile side were sand or sandy soil the profile would be recorded as sand. If two soil types are present, with no clear majority, the soil profile would be considered mixed. Soil type was characterized in

accordance with the Unified Soil Classification System (USCS). The 70% rule could also be interpreted as the soil type from which the pile derived 70% or more of its capacity. In fact, the second interpretation of the 70% rule would be preferable when classifying soil type, but sufficient strength information was not available to perform this type of classification for a number of the piles in the database.

3.1.2 Louisiana Load Cases

The report titled "Calibration of Resistance Factors Needed in the LRFD Design of Driven Piles" (Abu-Farsakh et al. 2009) was prepared for the Louisiana Department of Transportation and Development (LADOTD). The report presented information on SLT, DLT and Cone Penetration Testing (CPT) for 53 Precast-Prestressed-Concrete (PPC) piles tested to failure. The load-settlement information from SLT was evaluated using the Davisson Offset criterion for piles with diameter less than 24 inches and the modified Davisson Offset method for piles with diameter more than 24 inches. The DLT program employed signal matching at both EOD and BOR, with BOR testing taking place 14 days after driving. Soil profiles were characterized using CPT soundings and soil borings. Of the 53 pile load cases described in the report, 13 piles met the criteria for inclusion in the database by having both the SLT and DLT values recorded and the necessary soil profile information.

The soil deposits in the State of Louisiana are made up of alluviul, lacuastrine and coastal deposits of the Mississippi Embayment. Louisiana is divided into two main regions: the northern Louisiana region, and the southern Louisiana region. Soils in the northern Louisiana region are of the Tertiary Period, while the soils in the southern Louisiana region are of the Quaternary and Tertiary Period (DOI 2008). Northern Louisiana and Eastern and Southern Arkansas have similar

soil profiles therefore piles driven in Louisiana were determined to be acceptable for inclusion in the database.

3.1.3 Missouri Load Cases

Case studies from the Missouri Department of Transportation (MODOT) reports did not meet the criteria for inclusion into the data base. The report only contained signal matching predicted capacities. Though the MODOT report proved fruitless, a driving record was obtained for a pile driven in 2011. The single pipe pile was predrilled five feet in a predominately clay soil type. Dynamic load testing was conducted at EOD and at BOR with a 7 day waiting period. Static load testing was performed nine days after driving with the pile being loaded to failure according to the Davison Offset criterion (1972).

Missouri has four geologic regions: the Ozarks, Western Plains, Glaciated Plains, and Southeast Lowlands. The pile of interest was driven in the Glaciated Plains region that has a mix of clay, silt, sand, and rock fragments. The Glaciated Plains region is of the Pennsylvanian and Mississippian age with Quaternary formations are similar to those in North and Northwest Arkansas.

3.1.4 Alabama Load Cases

Data from Alabama was retrieved from a report titled ‘Evaluation of Load Tests for Driven Piles for the Alabama Department of Transportation’ (Hill 2007), where 30 projects were selected from the Alabama Department of Transportation database. Piles included in this study were PPC piles and steel H-piles that were tested statically and dynamically using signal matching. These piles were not loaded to failure, as the loading for the SLT was only to 2.0 or 3.0 times the design load. Load-settlement graphs from the project indicate that only one pile

was loaded to plunging failure. The load-settlement curves for the remaining piles suggest that the reported SLT capacities were not those at plunging failure and simply represent the highest load the pile was subjected to. This was typically 2.0 to 3.0 times the anticipated design load. Dynamic load tests were carried out using signal matching for EOD conditions and BOR testing were conducted on some of the piles with waiting periods ranging from 30 minutes to 60 days. The soil profiles were constructed from boring log data and the 70% rule was implemented to classify the soil type.

Alabama is made up five differing regions: Interior Low Plateau, Cumberland Plateau, Valley and Ridge, Piedmont, and the Coastal Plains. The region of interest is the Coastal Plains where all but one of the piles was tested. The Coastal Plains region consists of the Mesozoic and Cenozoic Period, with sediments of gravels, sands, silts, and clays. This region is similar to that found in eastern and southern Arkansas.

3.2 Other Data from Literature

3.2.1 WSDOT

The Washington State Department of Transportation (WSDOT) embarked on an effort to calibrate resistance factors for a state-developed pile driving formula in a report titled 'Development of the WSDOT Pile Driving Formula and Its Calibration for Load and Resistance Factor Design (LRFD)' (Allen 2005). Pile load test data from Paikowsky et al. (2004) database was used to develop a hammer efficiency factor for use in the WSDOT pile driving formula. The database included SLT and DLT data for 141 test piles at varying locations around the world. The soil profiles were identified along the pile length for friction piles and at the pile tip for end

bearing piles. A total of 59 records were gathered from this report with soil profiles similar to those found in Arkansas.

3.2.2 PILOT - IOWA

PILOT (PIle LOad Test) is a database developed for the state of Iowa. It is modeled after the Federal Highway Administration's (FHWA) Deep Foundation Load Test Database (DFLTD) which has 1500 records of load test data from over 850 sites around the world. PILOT contained 274 SLT data with accompanying DLT and in-situ soil information. The types of piles in the study were H-steel, monotube, pipe, timber, and concrete piles. Of the 274 pile load tests considered, 12 piles (PPC Piles and H-Piles) met the criterion necessary to be included in this analysis: SLT evaluated by the Davisson Offset criterion and DLT from EOD testing conditions.

3.2.3 FHWA - Central Artery/Tunnel (CA/T) Project, Boston, Massachusetts

The Central Artery/Tunnel (CA/T) project was considered one of the largest and most complex highway projects in the United States (Bradshaw et al. 2006). The project took place between 1991 and 2005, where 15 pile load tests were performed for evaluation. The piles were precast prestressed concrete (PPC) or pipe piles and were driven into loamy soils, similar to those found in southeast Arkansas. Loamy soils are a mixture of sands, silts, and clays (Bradshaw et al. 2006). Dynamic load testing (ASTM D4945 2008) with signal matching was conducted at both EOD and at BOR after a 12 to 36 hour waiting period. Static load tests (ASTM D1143 2007) were carried to 2.0 to 2.25 times the required allowable axial capacities. The load test reported met the criterion of having SLT, DLT, soils information and being a PPC pile.

3.3 Data Analysis

After eliminating load tests that did not meet the initial screening criteria, 138 load tests remained in this study. The load tests were characterized by soil and pile type, then assigned to groups as detailed in Chapter 4. An initial scatter plot of capacities measured using SLT, to capacities predicted using DLT at EOD was created. The scatter plot was then fitted with a regression line that implemented robust regression with iterative least square fitting techniques. The next step was to calculate the ration of Qmeasured/Qpredicted from the raw SLT and DLT at EOD capacities that would be used in further analyses to determine the distribution of the sample population by the probability density function (PDF) and cumulative distribution function (CDF). The CDF was often used to determine the distribution of the sample. The selection of the appropriate mathematical distribution was further confirmed by the execution of the goodness-of-fit test, in this case, the Chi-Square Test was used to accept or reject the PDF and CDF given a hypothesis. A confidence interval (CI) of 95% was applied to the selected CDF using the Inverse Fisher Matrix, bounding the data points and identified any points that fell outside the CI. Once the distribution was decided upon, parameters of the mean bias, which was the mean of the Qmeasured/Qpredicted of the sample, and the coefficient of variation (COV) applicable to the distribution, were used in further reliability analysis. These analyses consist of the First Order Second Moment, First Order Reliability Method, and the Monte Carlo Simulation. The software programs used to perform these analyses were Microsoft Excel® and ReliaPile. ReliaPile is a program based in MATLAB and was developed by Joseph Jabo, a Ph.D. candidate at the University of Arkansas, Fayetteville, Arkansas.

3.3.1 Regression Analysis

Linear regression was carried out on the capacity values in the database by separating the piles into subgroups by pile and soil type and plotting SLT capacity versus DLT capacity. The best fit line of the data is the line that provides a minimum error (minimum distance) between the data points and the regression line. The dependent DLT values were plotted on the y-axis, while the corresponding independent SLT values were plotted on the x-axis. This type of analysis allowed any trends to emerge as the points scatter about the line of equality (LOE). Any outlying data point would be identified and investigated to possibly ascertain the reason it might be an outlier.

3.3.2 Robust Regression and Iterative Least Squares Fitting Techniques

Least square fitting provides a best fit model function to describe the data by minimizing the sum of the squares of the data point offsets to their perpendicular points on a curve described by the model function. However, this technique is sensitive to outlying data points that may have a large influence on the regression function (Heiberger et al. 1992). Because data in the collected set of pile load tests contained data points that could be considered outliers, modified fitting techniques were used to account for outlying data. Throughout the analysis of the data, a technique called Robust Regression and Iterative Least Squares Fitting is used to accurately represent the data and minimize any effect outliers may have on the data (Heiberger et al. 1992). Robust regression assigns a weight to the data points and iteratively adjusts the weighting function using least squares. While there are many weighting functions available in the literature, the bisquare function, with the default tuning constant of 4.685 was used. During the first iteration, the weight assigned is usually estimated using unweighted least squares. As iterations continue the weights are reassigned to the data points, applying lower weights to points further

away from the predicted model function (MathWorks 2005). The iterative process continues until the residuals are unchanged for at least two successive iterations (Heiberger et al. 1992).

Within the ReliaPile program, the robust fitting technique was initiated with the selection of the sample from the database. A model was built with non-parametric variables, and then a hypothesized theoretical distribution with unknown parameters was developed. In the case of a linear regression analysis, this theoretical distribution follows the equation of a line expressed in Eqn. 3.1:

$$y = mx + c \qquad \text{Eqn. 3.1}$$

Where: x and y are variables, in this case Q_{SLT} and Q_{DLT} respectively, m is the slope of the line, and c is the intercept, which is set to pass through the origin. The equation then became Eqn. 3.2:

$$y = mx \qquad \text{Eqn. 3.2}$$

The error vector was defined as the perpendicular distance between the data point from the sample to the hypothesized theoretical distribution. This distance was found using the weighted least squares method. The initial weights were usually derived from the residuals of the initial fit (Heiberger et al. 1992). Points closer to the regression line and in range are assigned a weight of one, and points outside of the range are assigned a weight less than one. Robust regression attempts to estimate b in the model expressed in the Eqn. 3.3, where Y, X and C are the vector from the sample data points, and b is the regression coefficient (Heiberger et al. 1992).

$$Y = Xb + C \qquad \text{Eqn. 3.3}$$

The process of least squares was implemented by taking the independent variable, SLT capacity, and estimating y given the x variable, which gives an unknown b. This estimation was repeated at each data point and a collection of variables were analyzed for the error. The error vector (R) was computed using Eqn. 3.4 and minimized by applying the condition in Eqn. 3.5, and n is the number of data points:

$$R = (y_1 - bx_1, y_2 - bx_2, \dots, y_n - bx_n) \quad \text{Eqn. 3.4}$$

$$\frac{\partial R}{\partial y_i} = 0, \quad i = 1, 2, \dots, n \quad \text{Eqn. 3.5}$$

The sum of squares for the first iteration was made with an unweighed weighting function (w) illustrated in Eqn. 3.6:

$$|R|^2 = \sum_{i=1}^{n} w_i (y_i - bx_i)^2 , i = 1, 2, \dots, n \quad \text{Eqn. 3.6}$$

As the robust fitting technique continued, with each iteration the weighting functions were revised. This process continued until b converged to a constant value.

3.3.3 Probability Density Function (PDF)

Determination of the sample distribution type is an important step in developing the parameters for use in the reliability methods. To do this the ration of measured (SLT) to predicted (DLT) capacities are separated into bins representing small ranges in the ration values. Then a histogram of the number of occurrences of the ration in a given bin was plotted against the value of the bin in ascending order. A plot of various theoretical probability density functions is then superimposed on the histogram to visually determine the distribution which more closely fits the data. The probability density function (PDF) describes the frequency at

which a variable appears in a distribution. It is defined as a continuous function (X), which is the Qmeasured/Qpredicted variable, by Eqn. 3.7 for a normal distribution and Eqn. 3.8 for a lognormal distribution. The ration of the measured capacities and the predicted capacities are ordered in ascending order and represent the variable (X) in Eqn. 3.7 and Eqn. 3.8 (Kroese et al. 2011):

$$f(x;\mu,\sigma) = \frac{1}{\sigma\sqrt{2\pi}} e^{-\frac{1}{2}\left(\frac{x-\mu}{\sigma}\right)^2} \qquad \text{Eqn. 3.7}$$

$$f(x;\mu,\sigma) = \frac{1}{x\sigma\sqrt{2\pi}} e^{\frac{-(ln(x)-\mu)^2}{2\sigma^2}}, \quad x > 0 \qquad \text{Eqn. 3.8}$$

The standard deviation of the sample population is represented by σ, and μ is the mean of the sample population. Both equations were used to create the theoretical density function from the sample statistics. The resulting curves were plotted with frequency on the y-axis and the ration Qmeasured/Qpredicted on the x-axis. The curve that best fit the data (plotted in the histogram) was visually chosen as the frequency distribution.

3.3.4 Cumulative Probability Function (CDF)

The cumulative distribution function (CDF) describes the value of the state function, in this case the ration of measured to predicted capacity, in terms of the probability the that random values from the population will be less than a given point on the cumulative distribution function (Miller et al. 1985). These probabilities range between zero and one. The measured capacity, (Q_m), divided by predicted capacity, (Q_p), are plotted in ascending order against the cumulative frequency of occurrence. The probability of occurrence of values of this ration were calculated using $i/(n+1)$, where i is the rank of each data point when sorted, and n is the total number of points in the sample. Both normal and lognormal distributions were analyzed using the

respective normal or lognormal variables. The resulting curves provided a more definitive way to determine if the sample was normally or lognormally distributed, when PDF curves were not conclusive. The mean (μ) and standard deviation (σ) were recorded for the selected distribution. The COV of the capacity rations were then calculated and used to determine the resistance (ϕ) factors by FOSM, FORM, and MCS.

3.3.5 Fisher Information Matrix and Confidence Interval

The approach to determine the confidence interval (CI) in the ReliaPile program employs the inverse of the Fisher Information Matrix. The Fisher Information Matrix measures how much information is known about a parameter by estimating the standard errors (Neale et al. 1997), and was used when determining the confidence intervals for both the regression line and the CDF of the sample. The errors used were the standard error vector determined from the Robust Regression and Iterative Least Squares Fitting Technique, described earlier. The error vector (R), expressed in Eqn. 3.4, was transformed into an error matrix, and then partially differentiated with respect to b, the parameter that was estimated. The Fisher Information Matrix (I) is defined in Eqn. 3.9:

$$I = -E\left[\frac{\partial R}{\partial b}\right] = \frac{1}{2\sigma^4}\begin{pmatrix} 2\sigma^2 & 0 \\ 0 & -1 \end{pmatrix} \qquad \text{Eqn. 3.9}$$

Where: E is the expected matrix, R is the score function (error matrix), and b is a function of the mean and standard deviation (μ, σ^2) (Woo 2013).

The inverse of the Fisher Matrix, $[I]^{-1}$, is called the covariance matrix (Coe 2009), which is used to determine the CI. The confidence interval is an estimate that the parameter will fall within the stated interval with a specified degree of certainty. The degree of certainty is known as the level of significance and is denoted as alpha (α). Once the distribution was identified, a

confidence interval was applied, for this study the interval was 95%; meaning 2.5% above and below the distribution function. The CDF was evaluated to confirm that 95% of the time the ration of measured to predicted capacity fell within this bound. The CI is then determined by Eqn. 3.10:

$$CI = b \pm t\sqrt{S} \qquad \text{Eqn. 3.10}$$

Where: b are the coefficients produced by the fit, [namely the data point, (Qm/Qp, probability) for the CDF and SLT/DLT for the regression], t is the percentile of the t-distribution for the required level of confidence level, and S is the vector of the diagonal elements of the inverse of the Fisher Matrix (covariance matrix).

3.3.6 Chi-Squared Goodness-Of-Fit Test

To verify that the visually selected distribution provided an appropriate fit to the data, a goodness-of-fit test was required. The selected goodness-of-fit test was the Chi-Squared test represented in Eqn. 3.11. First a null hypothesis about the distribution was made, from earlier analysis, the null hypothesis was that the distributions were lognormal. The goodness of fit technique minimizes error by the least-squares method. The Chi-Squared (χ^2) test evaluates the parameter of interest, in this case the distribution, in terms of frequency. The frequencies of the normal and lognormal distributions were grouped into bins, similar to the process of the histograms, then the frequencies were tallied. Chi-Squared values were calculated using Eqn. 3.11, where n is the number of bins used to group the frequencies, Observed is the actual observed frequency in the bin, and Expected is the expected frequency, which was the sum of the observed frequencies divided by the total number of bins. Once the Chi-Squared value was determined for each bin, they were summed to provide a χ^2 score, then compared to the critical

value for a 95% level of confidence for n–1 degrees of freedom. The critical value was selected from the appropriate table of Chi-Squared Critical values:

$$\chi^2_{STAT} = \sum_{i=1}^{n} \frac{(Observed - Expected)^2}{Expected} \qquad \text{Eqn. 3.11}$$

If the summed χ^2 score was less than the upper tail critical value, the hypothesis was accepted, if the χ^2 score was larger than the critical value, it was rejected.

3.4 Calculation of Resistance (ϕ) Factors

The previous sections explained the process of how the distribution of the samples were determined and confirmed. It provided parameters particular to the distribution that would be necessary in the following reliability analysis. In particular were the bias of the sample, which was the mean Qmeasure/Qpredicted of the sample, and the COV of the sample. These factors directly impact the reliability equations that produce the entity of interest, the resistance factor.

3.4.1 Parameters

The various reliability methods required statistical parameters of the sample populations to determine the resistance factors for a specific level of reliability. The level of reliability was defined by the target reliability index (β_T). For the purposes of this study values for the loading parameters in the reliability equations where taken as those used by Paikowsky in the original calibration of resistance factors used in the AASHTO Bridge Design Guide. These loading parameters are presented in Table 3.1 and were suggested in Paikowsky et al. (2004). These loading parameters are currently recommended by AASHTO for a Strength I load case, which is the basic load combination relating to the normal vehicular use of a bridge without wind (AASHTO 2010). The DL/LL ratio was taken to be 2.0, along with the use of the suggested

parameter values, to enable a comparison of the analysis presented in this study with the original analysis presented in 2004.

Table 3.1. Statistical characteristics of loads used for resistance factor calibration (Paikowsky 2004)

Probabilistic Characteristics from AASHTO	
Dead Load Bias (λ_{QD})	1.05
Live Load Bias (λ_{QL})	1.15
Load Factor - Dead Load (γ_D)	1.25
Load Factor - Live Load (γ_L)	1.75
Dead Load/Live Load Ratio (DL/LL)	2.00
Coefficient of Variation of Dead Load (COV_{DL})	0.10
Coefficient of Variation of Live Load (COV_{LL})	0.20

The value of β_T corresponds to a probability of failure (p_f), as illustrated in Table 3.2. The reliability index (β_T) can range from 2.0 to 2.5 for a pile group and from 2.5 to 3.0 for a single pile (Paikowsky et al. 2004). The AASHTO recommended β_T of 2.33, with a p_f = 1.0% (0.01), was used for a pile group of five or more piles per pile cap, while the AASHTO recommended β_T of 3.00, with a p_f = 0.1% (0.001), was used for four or less piles per pile cap (Paikowsky 2004). The probability of failure can also be expressed as the level of reliability, which is defined as 1-p_f.

Table 3.2 Relationship between reliability index and probability of failure (Paikowsky et al. 2010)

Reliability index β	Probability of failure p_f
1.0	0.159
1.2	0.115
1.4	0.0808
1.6	0.0548
1.8	0.0359
2.0	0.0228
2.2	0.0139
2.4	0.00820
2.6	0.00466
2.8	0.00256
3.0	0.00135
3.2	$6.87\ E^{-4}$
3.4	$3.37\ E^{-4}$
3.6	$1.59\ E^{-4}$
3.8	$7.23\ E^{-5}$
4.0	$3.16\ E^{-5}$

3.4.2 First Order Second Moment (FOSM)

Using the assumed statistical parameters for loading stated in Section 3.4.1 and the statistical parameters for resistance which were developed using the process described in Section 3.4, the resistance factors can be calculated for a given level of reliability. The first order second moment method utilized the simplified closed form equation stated in Eqn. 2.38 or the improved equation stated in Eqn. 2.40. The statistical parameters for load and resistance were entered directly into the equation. The reliability index, β_T, was entered as the target and a resistance factor is calculated in a single step for the simplified FOSM. The equation was solved directly in Microsoft Office Excel® and compared to the results of the ReliaPile program.

The ϕ factors were also obtained with the Improved FOSM equation, Eqn. 2.40, with the modification of the COV_Q term, as described in Section 2.12.2, using both Microsoft Excel® and ReliaPile. The ReliaPile program required the parameters listed in Table 3.1, which were the

same parameters as in the Excel® calculation. The ϕ factors obtained using the simplified FOSM in both the Microsoft Excel® and ReliaPile produced the same values. The ReliaPile program was used to evaluate the remaining cases due to the following: (1) in the FOSM, the resistance values calculated were consistent with the Excel® values, (2) in the regression analysis, ReliaPile produced consistent graphs in regard to the coefficient of determination (see Section 4.2.1), and (3) ReliaPile produced smooth PDF and CDF curves than Excel® (see Section 4.2.2).

3.4.3 First Order Reliability Method (FORM)

First Order Reliability Method (FORM) was performed in ReliaPile where the objective was to determine the probability of failure, by using a defined set of statistical parameters for resistance and loading and assuming a resistance factor. This assumed ϕ factor was entered into the performance function in Eqn. 3.13, which identified the design point. The location of the design point was used in the objective function, Eqn. 3.12 to determine the reliability index (β). This process was optimized through iterations until β converged to a constant minimum value. The process was repeated for a range of ϕ factors to obtain a corresponding set of β values.

The first step was to identify the objective function which is expressed in Eqn. 3.12, where β is the reliability index, and $\sqrt{z^t z}$ is the distance from β to the origin in standard space and z^t is the transpose of z:

$$\beta = \sqrt{z^t z} \quad for\ z: P(z) \leq 0 \qquad \text{Eqn. 3.12}$$

Next the performance function, which determined the location of the design point, was expressed using Eqn. 3.13 for a lognormal distribution. The parameters used in Eqn. 3.13 are listed in Table 3.1. An assumed ϕ factor was entered into Eqn. 3.13:

$$P = \ln \frac{\lambda_R \left(\gamma_D \frac{DL_n}{LL_n} + \gamma_L\right)}{\phi \left(\lambda_{QD} \frac{DL_n}{LL_n} + \lambda_{QL}\right)} \qquad \text{Eqn. 3.13}$$

The performance function (P) was then transformed from the original lognormal space into standard normal space through the use of $z = (z_1, z_2, z_3)^t$, where z_1 is the resistance, z_2 is the live load, z_3 is the dead load, and t is the transpose of z. The standard space variables are then substituted into the performance function. It was necessary to transform into standard normal space because the probability of failure in Eqn. 2.41 can only be solved with normal standard variables. This transformation gave the variables a mean of zero and a standard deviation of one (Maier 2001). The design point provided a location on the performance function to measure β in standard normal space. The previous steps were iterated until β converged then optimized by taking the derivative of Eqn. 3.12 and finding the critical values. The optimized β was then entered into Eqn. 2.41 to calculate the probability of failure. These procedures were repeated for a range of ϕ factors and produced corresponding β values. The β values of interest, 2.33 and 3.00, were selected from the array of data along with its corresponding ϕ.

3.4.4 Monte Carlo Simulation (MCS)

The Monte Carlo Simulation (MCS) is a method that provides an estimate of the probability of failure through an iterative process. The MCS method generates random variables based on the statistical parameters provided and produces a set of random samples following a prescribed distribution. These random variables were then analyzed with the performance function, Eqn. 2.26, generating an array of results which were stored for use later. Once the number of predetermined simulations was completed, the number of times the performance function was less than zero was counted and used to calculate the probability of failure. The reliability index was then determined from the probability of failure.

The MCS follows the steps outlined in the ReliaPile 1.0 User's Manual (Jabo unpublished) to obtain the probability of failure. The analysis began with an assumed resistance (ϕ) factor of zero to obtain a maximum value of bias (λ_{max}). The minimum number of simulations was calculated using Eqn. 2.51, the counts ranged from 100,000 for $p_f = 0.001$, and 10,000 for $p_f = 0.01$. Normal random variables were generated in MATLAB using the statistical properties for resistance, live load, and dead load described earlier. The normal random variables were then substituted into the performance function (Eqn. 2.55) which takes the form, g(x) = ln(R) - ln(Q), for a lognormal distribution. The design point (x'_i) is determined using Eqn. 2.52 where the parameters were transformed into normal space with Eqn. 2.53 and Eqn. 2.54. The results of the evaluation of the performance function were totaled once the number or iterations/simulations were reached. The number of failures (N_f) during the simulation, meaning when the performance function was less than zero ($g(x) < 0$), were counted then divided by the total number of simulations. The probability of failure (p_f) was calculated using Eqn. 2.56, where N is the number of simulations. With p_f known, the reliability index (β) was determined using Eqn. 2.57. The β of interest, 2.33 and 3.00, was then picked from the array of values with its corresponding ϕ factor.

3.5 Summary

To develop this database, more than 1000 load tests were investigated where about 10% that met the criterion of containing a static load test (SLT) capacity loaded to at least 2.0 the design load, dynamic load test (DLT) capacity at end-of-driving (EOD) and/or at the beginning-of-restrike (BOR) with signal matching analysis, accompanied with soil profile information. Pile load tests collected span the southern United States with an occasional international site obtained from an earlier Paikowsky database. The analysis techniques used to determine resistance factors

aim to provide the best results from the data, accounting for data points that may be considered outliers. Chapter 4 presents and discusses the results of the implementation of these techniques.

4 Results and Discussions

The relationship between pile capacity measured by static load testing (SLT) and the capacity predicted by dynamic load testing (DLT) is one of great importance because it offers the engineer an opportunity to predict measured capacity when SLT may not be an economical option. While SLT capacity is directly measured, the capacity determined by DLT is subject to many variables and assumptions when converting strain and acceleration measurements to a pile capacity. The analyses presented in this chapter were conducted on 138 load tests contained in the database found in Appendix A. The general characteristics of these load tests are summarized in Table 4.1. These analyses were used to establish appropriate capacity resistance factors for the various field acceptance procedures. The analyses included: direct comparison of DLT and SLT results with a simple linear regression analysis, creation of a Probability Density Function (PDF), a Cumulative Distribution Function (CDF) with a 95 percent confidence interval, First Order Second Moment Reliability Method (FOSM), First Order Reliability Method (FORM), and Monte Carlo Simulation (MCS). Through the initial analysis, the distribution of the data was identified as a normal distribution or lognormal distribution. The classification of the data distribution is important because the defining parameters of those distributions, mean and standard deviation, are the primary inputs used in the reliability analyses to determine the resistance (ϕ) factor.

Table 4.1. Summary characteristics of the 138 load tests contained in the load test database.

Paper/Project	Pile Type	Soil Type	No. of Piles
ALDOT-2007	H-Piles	Clay	7
	H-Piles	Mixed	7
	H-Piles	Sand	14
	PPC	Sand	3
C/A Tunnel Project	Pipe	Clay	2
	Pipe	Sand	2
	PPC	Clay	10
	PPC	Sand	1
LADOTD-2009	PPC	Clay	10
	PPC	Sand	3
MODOT	Pipe	Clay	1
Paikowsky-2004	H-Piles	Clay	6
	PPC	Clay	15
	H-Piles	Mixed	7
	PPC	Mixed	6
	H-Piles	Sand	16
	PPC	Sand	16
PILOT	H-Piles	Clay	5
	H-Piles	Mixed	3
	H-Piles	Sand	2
	PPC	Sand	2

The load tests were categorized into the eleven categories, or cases listed in Table 4.2. There were no records of pipe piles in mixed soils that met the initial selection criteria of having; SLT, DLT, and soil information.

While the ideal DLT data to compare with SLT data would be capacities determined at the beginning of restrike (BOR), the literature provided few piles that included BOR measurements. As a result, end of driving (EOD) capacities are the primary values used in this analysis. Where possible, analyses were performed if adequate BOR capacities were available. End of driving data was available for 123 piles in the subset of the database while BOR data was available for only 37 piles.

Cases with fewer than 15 load tests were not analyzed separately because there would be limited statistical significance from the results. As result, Cases 3, 5, 6, and 8 were eliminated from consideration because they contained too few data.

Table 4.2. Pile load tests cases with quantity of piles

Cases		No. of Piles
Case 1	All Piles - EOD	123
Case 2	H-Piles in Clay - EOD	18
Case 3	H-Piles in Mixed - EOD	14
Case 4	H-Piles in Sand - EOD	32
Case 5	Pipe Piles in Clay - EOD	3
Case 6	Pipe Piles in Sand - EOD	2
Case 7	PPC Piles in Clay - EOD	28
Case 8	PPC Piles in Mixed - EOD	5
Case 9	PPC Piles in Sand - EOD	20
Case 10	All Piles - BOR	37
Case 11	Paikowsky Piles - EOD Data	59

4.1 General Analysis of All Piles

The initial analysis (Case 1) considers all the pile and soil types in the database and is illustrated in Figure 4.1. A scatter graph of the SLT and DLT capacities of the 123 piles was plotted to observe trends or identify any unusual data points. Also shown in Figure 4.1 is the linear regression for the comparison of SLT to DLT capacities at the end-of-driving (EOD) condition. The data suggest that DLT at EOD, on average, under predicts capacity relative to the measured SLT capacities. The majority of the points appear below the dashed line which represents the line of equality (LOE). The trend developed from this data shows that, on average, DLT values at EOD are approximately 60 percent of SLT values which agrees with past

correlation studies (Thendean et al. 1996). The coefficient of determination (R^2) measures the relationship between the regression line (the solid line) and how well the data is represented by the model. The R^2 value indicates that 57 percent of the variation in the data can be explained by the model and 43 percent is attributed to unknown variables. Therefore, the linear model is not a good predictor of the relationship between dynamic and static load capacities. A model that fully describes the variation and the relationship between the DLT data and the SLT data using the regression line would have an R^2 value of 1.0.

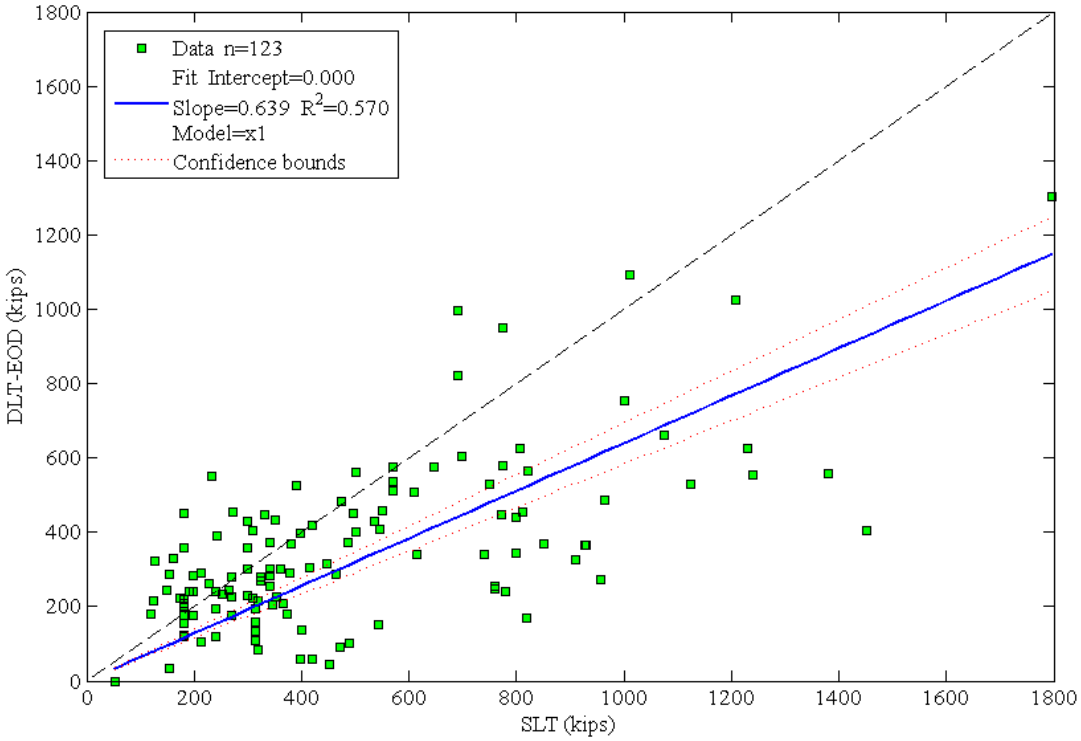

Figure 4.1. Scatter plot of all the load tests analyzed at EOD (Case 1)

The scatter plot for the 37 load tests which had beginning-of-restrike (BOR) data is presented in Figure 4.2 (Case 10). It is evident that the data groups more closely about the LOE. The regression line passes through the origin and indicates that, on average, predicted capacities at BOR are about 90 percent of SLT capacities. The coefficient of determination (R^2) indicates a

much better relationship of the data to the regression line than was observed for the EOD data presented in Figure 4.1. The R^2 of 0.81 indicates a model that better explains the variation in the data. The data presented in Figure 4.2 reinforces the notion that the time between EOD and BOR allows for pile capacity to increase or decrease to values more closely approximating the static load capacity. The change in pile capacity with time is dependent on the soil condition; when capacity increases after driving the increase is termed setup. Setup usually occurs in normally consolidated and uncemented soils. When capacity decreases after driving it is termed relaxation. Relaxation may occur in very dense silts, shales and clays.

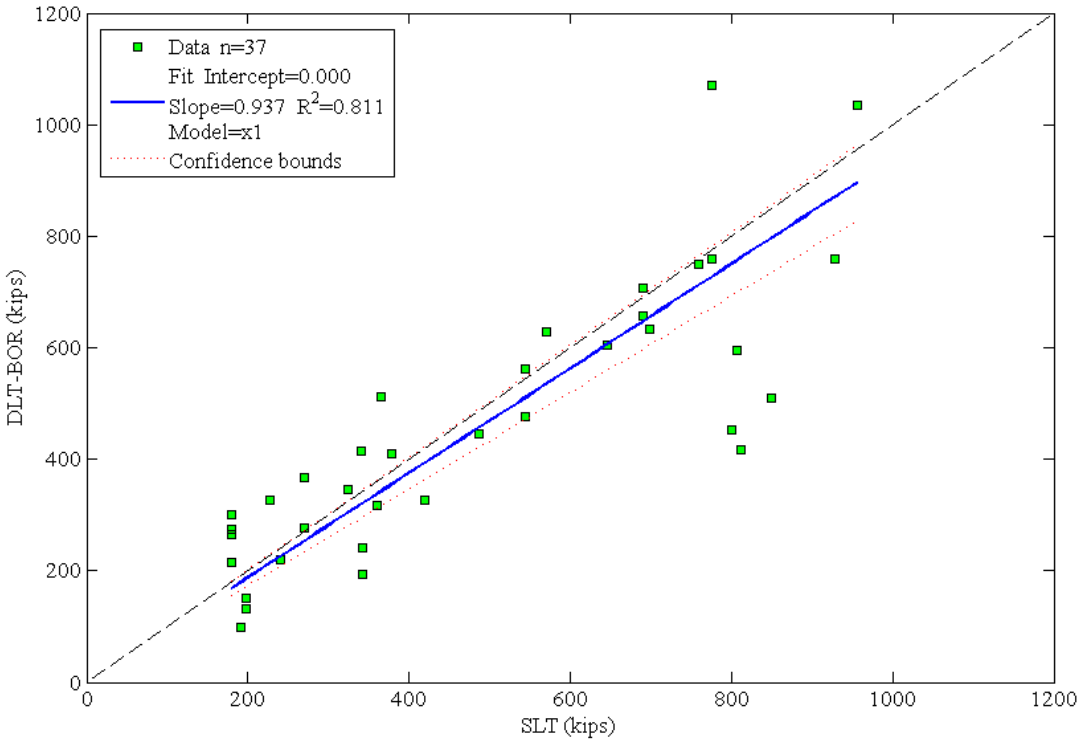

Figure 4.2. Scatter plot of all the load tests analyzed at BOR (Case 10)

4.2 Case 2: Steel H-Piles in Clay Soil

4.2.1 Linear Regression Analysis

Case 2 consists of 18 H-piles driven in clay soil. The scatter plots presented in Figure 4.3 created with Microsoft Excel® and Figure 4.4 created using ReliaPile, identify a cluster of data points about the LOE (the dashed line) at capacities less than 400 kips. The outlying data point at an SLT capacity of 740 kips was for a pile driven in Minnesota and was taken from the Paikowsky 2004 database where no additional information regarding driving was provided. If this data point were removed, the regression line would more closely follow the LOE with a slope near unity. The locations of the data points illustrated in Figure 4.3 and Figure 4.4 appear to be in agreement. However, the regression lines for the two figures which present the same data are slightly different. The graph created using the Excel® spreadsheet considered each data point to have an equal effect on the regression line, while the ReliaPile program used, robust regression techniques with iterative least squares fitting, as described in Section 3.4.2, to fit the regression line. A point of concern when comparing the regression lines in both graphs was that the value of the coefficient of determination (R^2) in the Excel® graph (Figure 4.3) was negative 0.804, when the range for the coefficient of determination should be between 0 and 1.0, and not negative. This error in internal calculations and reporting provided by Excel® dissuaded the use of Excel® in the analyses of further cases. The coefficient of determination provided by ReliaPile was 0.484, which seems more appropriate. Therefore it was decided that the ReliaPile program was more suitable to construct the scatter plots and other statistical operations for the subsequent cases.

A confidence interval (CI) of 95 percent is applied to the regression line in Figure 4.3 and Figure 4.4, which is indicated by the dotted lines above and below the regression line. The upper

and lower boundary of the CI in Figure 4.3 was created using the Excel® CONFIDENCE function. The input values for this function are the level of significance, the standard deviation of the sample, and the sample size. The CI was then added or subtracted to the y-coordinate of the regression line to generate values for the upper and lower confidence bounds.

In the ReliaPile graph, Figure 4.4, the CI was calculated based on the level of significance α (0.05) which corresponds to 95 percent confidence level. In the ReliaPile program the standard error of the parameter (Qmeasured/Qpredicted) is estimated by the Inverse Fisher Matrix, detailed in Section 3.4.5. Like the regression lines, the confidence intervals displayed in Figures 4.3 and 4.4 vary somewhat and it was felt that the ReliaPile program provided a more reasonable representation of the confidence intervals due to its more robust technique of creating a model to fit the data.

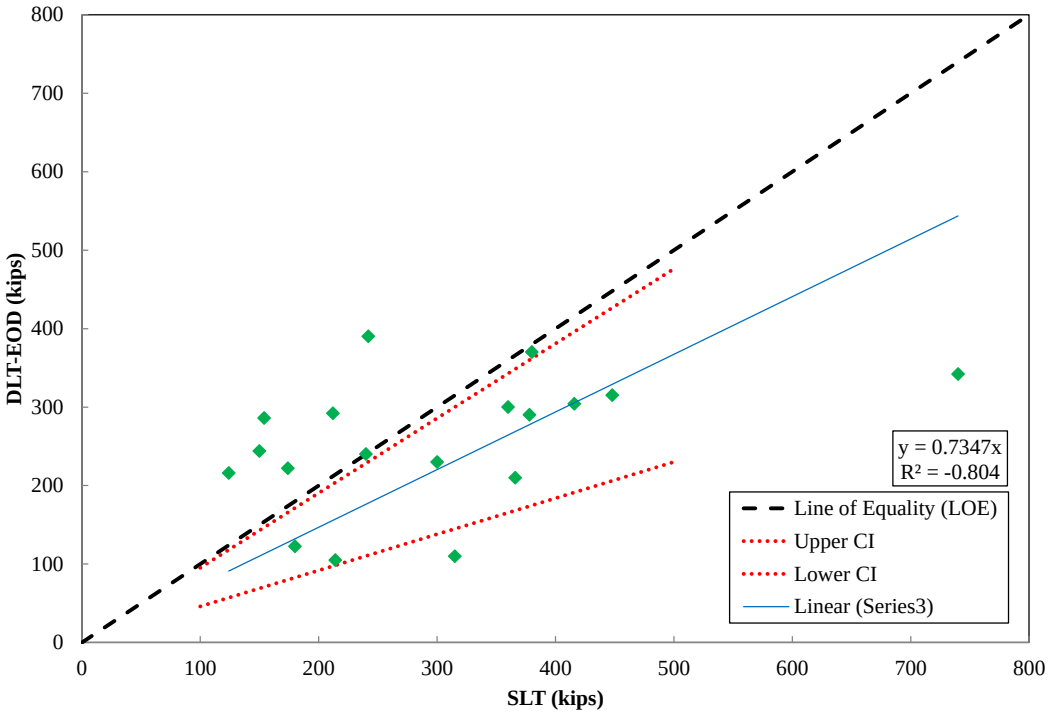

Figure 4.3. Microsoft Excel® linear regression plot for steel H-Piles in clay soil (Case 2)

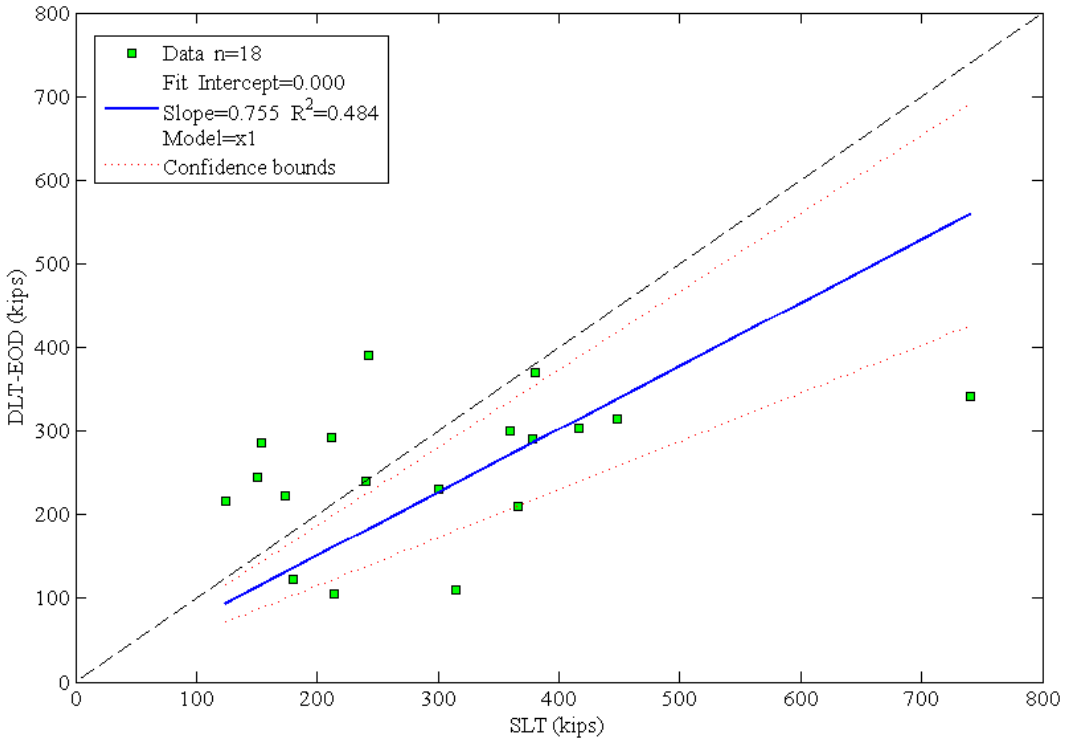

Figure 4.4. ReliaPile linear regression plot for steel H-Piles in clay soil (Case 2)

4.2.2 Probability Density Function (PDF)

The probability density function was established for every load case by following the procedure described below for Case 2. The probability density function (PDF) for steel H-Piles in clay soil (Case 2) is illustrated in Figure 4.5 and Figure 4.6. The histogram groups the ratios of measured capacity from an SLT to predicted capacity from a DLT into ranges of values (bins). The plot illustrates the frequency, or number of values in each of the bins. The statistical properties of the sample populations were used to superimpose a normal and lognormal distribution curve, produced by Excel® functions in Figure 4.5 and ReliaPile in Figure 4.6, onto the histogram. The values of both the normal and lognormal PDF are plotted on the secondary axes.

The graph constructed in Excel® used the NORM.S.DIST function for the normal distribution and the LOGNORM.DIST function for the lognormal distribution. Both of the Excel® functions require value of interest (X), the mean, the standard deviation, and the logical value (True or False) that determined the function. For the PDF function, the logical value required was False. In the ReliaPile software, the PDF was created by representing the data as a cumulative function, then fitting normal and lognormal distributions to the nonparametric data using the weighted least squares regression method to determine the parameters (μ, σ) which will determine the density function. The PDF graph is plotted in similar fashion to the Excel® process.

The difference in the PDF curves between Figure 4.5 and Figure 4.6, is the result of how the position of the value of interest (X) is measured in relation to the other points within the sample. The Excel® program identified the position by standard score (z), expressed in Eqn. 3.1, which measures how many standard deviations the value of interest (X) is away from the mean.

$$z = \frac{(X - \mu)}{\sigma} \qquad \text{Eqn. 4.1}$$

Where: X is the ratio of Qmeasured/Qpredicted, μ is the mean, and σ is the standard deviation. Whereas, ReliaPile assumes a nonparametric cumulative distribution function (Jabo unpublished) of the data by identifying the position of the value by quantile (x_j), expressed in Eqn.4.2, in which the sample is divided into equal parts and ranked in ascending order (Martinez et al. 2001).

$$x_j = \frac{(j - 0.5)}{n}, j = 1, 2, 3, \ldots n \qquad \text{Eqn. 4.2}$$

Where: n is the sample size. Using the quantile, along with the known mean and standard deviation, the PDF was graphed. The location of the mean value in relation to the x-axis (the Qmeasured/Qpredicted) for the PDF normal distribution is around 1.2 in both the Excel® and ReliaPile graphs. For the PDF lognormal distributions, was around 1.3 in both the Excel® and ReliaPile graphs.

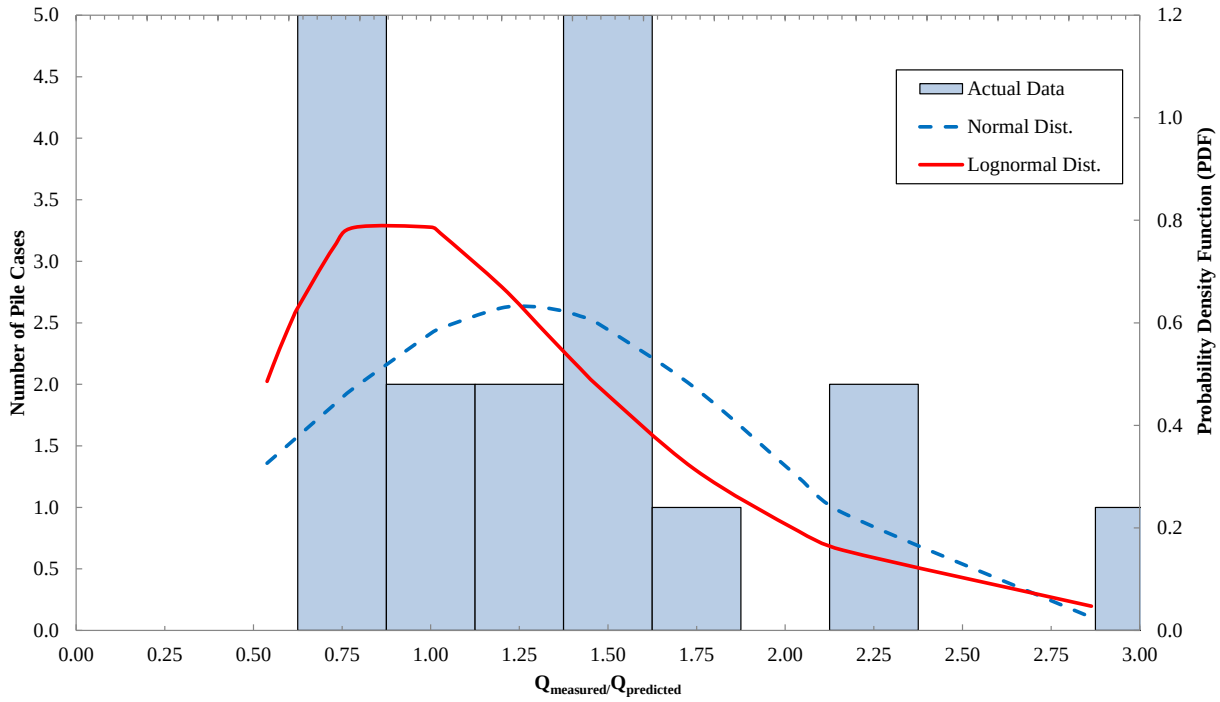

Figure 4.5. Microsoft Excel® probability density function plot (PDF) of steel H-Piles in clay soil (Case 2)

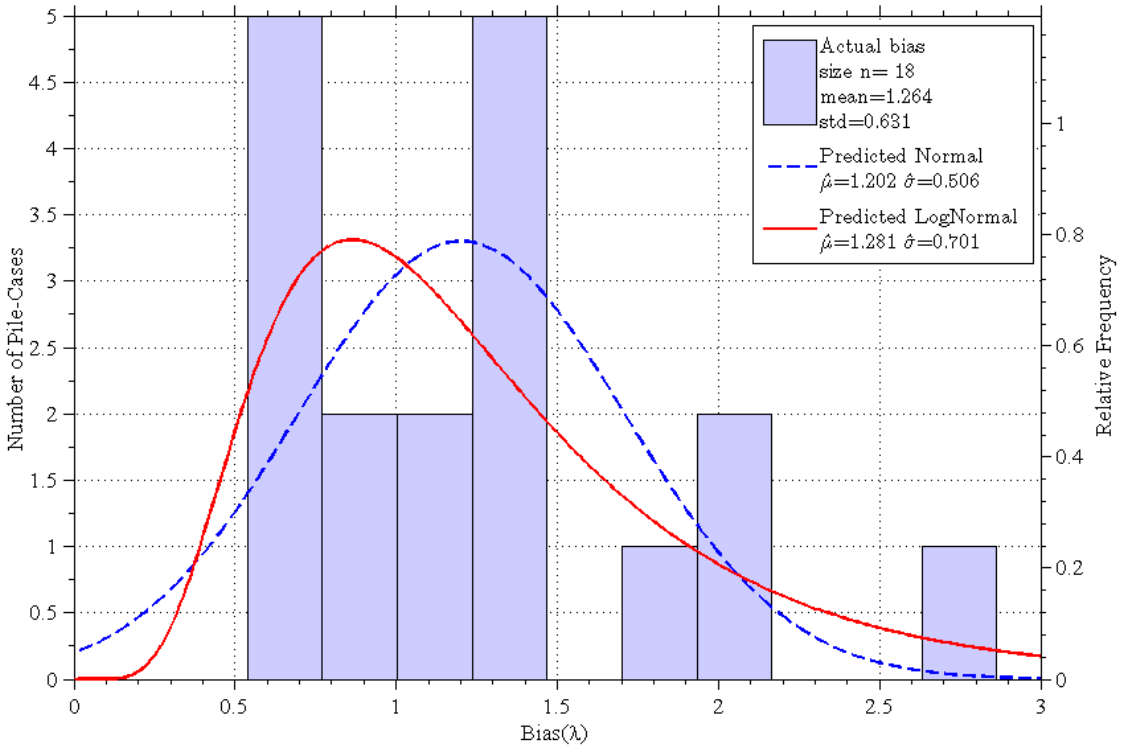

Figure 4.6. ReliaPile probability density function plot (PDF) of steel H-Piles in clay soil (Case 2)

The non-smooth nature of the PDF curve in Figure 4.5 produced in Excel® can be attributed to the fact that the points used in the calculation were specific data points, not data points produced at a regular interval. The PDF curves produced in ReliaPile were more smooth because the points used in the calculations were evenly spaced at regular intervals and smoothing functions were implemented in the program. The more visually appealing presentation of the PDF curves in ReliaPile was further reason to abandon Excel® as a tool for these analyses.

4.2.3 Cumulative Distribution Function (CDF)

The cumulative distribution function (CDF) was established for every load case by following the procedure described below for Case 2. The CDF for steel H-Piles in clay soil (Case 2) is presented in Figure 4.7 and Figure 4.8. Both the normal and lognormal distribution curves were fitted to the data to determine which CDF fit the data the best. In Excel®, the same

functions were utilized as in the PDF, but the logical value required was True to produce a cumulative distribution. In ReliaPile, the CDF follows the procedure expressed in the previous section and graphs the quantile against the ration of Qm/Qp. Visual interpretation of Figures 4.7 and 4.8 indicate that the lognormal distribution appears to fit the data better than the normal distribution. The lognormal statistical parameters for Case 2 are a mean (μ) of 1.281 and standard deviation (σ) 0.701. Table 4.3 summarizes the statistical parameters derived from ReliaPile for all cases.

It is important to note the title of the horizontal axis in both graphs. The Excel® graph in Figure 4.7 identifies the variable as Qmeasured/Qpredicted, while the ReliaPile graph in Figure 4.8 identifies the same variable, Qmeasured/Qpredicted, as the bias (λ), which is a descriptor used in the ReliaPile program. The use of the term bias in ReliaPile to represent the ratio of Qmeasured/Qpredicted must not be confused with the bias (λ_R) in Table 4.3 which represents the mean of Qmeasured/Qpredicted for each case.

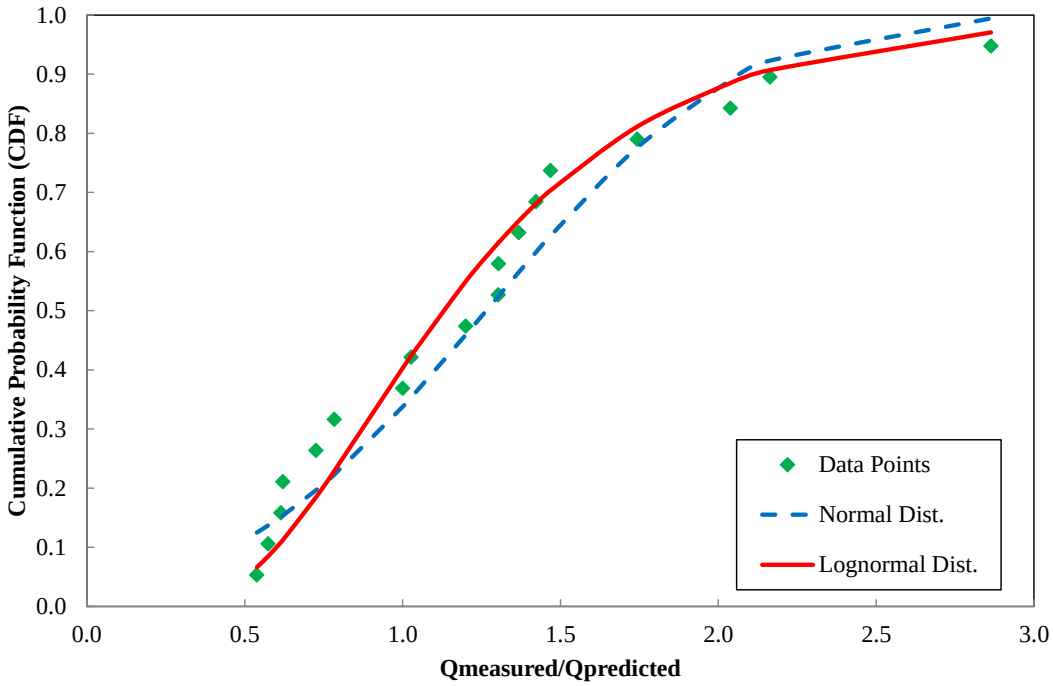

Figure 4.7. Microsoft Excel® cumulative distribution function plot (CDF) of steel H-Piles in clay soil (Case 2)

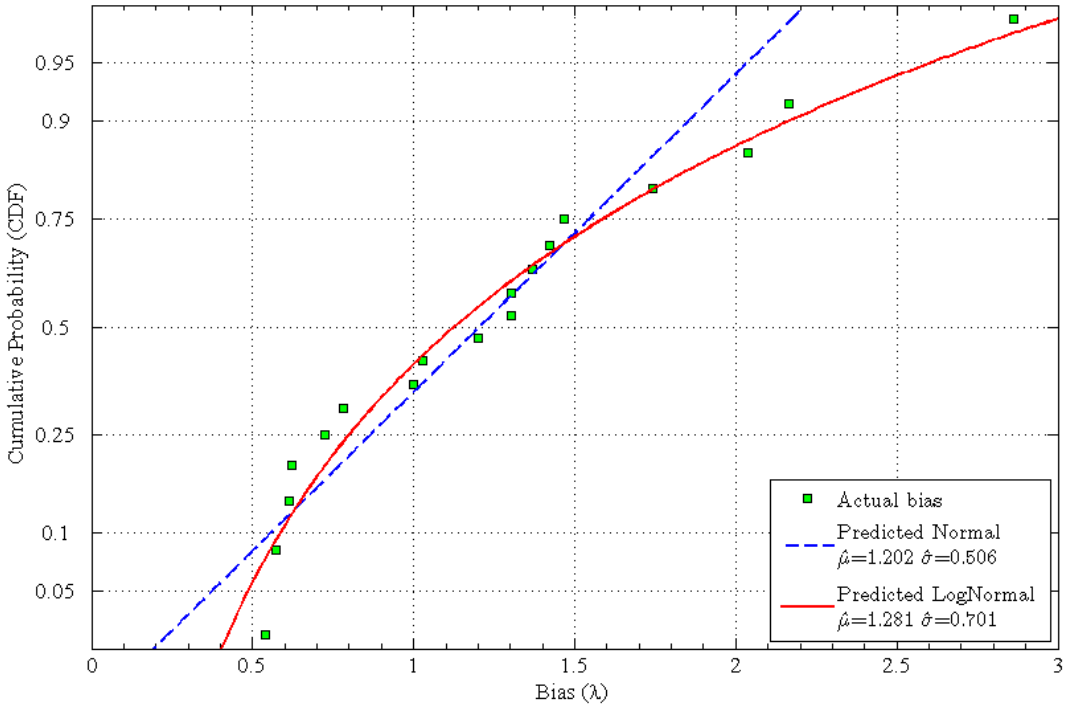

Figure 4.8. ReliaPile cumulative distribution function plot (CDF) of steel H-Piles in clay soil (Case 2)

In reviewing the previous graphs, the y-axis in the CDF graphs, Figure 4.7 for the Excel®, and Figure 4.8 for ReliaPile do not appear to be the same. The y-axis in Excel® plots the corresponding probabilities from the z values at a regular interval. Whereas, the y-axis in ReliaPile plots the quantile values with the corresponding probabilities. Upon identification of the distribution which best represented the sample, the coefficient of variation (COV) was calculated with Eqn. 2.32, using the relevant σ and μ. The COV is an indication of the scatter of the data and a tool used to compare data sets. The COV for Case 2 was determined to be 0.55, which is considered highly variability. High variability in the data is indicated when the COV is ≥ 40%, low variability is indicated when the $COV_x \leq 25\%$, medium variability is identified when $25\% \leq COV_x \leq 40\%$ (Paikowsky 2004). The COV is an important input parameter when evaluating the resistance factor using the various reliability methods.

Table 4.3. Summary of statistical parameters for each group of pile load cases.

Lognormal Distribution		**No. of Piles**	**Mean of the Bias**	**St. Dev. of Qm/Qp**	**COV**	**Variance**
			(λ_R)	(σ_λ)		(σ^2)
Case 1	All Piles EOD	123	1.59	1.00	0.63	0.39
Case 2	H-Piles in Clay EOD	18	1.28	0.70	0.55	0.30
Case 4	H-Piles in Sand EOD	32	1.13	0.46	0.40	0.16
Case 7	PPC Piles in Clay EOD	28	2.91	2.38	0.82	0.66
Case 9	PPC Piles in Sand EOD	20	1.86	1.13	0.60	0.37
Case 10	All Piles BOR	37	1.10	0.36	0.32	0.11
Case 11	Paikowsky Piles EOD	59	1.92	1.14	0.59	0.35

4.2.4 Chi-Squared Goodness-Of-Fit Test

Through visual inspection, the lognormal distribution appeared to fit the data better than the normal distribution, but this must be verified through statistical testing by the goodness of fit test. The Chi-Squared Test was conducted on Case 1 through Case 11 for the CDF data at 95% confidence level to confirm which distribution (normal or lognormal) best fit the data. The results of these analyses are presented in Table 4.4. These analyses were performed using the arithmetic standard deviations determined from Excel® functions and confirmed with the ReliaPile results. To perform the test, the null hypothesis that the distributions were lognormal was evaluated and a Chi-Squared statistical value calculated. The Chi-Squared statistical values were compared against the critical value for the upper bound of a 95% confidence level with nine degrees of freedom. If both the normal and lognormal distributions were accepted (a value less than the critical value), the distribution with the smaller Chi-Squared statistical value had the stronger correlation to the data, and was the chosen distribution. Table 4.4 tabulates the calculated Chi-Squared statistical values determined from Excel® for both distributions in each case and the ReliaPile program check. In the Excel® calculations, the lognormal distributions meet the null hypothesis and were the smaller of the statistical values if both the normal and lognormal met the criteria.

Table 4.4. Chi-Squared Test for Cumulative Distribution Function (CDF) for Case 1 through Case 11

	Excel®		ReliaPile	
Crit. Value	16.92			
	Chi-Square Values (χ^2)			
	Normal	Lognormal	Normal	Lognormal
Case 1	98.49	8.00	Accept	Accept
Case 2	12.00	6.44	Accept	Accept
Case 4	13.63	8.63	Accept	Accept
Case 7	13.43	4.14	Accept	Accept
Case 9	18.00	14.00	Accept	Accept
Case 10	13.13	9.22	Accept	Accept
Case 11	56.42	5.58	Accept	Accept

4.2.5 Confidence Bounds at 95.0% Confidence Level

The confidence interval (CI) provides an estimate of the likelihood a data point will fall within the stated range and a measure of the goodness-of-fit of the distribution. A 95% CI means that 95% of the time, data points will be located within this range. The CI was constructed for the lognormal distribution as described in Section 3.4.5. These confidence bounds are illustrated in Figure 4.9 with Excel® and Figure 4.10 with ReliaPile and demonstrated that the data points for Case 2 did fall with the stated CI. A CI of 95% captured all of the data points for each case with exceptions illustrated in Case 4 and Case 7, each with one data point just outside the bounds.

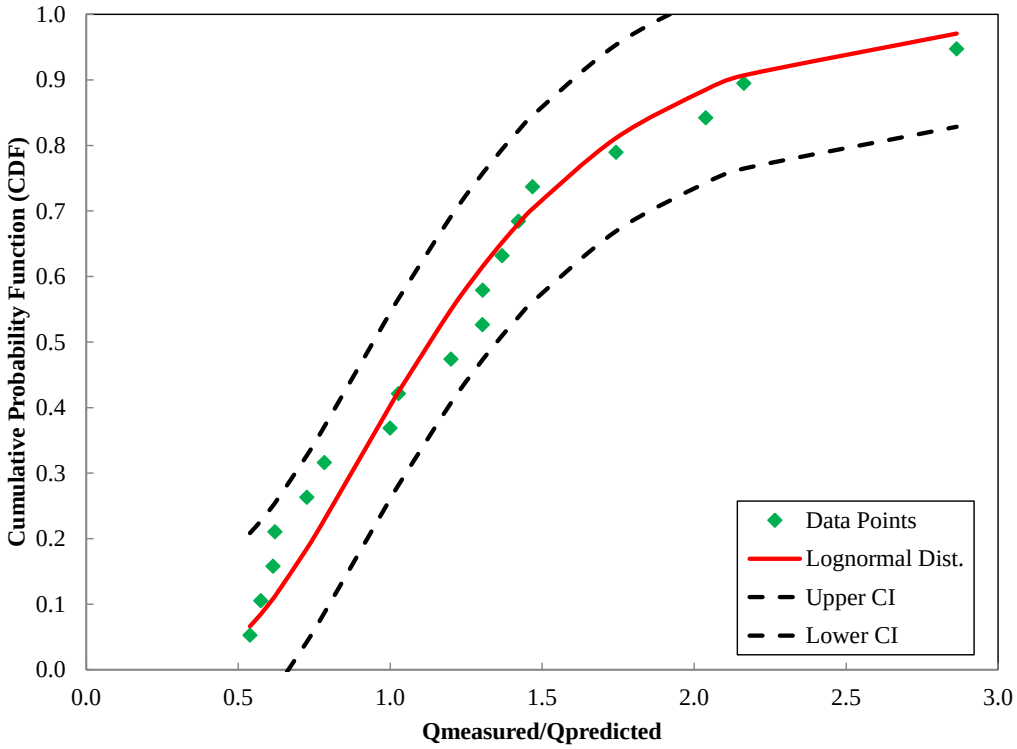

Figure 4.9. Microsoft Excel® confidence bounds for Predicted Log-Normal Distribution at 95.0% Confidence Level of steel H-Piles in clay soil (Case 2)

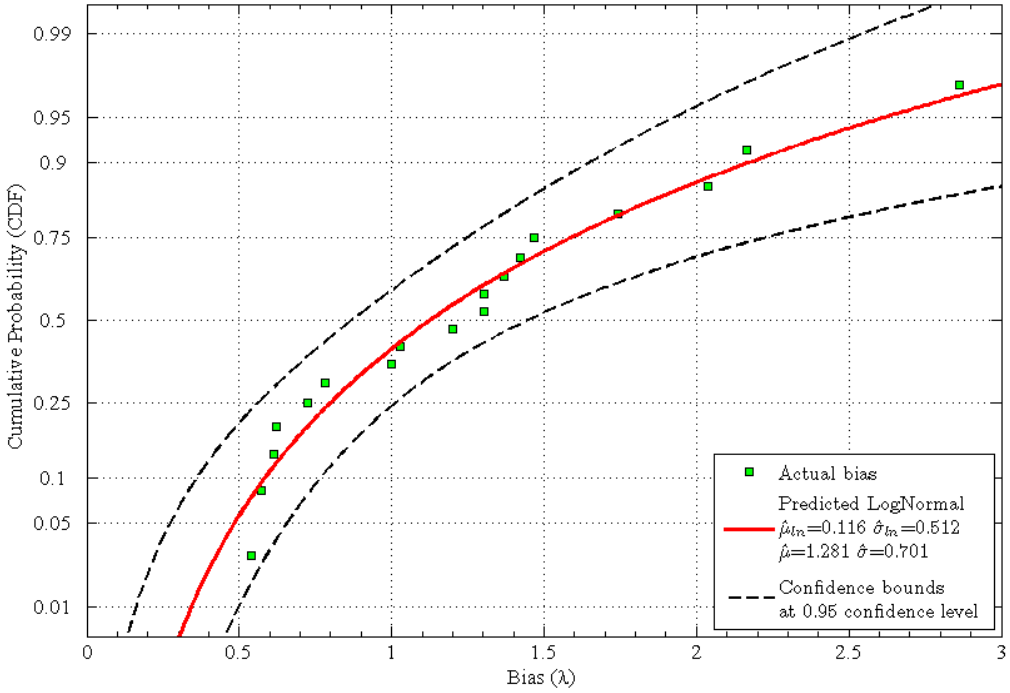

Figure 4.10. ReliaPile confidence bounds for Predicted Log-Normal Distribution at 95.0% Confidence Level of steel H-Piles in clay soil (Case 2)

4.3 Case 4: Steel H-Piles in Sand Soil

Case 4 represents the 32 steel H-piles driven in sandy soil. The regression analysis presented in Figure 4.11 shows a good balance about the LOE, with the regression line having nearly perfect agreement with the LOE at capacities less than 600 kips. An outlying data point with a SLT capacity of 900 kips was identified as a pile from the Paikowsky 2004 report driven in Iowa. Sufficient information was not available to ascertain why this data point was an outlier.

The PDF for steel H-piles in sand soil is represented in Figure 4.12. The observed distribution can be considered log-normally distributed. A lognormal distribution is identified by the CDF in Figure 4.13 and confirmed by the Chi-Squared Test results presented in Table 4.4. The lognormal mean (μ) was 1.130 and the corresponding standard deviation (σ) was 0.456. When a 95% confidence level was applied to the distribution all but one data point fell within the bounds. That single data point was located just outside the CI boundary. Case 4 had a resulting COV of 0.40 (medium variability of λ) and a variance of 0.16.

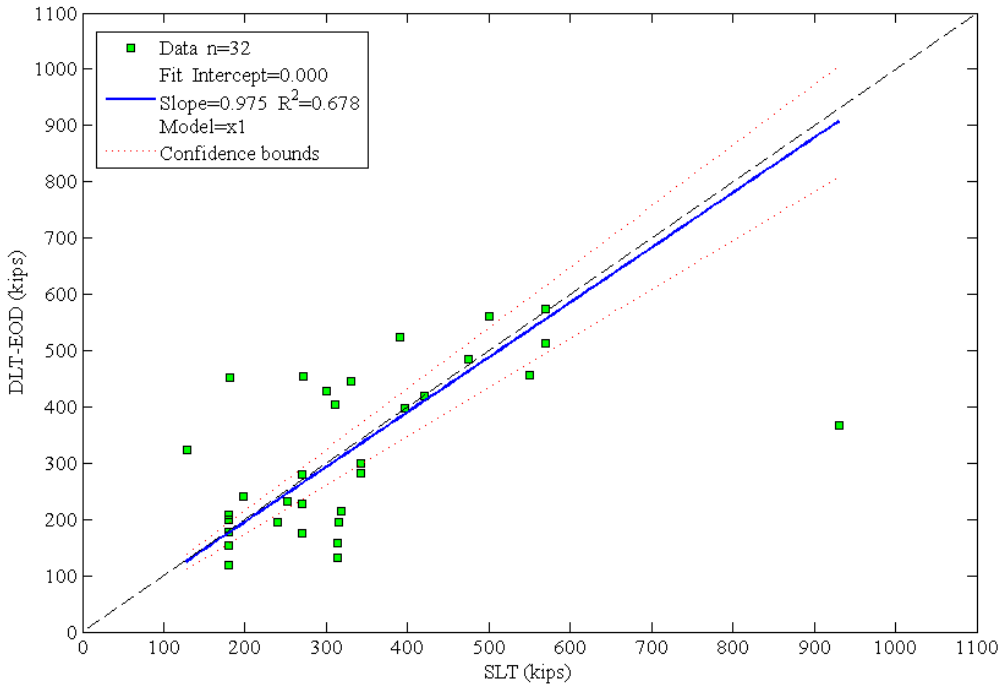

Figure 4.11. ReliaPile linear regression plot for steel H-Piles in sandy soil (Case 4)

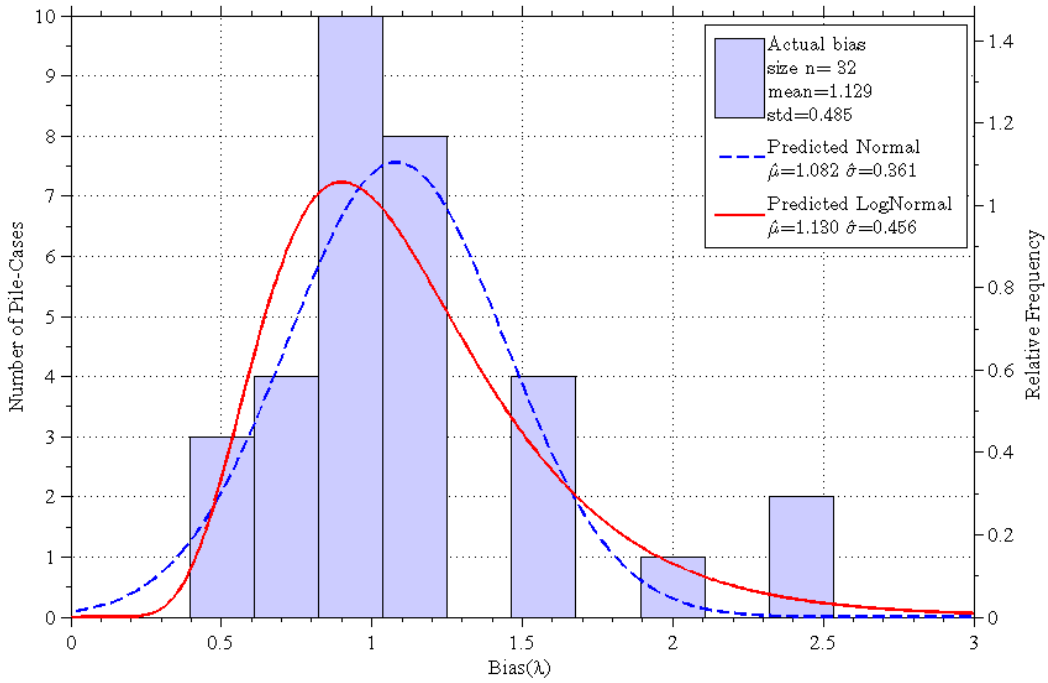

Figure 4.12. ReliaPile probability density function plot (PDF) of steel H-Piles in sandy soil (Case 4)

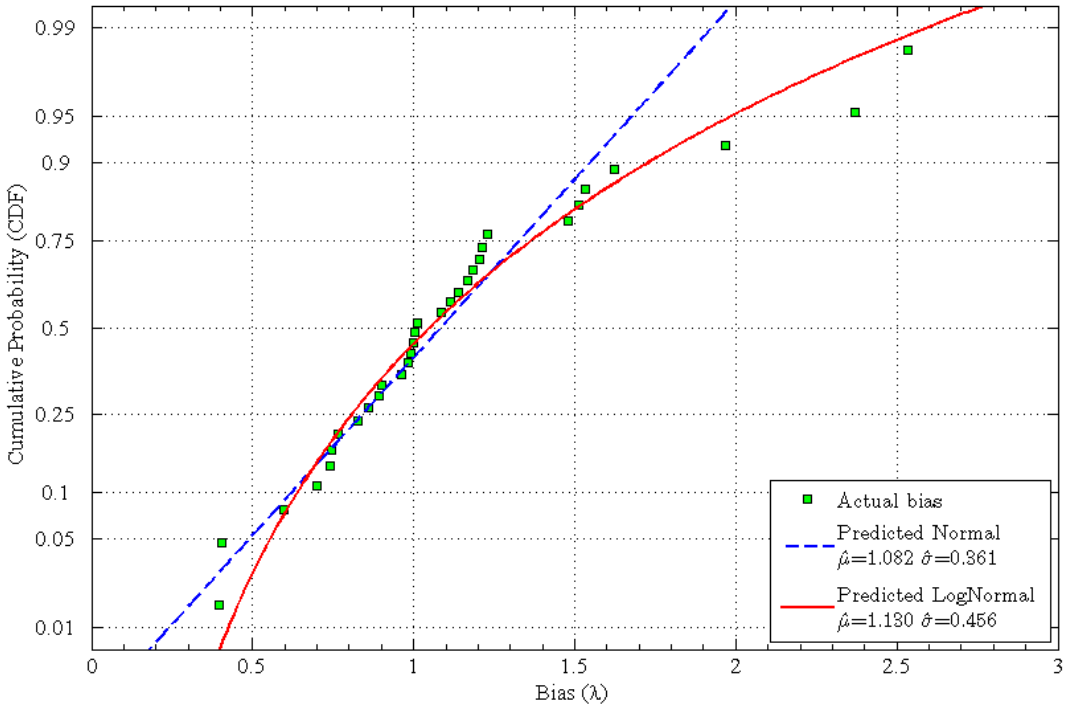

Figure 4.13. ReliaPile cumulative distribution function plot (CDF) of steel H-Piles in sandy soil (Case 4)

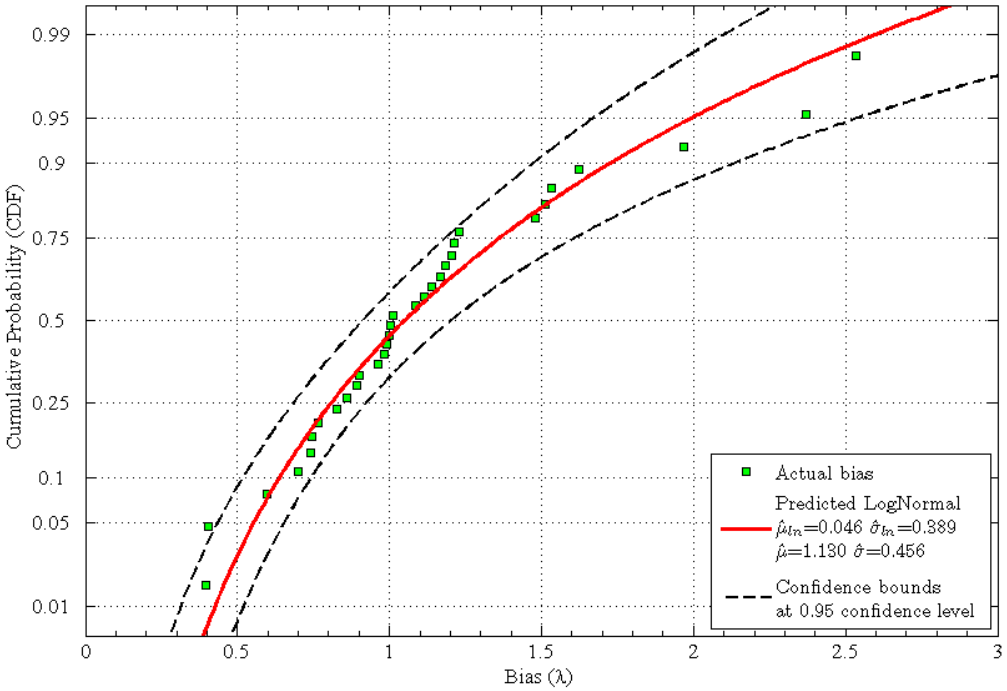

Figure 4.14. ReliaPile confidence bounds for Predicted Log-Normal Distribution at 95.0% Confidence Level of steel H-Piles in sandy soil (Case 4)

4.4 Case 7 and Case 9: Precast Pre-stressed Concrete Piles (PPC/PSC) in Clay and Sand

Case 7 represents precast pre-stressed concrete piles (PPC/PSC) in clay soil and Case 9 represents PPC/PSC piles in sandy soil. The analysis for these cases follows the previous format presented in Section 4.3 and Section 4.4. A summary of properties found are presented in Table 4.3 and the corresponding graphs are located in Appendix B.

4.5 Case 10: All Piles with Beginning of Restrike Capacities

The load tests included in Case 10 were piles where beginning of restrike (BOR) testing occurred and the capacities were recorded. There were 37 load cases where the BOR capacity was available. The regression analysis, as discussed in Section 4.1 and presented in Figure 4.2 indicate a slope of 0.937, near unity, which is expected when comparing SLT to DLT at BOR capacities. The PDF curves in Figure 4.15 did not definitively identify the distribution that best fit the data. However, the subsequent CDF in Figure 4.16 confirms a lognormal distribution with a μ of 1.099 and corresponding σ of 0.357. The Chi-Squared Test further confirmed the lognormal distribution. The applied 95% CI blankets the sample. The COV was 0.32, the lowest of all the cases, indicating low variability within the data expressed in Table 4.3.

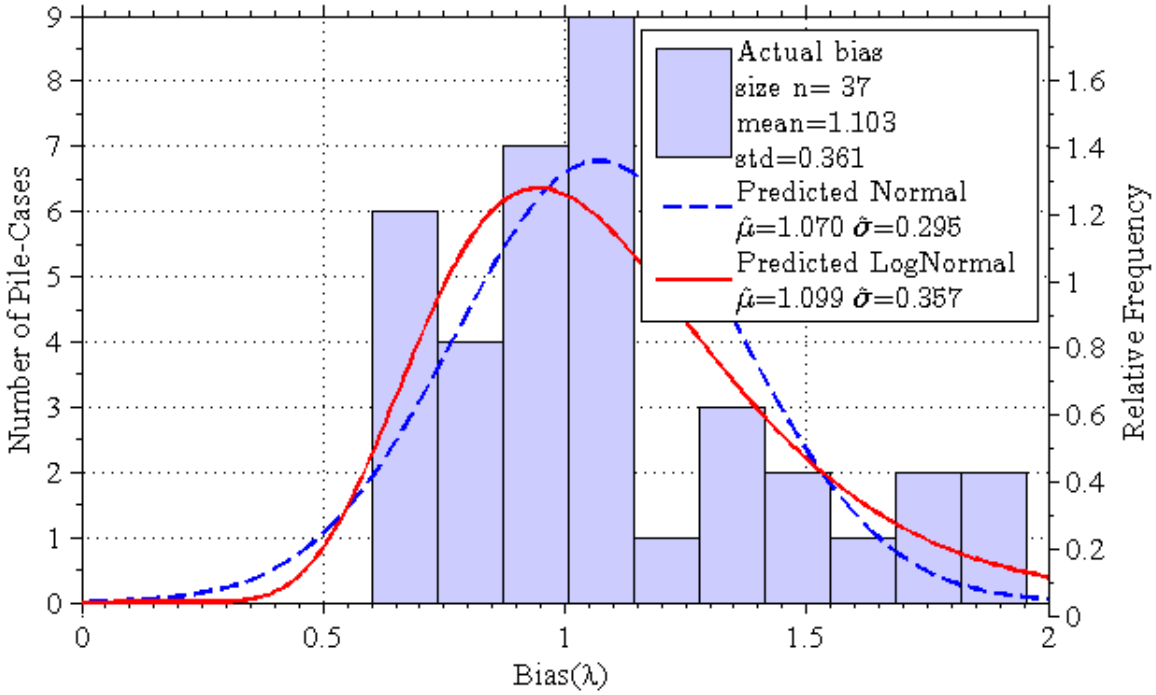

Figure 4.15. ReliaPile probability density function plot (PDF) of all piles with BOR data (Case 10)

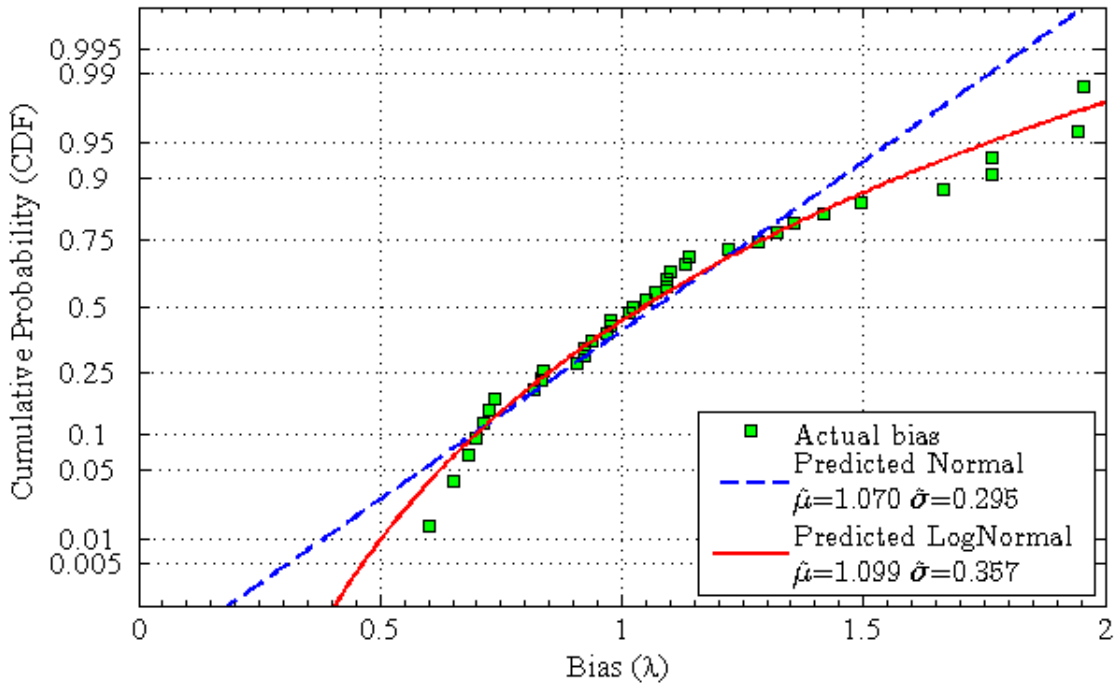

Figure 4.16. ReliaPile cumulative distribution function plot (CDF) of all piles with BOR data (Case 10)

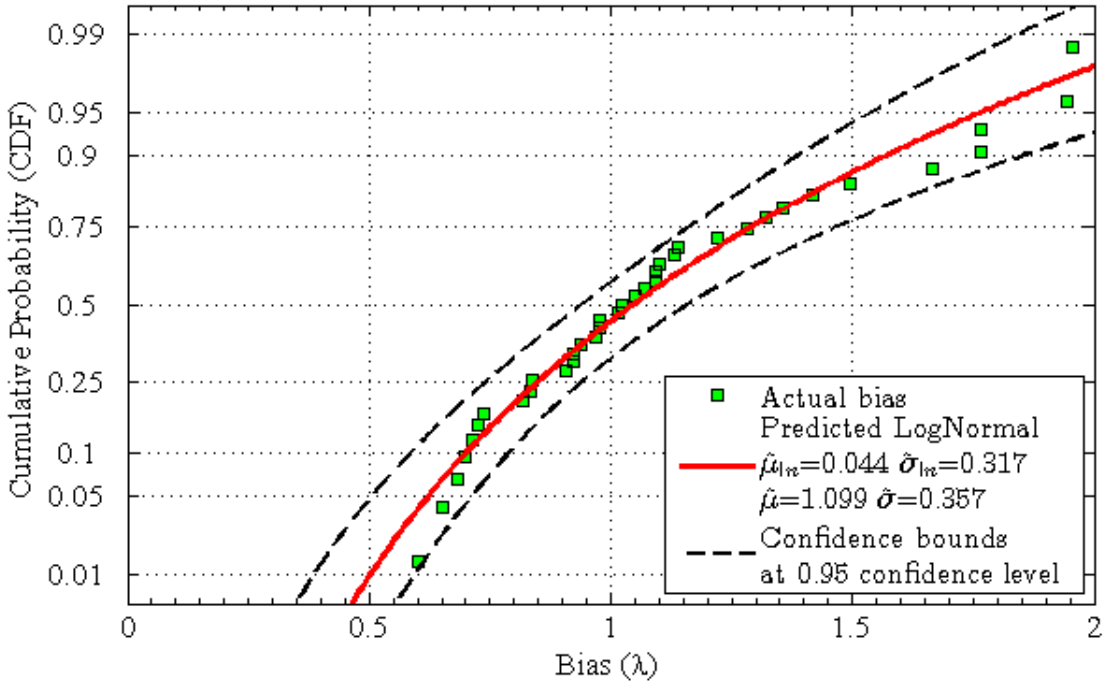

Figure 4.17. ReliaPile confidence bounds for Predicted Log-Normal Distribution at 95% Confidence Level of all piles with BOR data (Case 10).

4.6 Calibration of Resistance (ϕ) Factors

The preliminary steps described in previous sections, which include regression analysis and probability analysis provided necessary parameters, such as the coefficient of variation, the mean, and the standard deviation which were required to proceed with the reliability analysis in the calibration of the resistance factors. The process to determine these resistance factors took a probabilistic approach and utilized the methods of FOSM, FORM, and MCS. This approach required a target reliability index (β_T) which is related to the probability of failure. The probability of failure (p_f) is the percentage failure is expected. This study evaluated two main instances: (1) single piles and non-redundant pile groups with four or fewer piles per pile cap

with β=3.00, resulting in a pf of 0.1%, and (2) pile groups with five or more piles per pile cap with β=2.33 resulting in a pf of 1.0% (Paikowsky et al. 2004).

As described in Chapter 3, the FOSM had two approaches: The Simplified FOSM method utilizes a closed form solution with the assumption that the sum of the COV_Q is simply the sum of the COV for the dead load and COV of the live load (Eqn. 2.24), the second approach, called the Improved FOSM where the COV_Q in the closed form expression is expanded as illustrated in Eqn. 2.40. The resistance factors obtained from the Improved FOSM were higher than those found with the Simplified FOSM. This slight difference was attributed to how the COV_Q term is expressed in Eqn. 2.38 and Eqn. 2.40.

The ϕ factors obtained from FOSM Simplified method were approximately eight percent lower than the ϕ factors obtained by all other reliability methods. The resistance factors derived from the Improved FOSM method were in better agreement with the values obtained from the FORM and MCS methods. Values of resistance (ϕ) factors for both β = 3.00 and β = 2.33, for each load case are presented in Table 4.5.

The cases in this study were evaluated at both β=3.00 and β=2.33 and reported in Table 4.5. The reliability indexes that were selected for comparison are from AASHTO Table 10.5.5.2.3-1 (Table 2.3). According to AASHTO, the resistance factor recommended for a single or non-redundant pile group using DLT with signal matching at BOR conditions is 0.50 (AASHTO 2010), and for a redundant pile group, the resistance factor is 0.65 (AASHTO 2010). It is important to note that Cases 1, 2, 4, 7, 9, and 11 are EOD conditions, not the recommended condition under which to determine resistance factors. These cases clearly show a lower

resistance factor than the AASHTO recommended value of 0.50 and 0.65 for non-redundant and redundant pile group systems.

Table 4.5. Resistance factors (ϕ) for target reliability index (β_T) of 3.0 (non-redundant piles) and 2.33 (redundant piles)

Lognormal Distribution		No. of Piles	Mean of the Bias (λ_R)	COV	Rel. Index (β)	ϕ				AASHTO 2010 BOR	MCS ϕ/λ
						FOSM Simp.	FOSM Imp.	FORM	MCS		
Case 1	All Piles EOD	123	1.59	0.63	3.00	0.28	0.31	0.31	0.31	0.50	0.19
					2.33	0.43	0.46	0.46	0.45	0.65	0.28
Case 2	H-Piles in Clay EOD	18	1.28	0.55	3.00	0.28	0.31	0.31	0.31	0.50	0.24
					2.33	0.41	0.44	0.44	0.44	0.65	0.34
Case 4	H-Piles in Sand EOD	32	1.13	0.40	3.00	0.37	0.41	0.42	0.42	0.50	0.37
					2.33	0.50	0.54	0.54	0.54	0.65	0.48
Case 7	PPC Piles in Clay EOD	28	2.91	0.82	3.00	0.32	0.34	0.34	0.34	0.50	0.12
					2.33	0.53	0.55	0.56	0.55	0.65	0.19
Case 9	PPC Piles in Sand EOD	20	1.86	0.60	3.00	0.35	0.38	0.39	0.38	0.50	0.20
					2.33	0.53	0.56	0.56	0.56	0.65	0.30
Case 10	All Piles BOR	37	1.10	0.32	3.00	0.44	0.51	0.51	0.51	0.50	0.46
					2.33	0.57	0.64	0.64	0.63	0.65	0.58
Case 11	Paikowsky Piles EOD	59	1.92	0.59	3.00	0.37	0.41	0.41	0.41	0.50	0.21
					2.33	0.56	0.59	0.59	0.59	0.65	0.31

However, Case 10 is relevant for AASHTO resistance factor comparison because it contains BOR testing condition; the preferred condition to obtain resistance factors. Analyzing piles at beginning-of-restrike (BOR) produces which is better correlated with the results of static load testing and leads to a ratio of Qmeasured/Qpredicted, closer to unity (Table 4.5). Based on the data collected in this study, both the non-redundant and redundant pile group systems resistance factors of 0.51 and 0.63, respectively, show strong agreement with the AASHTO recommended values.

Another aspect of this analysis was to determine if the soil type (clay, sand, or mixed) and pile type affected the value of the resistance factor. In Table 4.5, of the non-redundant pile group cases at EOD, H-Piles in sand produced the highest resistance factor of 0.42, nearest to the AASHTO recommended. For the redundant pile group cases at EOD, PPC Piles in sand produced the highest resistance factor of 0.56. These observations are preceded with the caveat that these factors were determined with EOD testing and analysis, not the BOR testing and analysis suggested. However, it suggests that a larger database of load tests taken at BOR would possibly allow the segregation of piles by type and soil profile which could lead to higher resistance factors.

4.7 Analysis of Piles in Paikowsky 2004 Report

The resistance factors calculated in Section 4.6 from the reliability methods were in agreement with each other, but they should be checked against a proven baseline. The Paikowsky et al. (2004) report presents a worldwide database, from which the current AASHTO recommended resistance factors were determined. The Paikowsky et al. (2004) study included 338 load tests with SLT and DLT at EOD.

Case 11 was a subset of that database containing 59 piles that were analyzed independently to determine the resistance factors using FOSM, FORM, and MCS. The ϕ factor presented in Table 4.5 for β=3.00 was within 18% of the AASHTO recommended ϕ factor. For β=2.33, the ϕ factor was within 9 % of the AASHTO recommended value presented in Table 4.5. The agreement in resistance factors between this subset of data and the full Paikowsky database tends to validate the process of resistance factor calibration used in this study.

4.8 Efficiency

The resistance factor alone cannot always determine which deign method or, in this instance, which case was most efficient. The efficiency of a given resistance factor is defined in this study to be the ration of the resistance factor over the mean value of the ratio of measured to predicted capacity, ϕ/λ. The ϕ factors use to determine efficiency were taken from the MCS analyses because MCS is the AASAHTO recommended method for reliability analysis. When comparing the 11 cases, high levels of efficiency correspond to those cases where the COV values were low. The data, presented in Table 4.5, indicates Case 10 is the most efficient of all the cases with an efficiency of 0.46 (non-redundant piles) and 0.58 (redundant piles). This further confirms the fact that BOR data is a better indicator of static capacity.

4.9 BOR Resistance Factors with Reliability Indexes

From the information developed in this study it is clear that evaluation of driven piles at BOR is the preferred method to determine resistance factors. Case 10 allowed for a comparison between the AASHTO recommended resistance factors at two reliability indexes with the values determined using this database. The database objective was to contain load cases that were representative of piles driven in soils similar to those found in Arkansas, to evaluate the suitability of the AASHTO recommended resistance factors for the Arkansan environment. The

comparison included only the values obtained from the MCS analysis, as this is the preferred probability analysis (Paikowsky et al. 2010). The analysis correlated with the reliability indexes of 3.05 and 2.28 for redundant and non-redundant groups when evaluated with the AASHTO criteria using the MCS results.

4.10 Summary

In general the ϕ factors determined in this study for EOD capacities were lower than the AASHTO recommended values by 30% when considering only EOD capacities. However, when considering Case 10, where the BOR capacities were used, the factors were very similar to the AASHTO recommended values. The low resistance factors obtained for EOD capacities further reinforces the AASHTO recommendation that EOD data should not be used for pile acceptance. The lack of improvement in resistance factors from this study may be due to the quality of the data reported in the literature or the limited quantity of data in some of the load cases categories considered in this study. Some data points, that might be considered outliers, could not be fully evaluated because the information necessary to make such a decision was not included in the parent document. The grouping of the data may also have impacted the results; more detailed soil information which would allow better soil classification, pile capacity development information (end bearing versus friction piles), or more load tests for each case may have changed the way pile load tests were grouped with a resulting positive impact on the resistance factors. Improvements are possible with more BOR data in each pile/soil groupings.

5 Conclusions

Pile capacity prediction is a necessity to insure safe and economical foundations for structures of all types. Pile capacity is most accurately measured through static load testing (SLT) but with an associated high cost and time requirement. More economical methods, such as dynamic load testing (DLT), are available to predict pile capacity. The comparison of capacities measured using SLT to those derived through DLT provides a reference tool when only DLT methods are used to determine pile capacity in the field.

Resistance factors were developed in this study that may be considered specific to the landforms found in the State of Arkansas. These resistance factors were obtained by conducting reliability analyses on a database of 138 load tests. The load tests were conducted at sites with subsurface conditions similar to the conditions found within the State of Arkansas. The reliability analyses consisted of First Order Second Moment, First Order Reliability Method, and Monte Carlo Simulation. The following conclusions may be inferred from the data:

1. In many cases the data available in the literature for individual load tests was insufficient to determine why a load test might be considered an outlier; this resulted in potentially higher coefficients of variation and correspondingly lowers resistance factors.
2. Segregating piles into categories had the general effect of reducing resistance factors rather than improving them.
3. The simplified FOSM method resulted in lower values for resistance factors and should not be used for the calibration of resistance factors.
4. The Improved-FOSM, FORM or MCS all produce resistance factors (ϕ) that are nearly identical and are approximately 10% higher than the resistance factors derived from the simplified FOSM method. While the MCS is the AASHTO preferred reliability method,

the analyses show the Improved-FOSM produces similar resistance factors and requires far less computing capability.

5. Capacities derived from BOR information more closely mirror the capacities measured from static load tests with less variance than capacities derived from EOD data.
6. Resistance factors derived from this study when using cases with EOD data are approximately 30 percent lower than those suggested by AASHTO 2010.
7. Based on the results of this study, only data from the BOR dynamic testing should be used to ascertain pile capacity.

5.1 Future Work

With the observed results from the resistance factor determination, it is evident that subsequent research is required to achieve more definitive results in the classification of soil and more data is required to create statistically significant sample populations when grouping by pile type. It is recommended that:

1. Since segregating piles into categories had the general effect of reducing resistance factors rather than improving them. The creation of a more complete database that includes:
    a. Significantly more load cases.
    b. Complete soil information, for all load test which includes strength parameters
    c. Contain SLT information from load tests carried to the Davison Offset failure criteria and contain DLT information at BOR.
    d. Contain sufficient driving information to determine why a load test might be considered an outlier.
    e. Known the time lapse between driving and BOR or SLT

f. More complete information from signal matching to include damping factors (quakes and side resistance) and the level of signal match quality.

2. Generate new load test data within the State of Arkansas that includes high quality soils data and well supervised SLT and DLT information.

References

AASHTO. (2010). LRFD Bridge Design Specifications (5th ed.) with 2010 Interim Revisions. Washington, D. C. American Association of State Highway and Transportation Officials. Online: http://app.knovel.com/hotlink/toc/id:kpAASHTO11/aashto-lrfd-bridge-design-3. Accessed June 2013.

Abu-Farsakh, M. Y., Yoon, S., and Tsai, C. (2009). Calibration of Resistance Factors Needed in the LRFD Design of Driven Piles. No. FHWA/LA. 09/449.

AHTD. (2007). Arkansas 2003 Standard Specification for Highway Construction. Arkansas State Highway and Transportation Department. Section 805. 731-759.

Allen, T. M. (2005). Development of the WSDOT Pile Driving Formula and its Calibration for Load and Resistance Factor Design (LRFD). No. WA-RD 610.1.

Alvarez, C., Zuckerman, B., and Lemke, J. (2006). Dynamic Pile Analysis Using CAPWAP and Multiple Sensors. In ASCE GEO Congress: Atlanta, Georgia. (CD-ROM).

American Petroleum Institute. (1984). Recommended Practice for Planning, Designing and Constructing Fixed Offshore Platforms (15th ed.). Code RP 2A. Dallas, TX.

Arkansas Geological Survey (AGS). General Geology. Online: http://www.geology.ar.gov/geology/general_geology.htm. Accessed September 2012.

ASTM Standard D1143/D1143M. (2007). Standard Test Method for Deep Foundations under Axial Compressive Load. ASTM International. West Conshohocken, PA.

ASTM Standard D4945. (2008). Standard Test Method of High-Strain Dynamic Testing of Deep Foundations. ASTM International, West Conshohocken, PA.

ASTM Standard D7383. (2008). Standard Test Methods for Axial Compressive Force Pulse (Rapid) Testing of Deep Foundations. ASTM International, West Conshohocken, PA.

Baecher, G. B., and Christian, J. T. (2003). Reliability and Statistics in Geotechnical Engineering. John Wiley & Sons Inc.

Barker, R., Duncan, J., Rojiani, K., Ooi, P., Tan, C., and Kim, S. (1991). NCHRP Report 343: Manuals for the Design of Bridge Foundations. TRB, National Research Council, Washington, DC.

Bradshaw, A. S., and Baxter, C. D. (2006). Design and Construction of Driven Pile Foundations-Lessons Learned on the Central Artery/Tunnel Project. No. FHWA-HRT-05-159.

Brown, D. A., & Thompson, W. R. (2011). Developing Production Pile Driving Criteria from Test Pile Data. NCHRP Synthesis 418. Transportation Research Board.

Chrimes, M. (2008). Geotechnical Publications before Geotechnique. Geotechnique, 58(5), 343-355.

Coduto, D.P. (2001). Foundation Design: Principles and Practices (2nd ed.). Prentice Hall Inc., New Jersey.

Coe, D. (2009). Fisher Matrices and Confidence Ellipses: A Quick-Start Guide and Software. Accessed June 2013.

Davisson, M. T. (1972). High Capacity Piles. In Proceedings of Soil Mechanics Lecture Series on Innovations in Foundation Construction. American Society of Civil Engineers. Illinois Section. Chicago, IL. 81 - 112.

DeBeer, E. E. (1968). Proefondervindlijke bijdrage tot de studie van het grensdraag vermogen van zand onder funderingen op staal. Tijdshift der Openbar Verken van Belgie, No. 6.

Decourt, L. (1999). Behavior of Foundations under Working Load Conditions. Proceedings of the 11th Pan-American Conference on Soil Mechanics and Geotechnical Engineering. Foz DoIguassu, Brazil. Vol. 4. 453 - 488.

DOI. (2008). Louisiana: Reasonably Foreseeable Development Scenario for Fluid Minerals. U.S. Department of the Interior. Bureau of Land Management Eastern States, Jackson Field Office. Jackson, MS. Online: http://www.blm.gov. Accessed September 2012.

Fellenius, B. H. (1999). Using the Pile Driving Analyzer. Pile Driving Contractors Association, PDCA. Annual Meeting, San Diego, CA.

Fellenius, B. H. (2001). What Capacity Value to choose from the Results of a Static Loading Test. Paper presented at the Fulcrum, Deep Foundation Institute New Jersey.

FHWA. (1998). Driven 1.0: A Microsoft Windows™ Based Program for Determining Ultimate Vertical Static Pile Capacity. Federal Highway Administration. Publication No. FHWA-SA-98-074.

FHWA. (2001). Load and Resistance Factor Design (LRFD) for Highway Bridge Substructures. Reference Manual and Participant Workbook. Federal Highway Administration. NHI Course No. 132068. Publication No. FHWA HI-98-032.

Fragaszy, R. J., Higgins, J. D., & Lawton, E. C. (1985). Development of Guidelines for Construction Control of Pile Driving and Estimation of Pile Capacity-Phase I-Final Report. WA-RD 68.1, Washington State Transportation Center (TRAC).

GRL Engineers, Inc. (2014). About Dynamic Foundation Testing. Online: http://www.pile.com/aboutdynamictesting/. Accessed May 7, 2014.

Goble, G. (2008). Driven Pile Installation and Capacity Determination. Application of Dynamic Methods to the Design and Installation of Driven Piles. The 2007 Karl Terzaghi Lecture. American Society of Civil Engineers.

Goble, G. G., and Hussein, M. H. (2000). Deep foundation capacity—What is it? Proceeding. Performance Confirmation of Constructed Geotechnical Facilities. GSP No. 94, ASCE, Reston, VA.

Goble, G. G., Likins, G. E., and Rausche, F. (1975). Bearing Capacity of Piles from Dynamic Measurements. Ohio Department of Transportation. Cleveland, OH.

GRL-PDI. (2000). Deep Foundations: Believing Without Seeing. Newsletter No. 38. Goble Rausche Likins and Associates, Inc. and Pile Dynamics, Inc. Cleveland, OH.

Hammersley, J. M., and Handscomb, D. C. (1964). Monte Carlo Methods, Methuen's Monographs on Applied Probability and Statistics. Methuen & Co., London.

Hannigan, P. (2009). Special Design and Construction Considerations. Pile Driving Contractors Association. Online: http://www.piledrivers.org/pdpi-lectures.htm. Accessed May 2013.

Hannigan, P.J., Goble, G.G., Likins, G.E. and Rausche, F. (2006). Design and Construction of Driven Pile Foundations Reference Manual –Volume II. Publication No. FHWA NHI-05-043. National Highway Institute. Federal Highway Administration.

Hannigan, P. J., Goble, G. G., Thendean, G., Likins, G. E., and Rausche, F. (1998). Design and Construction of Driven Pile Foundations, Workshop Manual. Vol. 2. Publication No. FHWA-HI-97-014. Federal Highway Administration. Washington, DC.

Hansen, J. B. (1963). Discussion on Hyperbolic Stress-Strain Response. Cohesive Soils. American Society of Civil Engineers. Journal for Soil Mechanics and Foundation Engineering. Vol. 89 (SM 4). 241 – 242.

Heiberger, R. M. and Becker, R. A. (1992). Design of an S Function for Robust Regression Using Iteratively Reweighted Least Squares. Journal of Computational and Graphical Statistics, American Statistical Association, Institute of Mathematical Statistics, and Interface Foundation of America. Vol. 1. No. 3. Article DOI: 10.2307/1390715. 181-196.

Hill, J. W. (2007). Evaluation of Load Tests for Driven Piles for the Alabama Department of Transportation. (Master's Thesis). Auburn University, Auburn, AL.

Jabo, J. (unpublished b). ReliaPile 1.0: A MATLAB® Based Program for Analyzing Pile Capacity Distribution and LRFD Calibration for Driven Piles. User's Manual.

Kolsky, H. (1963). Stress Waves in Solids (Vol. 1098). Dover Publication, Inc.

Kraft, L. M., Amerasinghe, S. F., and Focht, J. A. (1981). Friction Capacity of Piles Driven into Clay. Journal of the Geotechnical Engineering Division. Vol. 107(11). 1521-1541.

Kroese, D. P., Taimre, T., & Botev, Z. I. (2011). Handbook of Monte Carlo Methods. John Wiley & Sons, Inc. Hoboken, New Jersey

Kyfor, Z.G., Schnore, A.S., Carlo, T.A. and Bailey, P.F. (1992). Static Testing of Deep Foundations. Federal Highway Administration. Report No. FHWA-SA-91-042, U.S. Department of Transportation

Likins, G., Fellenius, B., and Holtz, R. (2012). Pile Driving Formulas: Past and Present. Full-Scale Testing and Foundation Design. 737-753.

Loadtest USA. (2012). Telephone interview.

Long, J. H., Hendrix, J., and Jaromin, D. (2009). Comparison of Five Different Methods for Determining Pile Bearing Capacities. No. WisDOT 0092-07-04. Wisconsin Highway Research Program.

Long, J. H., Kerrigan, J. A., and Wysockey, M. H. (1999). Measured Time Effects for Axial Capacity of Driven Piling. Transportation Research Record: Journal of the Transportation Research Board. 1663(1). 8-15.

MathWorks, Inc. (2005). MATLAB: the language of technical computing. Desktop tools and development environment, version 7. Vol. 9. MathWorks.

Maier, H. R., Lence, B. J., Tolson, B. A., and Foschi, R. O. (2001). First-order reliability method for estimating reliability, vulnerability, and resilience. Water Resources Research. 37(3). 779-790.

Meyerhof, G. (1976). Bearing Capacity and Settlement of Pile Foundations. Journal of the Geotechnical Engineering Division. American Society of Civil Engineers. 102(3). 195-228.

Middendorp, P. (2000). Statnamic: The Engineering of Art. In Proceedings of the 6th International Conference on the Application of Stress Wave Theory to Piles. Sao Paulo, Brazil.

Miller, I. and Freund, J. E. (1985). Probability and Statistics for Engineers. Third edition. Englewood Cliffs, NJ: Prentice-Hall.

Neale, M. C., & Miller, M. B. (1997). The Use of Likelihood-Based Confidence Intervals in Genetic Models. Behavior Genetics, 27(2), Kluwer Academic Publishers-Plenum Publishers, pp. 113-120.

Nordlund, R. L. (1963). Bearing Capacity of Piles in Cohesionless Soils. American Society of Civil Engineers. Journal of Soil Mechanics and Foundation Engineering. Vol. 89 (SM 3). 1-35.

Olson, R. E., and Flaate, K. S. (1967). Pile-Driving Formulas for Friction Piles in Sand. Journal of Soil Mechanics and Foundation Division. ASCE, No. SM 6, 279−296.

Paikowsky, S. G. (2002). Load and Resistance Factor Design (LRFD) for Deep Foundations. Proceedings of IWS Kamakura 2002 Foundation Design Codes and Soil

Investigation in view of International Harmonization and Performance. Tokyo, Japan. 59-94

Paikowsky, S. G., Canniff, M. C., Lesny, K., Kisse, A., Amatya, S., and Muganga, R. (2010). LRFD design and construction of shallow foundations for highway bridge structures. NCHRP Report 651. Transportation Research Board. Washington, DC.

Paikowsky, S. G., Kuo, C., Baecher, G., Ayyub, B., Stenersen, K., .,…and O'Neill, M. (2004). Load and Resistance Factor Design (LRFD) for Deep Foundations. NCHRP Report 507. Transportation Research Board. Washington, DC.

Patev, R. C. (2010). Risk Technology Workshop: Engineering Reliability Concepts, Introduction to Engineering Reliability. United States Army Corps of Engineers.

PDI. (2002). Dynamic Pile Testing with the Pile Driving Analyzer. Quality Assurance for Deep Foundations. Pile Dynamics, Inc. Online: http://www.dot.state.oh.us/Divisions/ Engineering/ Structures/standard/Geotechnical/Documents/ODOT. Accessed October 2012.

PDI. (2012). Pile Dynamics, Inc. Telephone interview.

Phoon, K. K., Kulhawy, F. H., & Grigoriu, M. D. (2003). Development of a reliability-based design framework for transmission line structure foundations. Journal of Geotechnical and Geoenvironmental Engineering. 129(9). 798-806.

Raychaudhuri, S. (2008). Introduction to Monte Carlo Simulation. In Simulation Conference, 2008. WSC 2008. IEEE. 91-100.

Reese, L. C., Isenhower, W. M., Wang, and Shin-Tower (2006). Analysis and Design of Shallow and Deep Foundations. John Wiley & Sons, Inc. Hoboken, New Jersey.

Rubinstein, R. Y. (1981). Simulation and the Monte Carlo Method. John Wiley & Sons, Inc. New York.

Smith, E. A. (1962). Pile-Driving Analysis by the Wave Equation. American Society of Civil Engineers Transactions. Vol. 27. 1145–1193.

Statnamic Load Testing Overview. Applied Foundation Testing. Inc. Online: http://www.testpile.com/PDF/Statnamic%20Testing%20Brief%20Overview%20for%20Web%20Site.pdf. Accessed August 2012.

Steele, R., Seidel, J., and Klingberg, D., (1990). Test Piling Program for Bridges on the Sunshine Motorway in Queensland. Australian Road Research Board (ARRB) Conference. 15th. Darwin, Northern Territory. 139-153.

Terzaghi, K., Peck, R. B., and Casagrande, A. (1942). Discussion of Pile Driving Formulas: Progress Report of the Committee on the Bearing Value of Pile Foundation. Proceedings of the American Society of Civil Engineers. Vol. 68. 311-323.

Thendean, G., Rausche, F., Svinkin, M., Likins, G. E. (1996). Wave Equation Correlation Studies. Proceedings of the Fifth International Conference on the Application of Stress-wave Theory to Piles 1996. Orlando, FL. 144-162.

Tomlinson, M. J. (1957). The Adhesion of Piles Driven in Clay Soils. In Proceedings of the 4th International Conference on Soil Mechanics and Foundation Engineering. London, England.

Ulitskii, V. M. (1995). History of Pile Foundation Engineering. Soil Mechanics and Foundation Engineering. 32(3). 110-114.

Valsamosa, G., Casadeia, F., Solomos, G. (2013). A Numerical Study of Wave Dispersion Curves in Cylindrical Rods with Circular Cross-Section. Applied and Computational Mechanics. Vol. 7. 99–114.

Vijayvergiya, V. N. and Focht, J. A. (1972). A New Way to Predict the Capacity of Piles in Clay.

Proceeding: 4th Offshore Technology Conference. Houston, TX. Vol. 2. 865-874.

Walton, P. A., and Borg, S. L. (1998). Using Dynamic Pile Testing To Evaluate Quality and Verify Capacity of Driven Piles. Transportation Research Record. Journal of the Transportation Research Board. Vol. 1633(1). 117-119.

Woo, C. (2013). Fisher Information Matrix. http://planetmath.org/sites/default/files/texpdf /36041.pdf. Accessed June 20, 2014.

Yoon, S., Tsai, C., and Melton, J. M. (2011). Pile Load Test and Implementation of Specifications of Load and Resistance Factor Design. Transportation Research Record. Journal of the Transportation Research Board. 2212(1), 23-33.

Appendix A – Load Test Database

Table A.1. Load test database

Pile No.	Location	Paper/Project	Pile Type	Soil Type	SLT (kips)	DLT - EOD (kips)	DLT-BOR w/PDA (kips)
1	Alabama	ALDOT-2007	HP 10x42	clay	240	240	
2	Alabama	ALDOT-2007	HP 10x42	clay	174	222	
3	Alabama	ALDOT-2007	HP 10x42	Mixed	120	180	
4	Alabama	ALDOT-2007	HP 10x42	sand	252	232	
5	Alabama	ALDOT-2007	HP 10x42	sand	240	195	220
6	Alabama	ALDOT-2007	HP 12x53	clay	360	300	318
7	Alabama	ALDOT-2007	HP 12x53	clay	366	210	512.8
8	Alabama	ALDOT-2007	HP 12x53	Mixed	180	358	275.4
9	Alabama	ALDOT-2007	HP 12x53	Mixed	180	220	264
10	Alabama	ALDOT-2007	HP 12x53	MIxed	192	240	98.2
11	Alabama	ALDOT-2007	HP 12x53	Mixed	198	176	149.8
12	Alabama	ALDOT-2007	HP 12x53	sand	180	154	
13	Alabama	ALDOT-2007	HP 12x53	sand	270	176	276
14	Alabama	ALDOT-2007	HP 12x53	sand	270	228	
15	Alabama	ALDOT-2007	HP 12x53	sand	180	178	
16	Alabama	ALDOT-2007	HP 12x53	sand	180	200	214.8
17	Alabama	ALDOT-2007	HP 12x53	sand	180	209	300
18	Alabama	ALDOT-2007	HP 12x53	sand	180	119	216
19	Alabama	ALDOT-2007	HP 12x53	sand	420	419	327.4
20	Alabama	ALDOT-2007	HP 12x53	sand	198	240	132.4
21	Alabama	ALDOT-2007	HP 12x84	clay	180	122.6	
22	Alabama	ALDOT-2007	HP 14x73	clay	378	290	410
23	Alabama	ALDOT-2007	HP 14x73	clay	380	370	
24	Alabama	ALDOT-2007	HP 14x73	Mixed	324	268	346
25	Alabama	ALDOT-2007	HP 14x73	sand	342	282	241.4
26	Alabama	ALDOT-2007	HP 14x89	Mixed	342	256	
27	Alabama	ALDOT-2007	HP 14x89	sand	270	280	366
28	Alabama	ALDOT-2007	HP 14x89	sand	342	300	193.8
29	Alabama	ALDOT-2007	PSC 14" Square	sand	300	360	
30	Alabama	ALDOT-2007	PSC 24" Square	sand	690	998	657

Table A.1 Cont.

Pile No. (Cont.)	Location (Cont.)	Paper/Project (Cont.)	Pile Type (Cont.)	Soil Type (Cont.)	SLT (kips) (Cont.)	DLT - EOD (kips) (Cont.)	DLT-BOR w/PDA (kips) (Cont.)
31	Alabama	ALDOT-2007	PSC 24" Square	sand	690	820	707.2
32	MA	C/A Tunnel Project	PIPE	clay	807	626	595
33	MA	C/A Tunnel Project	PIPE	clay	646	575	604
34	MA	C/A Tunnel Project	PIPE	sand	486	372	445
35	MA	C/A Tunnel Project	PIPE	sand	544	408	562
36	MA	C/A Tunnel Project	PPC 31 cm	clay	340	374	415
37	MA	C/A Tunnel Project	PPC 31 cm	clay	228	261	327
38	MA	C/A Tunnel Project	PPC 41 cm	clay	702		730
39	MA	C/A Tunnel Project	PPC 41 cm	clay	800		836
40	MA	C/A Tunnel Project	PPC 41 cm	clay	775	950	1070
41	MA	C/A Tunnel Project	PPC 41 cm	clay	775	578	758
42	MA	C/A Tunnel Project	PPC 41 cm	clay	850	370	510
43	MA	C/A Tunnel Project	PPC 41 cm	clay	698	604	634
44	MA	C/A Tunnel Project	PPC 41 cm	clay	812	453	418
45	MA	C/A Tunnel Project	PPC 41 cm	clay	800	344	453
46	MA	C/A Tunnel Project	PPC 41 cm	sand	570	537	628
47	Louisiana	LADOTD-2009	PPC 14" Square	clay	230		226.8
48	Louisiana	LADOTD-2009	PPC 14" Square	clay	344		300.2
49	Louisiana	LADOTD-2009	PPC 14" Square	clay	330		133

Table A.1. Cont.

Pile No. (Cont.)	Location (Cont.)	Paper/Project (Cont.)	Pile Type (Cont.)	Soil Type (Cont.)	SLT (kips) (Cont.)	DLT - EOD (kips) (Cont.)	DLT-BOR w/PDA (kips) (Cont.)
50	Louisiana	LADOTD-2009	PPC 16" Square	clay	200		192
51	Louisiana	LADOTD-2009	PPC 24" Square	clay	544	150	477.6
52	Louisiana	LADOTD-2009	PPC 24" Square	clay	298	300	
53	Louisiana	LADOTD-2009	PPC 24" Square	sand	154	35	
54	Louisiana	LADOTD-2009	PPC 24" Square	sand	240	120	
55	Louisiana	LADOTD-2009	PPC 30" Square	clay	956	273	1034.2
56	Louisiana	LADOTD-2009	PPC 30" Square	clay	928	365	759.2
57	Louisiana	LADOTD-2009	PPC 30" Square	clay	760	247	749.2
58	Louisiana	LADOTD-2009	PPC 30" Square	clay	910	325	
59	Louisiana	LADOTD-2009	PPC 30" Square	sand	780	240	
60	MO	MODOT	PIPE	clay	233	550	
61	H.Kong	Paikowsky-2004	HP 10x120	mixed	1055		978
62	NE	Paikowsky-2004	HP 10x42	clay	300	230	
63	PA	Paikowsky-2004	HP 10x42	sand	397	398	
64	PA	Paikowsky-2004	HP 10x57	sand	330	446	
65	PA	Paikowsky-2004	HP 10x57	sand	300	428	
66	PA	Paikowsky-2004	HP 10x57	sand	390	524	
67	CAN	Paikowsky-2004	HP 10X74	mixed	350	432	
68	H.Kong	Paikowsky-2004	HP 12x120	mixed	1011	1091	
69	HOL	Paikowsky-2004	HP 12x120	mixed	223		156

Table A.1. Cont.

Pile No. (Cont.)	Location (Cont.)	Paper/Project (Cont.)	Pile Type (Cont.)	Soil Type (Cont.)	SLT (kips) (Cont.)	DLT - EOD (kips) (Cont.)	DLT-BOR w/PDA (kips) (Cont.)
70	CAN	Paikowsky-2004	HP 12X53	sand	475	484	
71	MA	Paikowsky-2004	HP 12x74	clay	416	304	
72	MA	Paikowsky-2004	HP 12x74	clay	448	315	
73	CAN	Paikowsky-2004	HP 12x74	mixed	800	439	
74	CAN	Paikowsky-2004	HP 12x74	sand	570	575	
75	PA	Paikowsky-2004	HP 12x74	sand	550	457	
76	PA	Paikowsky-2004	HP 12x74	sand	570	512	
77	PA	Paikowsky-2004	HP 12x74	sand	310	405	
78	PA	Paikowsky-2004	HP 12x74	sand	272	455	
79	PA	Paikowsky-2004	HP 12x74	sand	500	561	
80	OK	Paikowsky-2004	HP 14x117	mixed	820	566	
81	AZ	Paikowsky-2004	HP 14x117	mixed	1239	554	
82	MN	Paikowsky-2004	HP 14x73	clay	740	342	
83	S.C.	Paikowsky-2004	HP 14x73	sand	318	215	
84	VT	Paikowsky-2004	HP 14x73	sand	315	194	
85	VT	Paikowsky-2004	HP 14x73	sand	313	159	
86	IA	Paikowsky-2004	HP 14x89	sand	930	367	
87	NY	Paikowsky-2004	HP 10x24	sand	313	132	
88	WI	Paikowsky-2004	HP 12x63	clay	315	110	
89	WI	Paikowsky-2004	HP 12x63	clay	214	105	

Table A.1. Cont.

Pile No. (Cont.)	Location (Cont.)	Paper/Project (Cont.)	Pile Type (Cont.)	Soil Type (Cont.)	SLT (kips) (Cont.)	DLT - EOD (kips) (Cont.)	DLT-BOR w/PDA (kips) (Cont.)
90	NE	Paikowsky-2004	PSC 12" sq	clay	354	226	
91	CAN	Paikowsky-2004	PSC 12" sq	mixed	500	400	
92	NY	Paikowsky-2004	PSC 14" cyl	sand	324	279	
93	Florida	Paikowsky-2004	PSC 14" sq	clay	760	255	
94	NE	Paikowsky-2004	PSC 14" sq	clay	374	179	
95	MA	Paikowsky-2004	PSC 14" sq	clay	319	82	
96	KY	Paikowsky-2004	PSC 14" sq	clay	465	288	
97	AZ	Paikowsky-2004	PSC 16" sq	mixed	1123	529	
98	S.C.	Paikowsky-2004	PSC 16" sq	sand	819	170	
99	Florida	Paikowsky-2004	PSC 18" sq	clay	308	224	
100	AL	Paikowsky-2004	PSC 18" sq	sand	345	205	
101	AL	Paikowsky-2004	PSC 18" sq	sand	535	428	
102	Florida	Paikowsky-2004	PSC 18" sq	sand	265	245	
103	H.Kong	Paikowsky-2004	PSC 19.69" cyl	mixed	1000	755	
104	H.Kong	Paikowsky-2004	PSC 19.69" cyl	mixed	1021		1091
105	HOL	Paikowsky-2004	PSC 19.69" cyl	sand	124		147
106	OR	Paikowsky-2004	PSC 20" sq	mixed	1380	559	
107	OK	Paikowsky-2004	PSC 24" oct	sand	750	530	
108	Louisiana	Paikowsky-2004	PSC 24" sq	clay	400	136	

Table A.1. Cont.

Pile No. (Cont.)	Location (Cont.)	Paper/Project (Cont.)	Pile Type (Cont.)	Soil Type (Cont.)	SLT (kips) (Cont.)	DLT - EOD (kips) (Cont.)	DLT-BOR w/PDA (kips) (Cont.)
109	LA	Paikowsky-2004	PSC 24" sq	clay	398	60	
110	VA	Paikowsky-2004	PSC 24" sq	mixed	1230	626	
111	Florida	Paikowsky-2004	PSC 24" sq	sand	965	488	
112	AL	Paikowsky-2004	PSC 24" sq	sand	614	340	
113	AL	Paikowsky-2004	PSC 24" sq	sand	773	446	
114	Florida	Paikowsky-2004	PSC 24" sq	sand	610	509	
115	Florida	Paikowsky-2004	PSC 24" sq	sand	495	450	
116	Florida	Paikowsky-2004	PSC 30" sq	clay	1797	1301	
117	LA	Paikowsky-2004	PSC 30" sq	clay	453	45	
118	LA	Paikowsky-2004	PSC 30" sq	clay	420	59	
119	Florida	Paikowsky-2004	PSC 30" sq	clay	1209	1025	
120	LA	Paikowsky-2004	PSC 36" cyl	clay	471	91	
121	LA	Paikowsky-2004	PSC 36" cyl	clay	488	103	
122	AL	Paikowsky-2004	PSC 36" sq	sand	1074	662	
123	NY	Paikowsky-2004	PSC 54" cyl	sand	1452	405	
124	WI	Paikowsky-2004	PSC 9.7" sq	clay	214		335
125	HOL	Paikowsky-2004	PSC 9.7" sq	sand	228		296
126	NY	Paikowsky-2004	PSC 9.7" sq	sand	480		489
127	IA	PILOT	HP 10x42	Clay	124	216	
128	IA	PILOT	HP 10x42	Clay	150	244	
129	IA	PILOT	HP 10x42	Clay	154	286	

Table A.1. Cont.

Pile No. (Cont.)	Location (Cont.)	Paper/Project (Cont.)	Pile Type (Cont.)	Soil Type (Cont.)	SLT (kips) (Cont.)	DLT - EOD (kips) (Cont.)	DLT-BOR w/PDA (kips) (Cont.)
130	IA	PILOT	HP 10x42	Clay	242	390	
131	IA	PILOT	HP 10x42	Clay	212	292	
132	IA	PILOT	HP 10x42	Mixed	52		
133	IA	PILOT	HP 10x42	Mixed	162	328	
134	IA	PILOT	HP 10x42	Sand	182	452	
135	IA	PILOT	HP 10x42	Sand	128	324	
136	IA	PILOT	HP 10x57	Mixed	198	282	
137	AZ	PILOT	PSC 18.05" sq	sand	975		
138	AZ	PILOT	PSC 18.05" sq	sand	1115		

Appendix B – ReliaPile Graphs for Cases 7 and 9

Appendix B contain the ReliaPile graphs for Case 7 and Case 9 discussed in Chapter 4. The included graphs are a linear regression plot, probability density function plot (PDF), cumulative distribution function plot (CDF), and CDF with confidence bounds for the predicted lognormal distribution at a 95.0% confidence level.

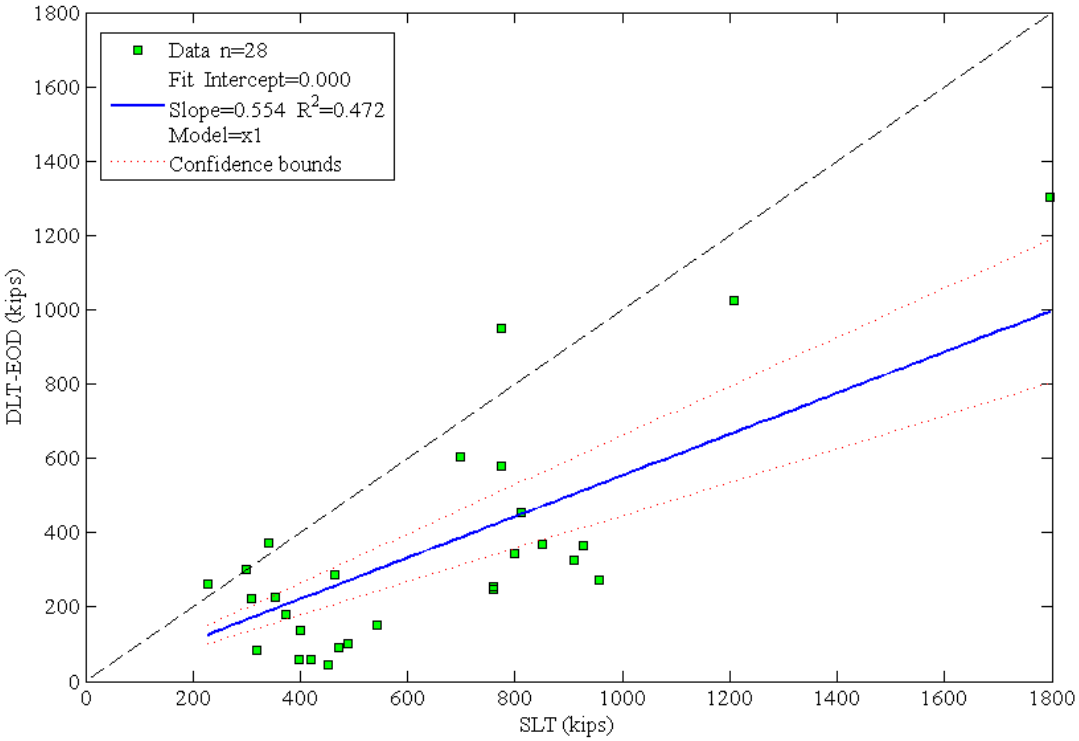

Figure B.1. ReliaPile Linear Regression Plot for PPC piles in clay soil (Case 7)

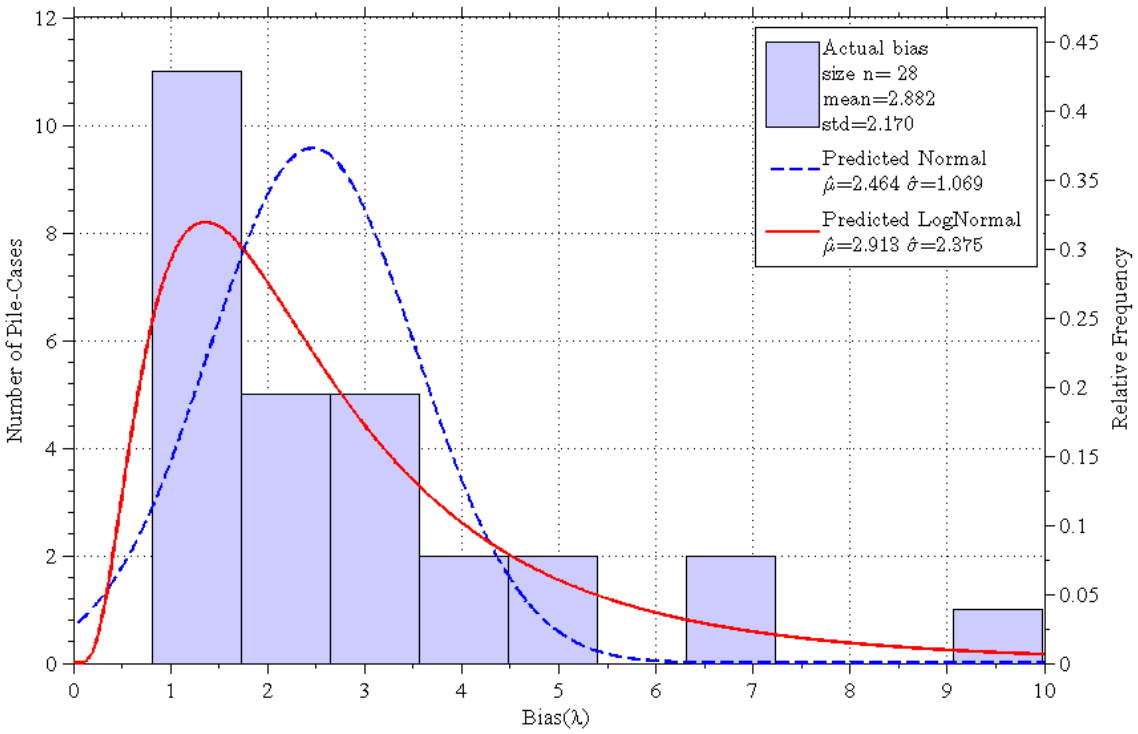

Figure B.2. ReliaPile Probability Density Function Plot (PDF) for PPC piles in clay soil (Case 7)

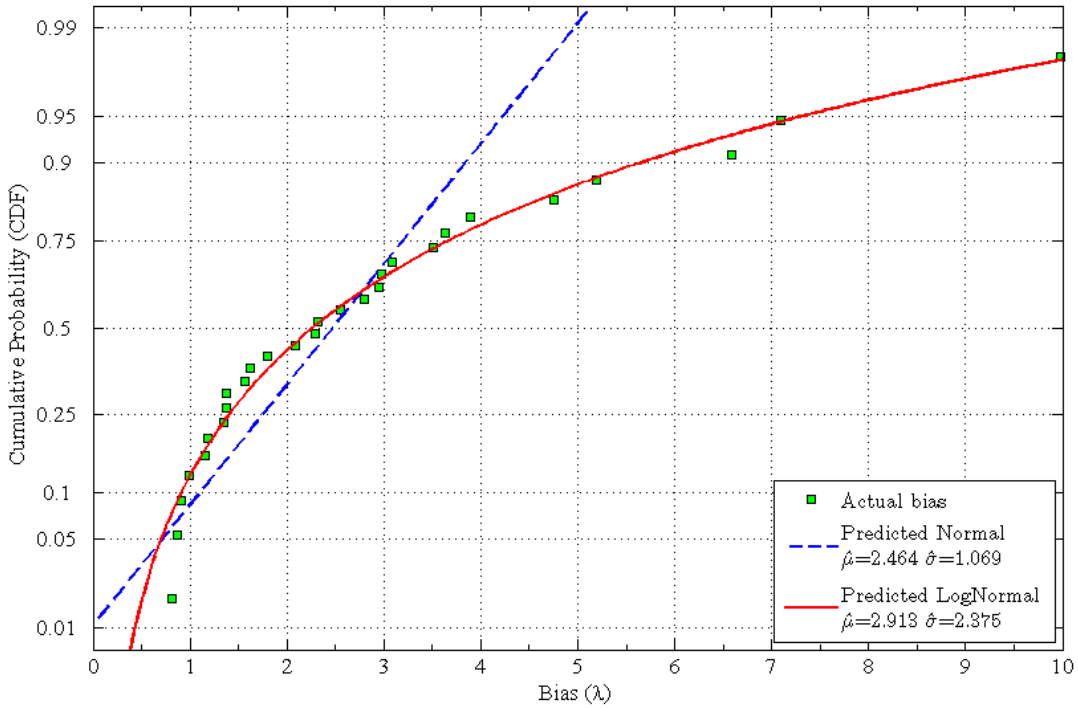

Figure B.3. ReliaPile Cumulative Distribution Function Plot (CDF) for PPC piles in clay soil (Case 7)

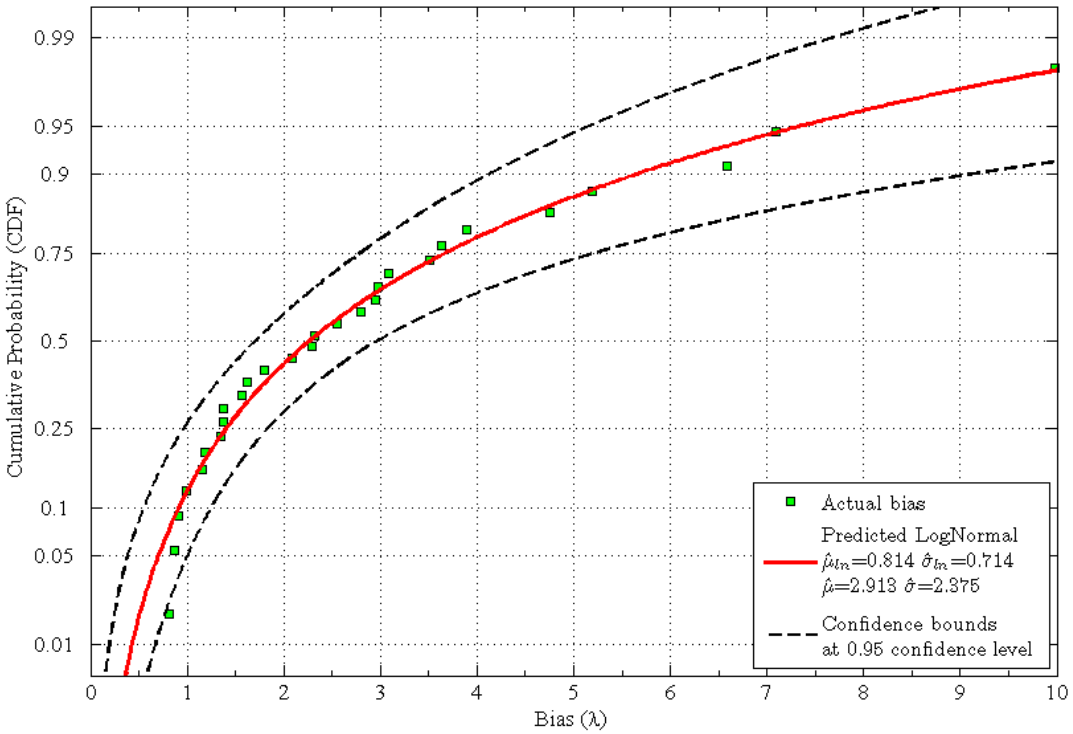

Figure B.4. ReliaPile Confidence Bounds for Predicted Log-Normal Distribution at 95.0% Confidence Level for PPC piles in clay soil (Case 7)

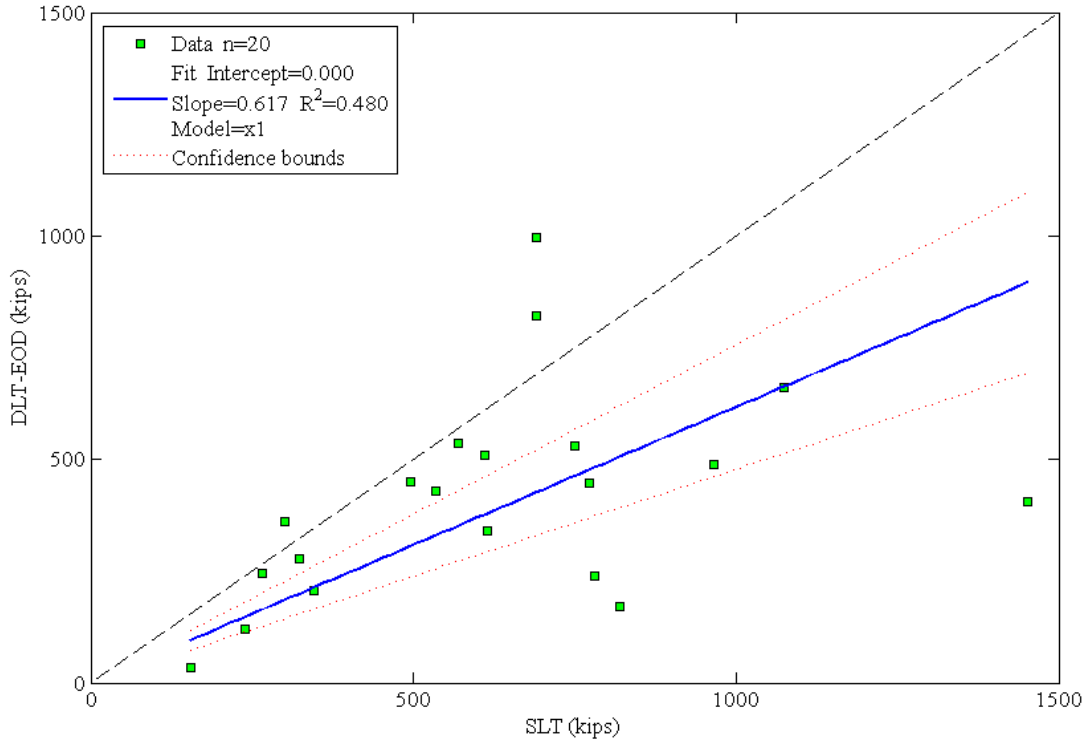

Figure B.5. ReliaPile Linear Regression Plot for PPC piles in sand soil (Case 9)

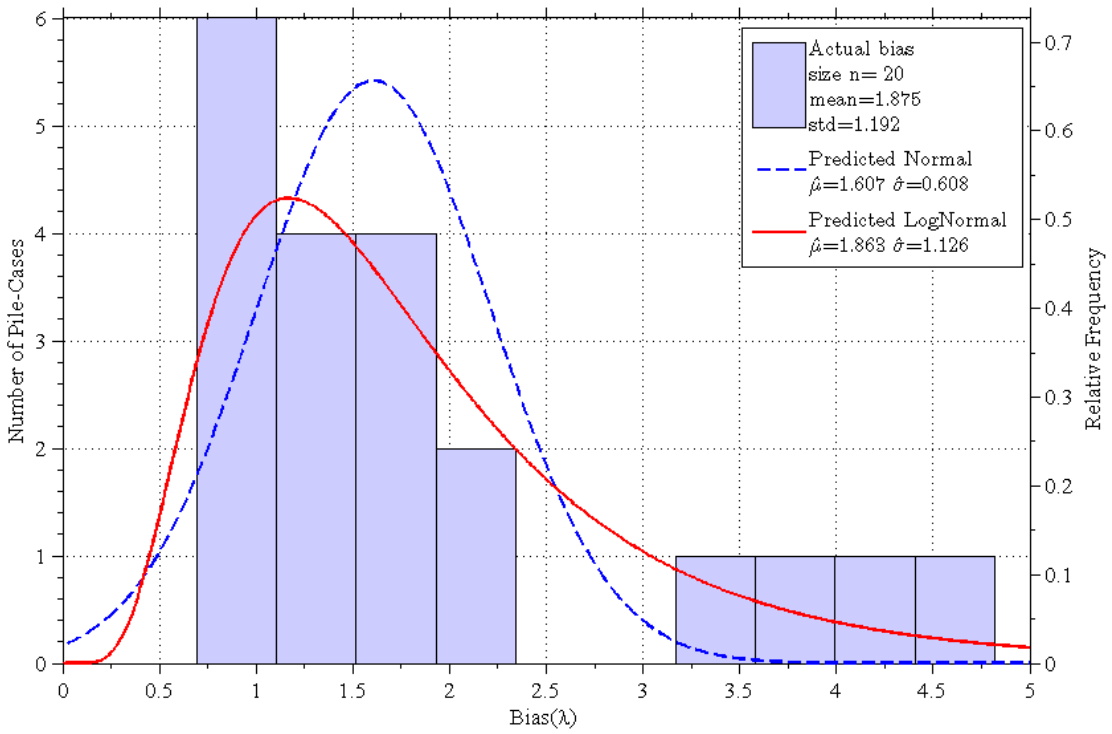

Figure B.6. ReliaPile Probability Density Function Plot (PDF) for PPC piles in sand soil (Case 9)

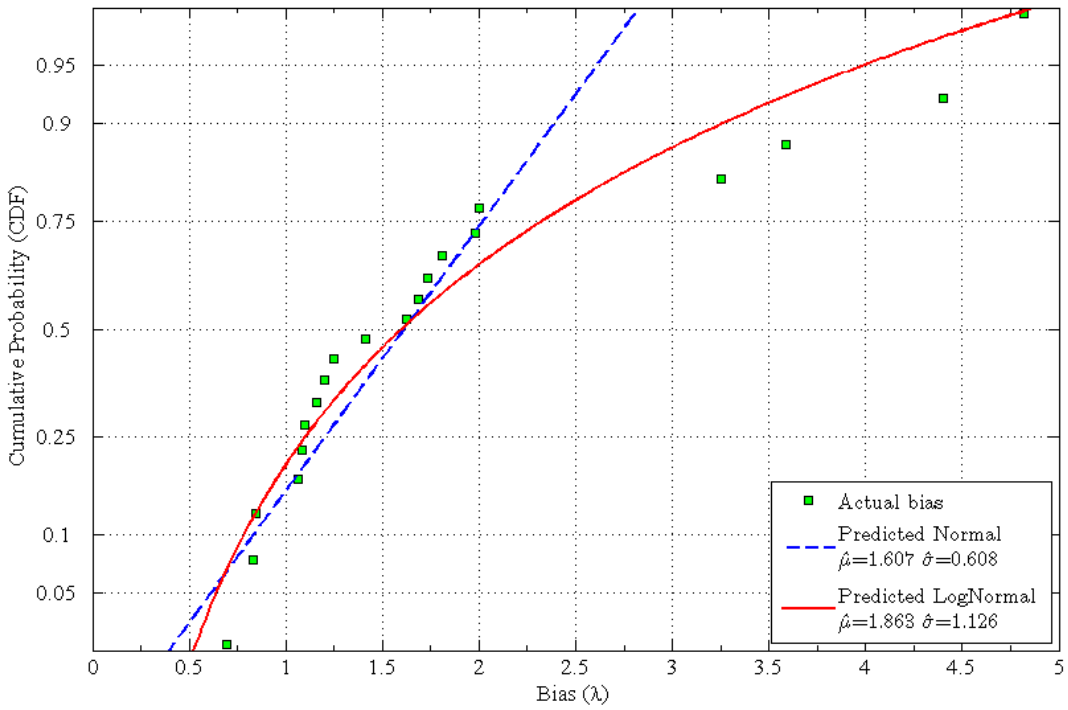

Figure B.7. ReliaPile Cumulative Distribution Function Plot (CDF) for PPC piles in sand soil (Case 9)

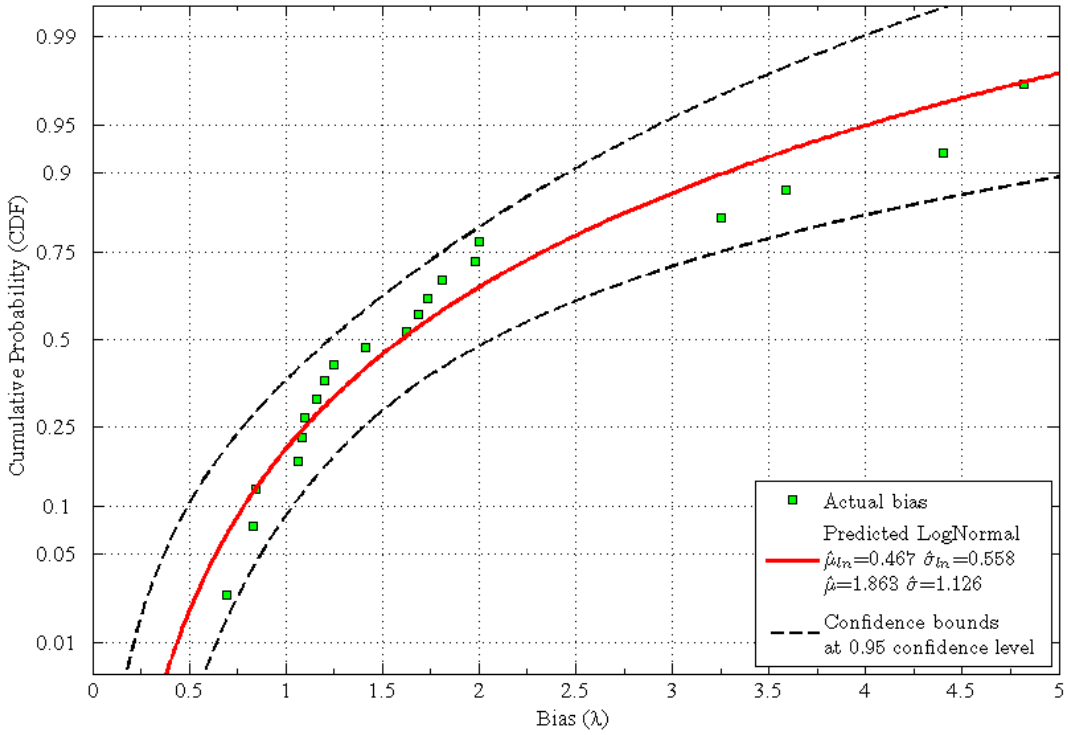

Figure B.8. ReliaPile Confidence Bounds for Predicted Log-Normal Distribution at 95.0% Confidence Level for PPC piles in sand soil (Case 9)